INVESTIGATION OF FANLESS PCs: DESIGN AND OPTIMIZATION

A thesis presented to the Faculty of the Mechanical and Aerospace Engineering Department and Graduate School at the University of Missouri

---

In Partial Fulfillment of the Requirements for the Degree

Master of Science

---

by

AUSTIN SHELNUTT

Dr. James Bryan, Thesis Supervisor

DECEMBER 2009

The undersigned, appointed by the dean of the Graduate School at the University of Missouri, have examined the thesis entitled

INVESTIGATION OF FANLESS PCs: DESIGN AND OPTIMIZATION

presented by Austin Shelnutt, a candidate for the degree of Master of Science, and hereby certify that, in their opinion, it is worthy of acceptance.

Dr. James Bryan	Date
Dr. Gary Solbrekken	Date
Dr. Stephen Montgomery-Smith	Date

I’ve dedicated the work in this thesis to my wife, Lorraine, for supporting me and encouraging me in ways words could never ascribe justice to.

Special Thanks

I would like to thank several people who have been absolutely instrumental in collaboration of this thesis work. First, I must thank my thesis advisor, Dr. James Bryan. Your passion and enthusiasm towards the science and education of heat transfer is infectious and my life was changed when I caught it. Working with you on a multitude of projects thoughout my stay at the University of Missouri has been an absolute blessing in spite of the inevitable obstacles encountered along the journey. As I depart from Mizzou, I hope to continue to learn from you in a whole new venue – the workplace. Next, I would like to thank an amazing Dell thermal engineer, Robert Prosperi. To speak honestly, I can't understand how any veteran of the engineering arts would be so patient, understanding, and insightful with a random college student, but your wisdom and guidance is what allowed for this research to reach fruition. Along those lines, I want to thank every Dell technician in the thermal lab at PS4 in Austin, TX. Words cannot describe the amount of undue help provided by that team in the heat pipe study. I would also like to thank Dr. Gary Solbrekken who has an amazing passion for educating students – a very rare desire to impart knowledge rather than just mindlessly teach a course. You are never afraid to ask more of students than they want to give you, and in doing so give them more than they could have asked. I also thank Dr. Stephen Montgomery-Smith for participating on my thesis defense committee. While I didn't get to know you as well as I had hoped, I very much enjoyed the few conversations we had on your seamless Christian undertones somehow meticulously worked into lectures on partial differential equations. I have to thank everyone in the MU thermal crew: Scott Thompson, Mike Campbell, Mike Lafser, Josh Harvey, Arron Hathaway, Corey Wilson, Chris Smoot, and Kyler Turner. Above all else, I thank the God of the heavens and earth; Jesus Christ, who has shown me that, through Him, unimaginable things are possible. God: you are real, wonderful, and amazing; I am unduely blessed in your willingness to carry me through this process and I am eternally greatful to have you in my life.

TABLE OF CONTENTS

- Special Thanks ii
- Nomenclature iv
- List of Figures v
- List of Tables viii
- Abstract ix
- Introduction 1
    - Heat Sink Fundamentals 4
    - Literature Review 9
    - Application of Theory – Heat Sink Investigation 16
- Natural Convection Enhancement 48
- Heat Diffusion within the heat sink 50
- Heat Pipe Implementation Investigation 65
- Research Conclusions 84
- Suggested Future Investigations 86
- Works Cited 87
- Appendix 89
    - Heat Sink Spreading Exp. Setup 90
    - Heat Pipe Investigation Setup 94
    - Table of Applied Correlations and Limitations 98
    - Composed Numerical Coding 99

Nomenclature

a,b	Empirical correlation consts. Eq. 12, or x/y-direction, rect. plate dimension
A	Surface area, m^2, (const. Eq. ref. 7)
B	Constant Equation reference 7
b	Half-height spacing, m
D^*	Dimensionless diameter
El	Elenbaas no. or $Ra_S = g\beta Pr\theta_b s^4/(Lv^2)$
F	Drag force
g	Gravitational acceleration, m/s^2
H	Fin Height, m
h	Heat transfer coefficient, W/m^2K
H^*	Dimensionless height
k	Thermal conductivity, W/mK
k_o	Drag factor
L	Heat Sink Length, m (see Fig. 2)
L^*	Dimensionless length
m	Fin parameter
N	Total number of fins in array
Nu_L	Nusselt no. based on length
Nu_S	Nusselt no. based on fin spacing
Pr	Prandtl number
q	Total heat transfer, W
q''	Heat flux, W/m^2
Ra_L	Raleigh's no. based on length
Re	Reynolds number
s	fin Spacing, m
S^*	Dimensionless spacing
t	fin thickness, m
W	heat Sink Width, m
W^*	Dimensionless width
T_s	surface Temperature, ºC, K
T_{surf}	surface Temperature, ºC, K
T_∞	ambient Temperature, ºC, K

Greek Symbols

α	thermal diffusivity, m^2/s, or dimensionless source width,$\Delta x/a$
β	thermal expansion coeff., K^{-1}, Porosity coefficient, or dimensionless source length,$\Delta y/a$
Γ	chimney contraction ratio
Δ	change, difference
ε	surface emissivity constant
θ_b	base excess temperature, K
λ	dimensionless constriction resis.
ρ	density, kg/m^3, or substrate aspect ratio, a/b
σ	Stephen-Boltzmann constant
τ	Dimensionless thickness, t/a
μ	mean dynamic viscosity
υ	mean kinematic viscosity, m^2/s
ϕ	heat-sink porosity
ψ	Dimensionless spread resistance

Subscripts

b, base	fin array base
fin, f	heat sink fin
hs	heat sink
i	inner, internal
o	external,outside
p	base plate
s	surface

List of Figures

Figure Page

1. Thermal resistance network……..... 2
2. Heat sink geometric depiction……..... 5
3. Natural Convection Fluidic Motion……..... 6
4. Inclined Surface Convection…… 7
5. Boundary layer between parallel plates…… 8

Vertically Oriented Heat Sinks – Rectangular Fins

6. HSA: Fin Height……... 19
7. HSA: Fin Thickness…… 21
8. HSA: Fin Spacing…….. 24
9. Combined Effects…….. 26

Vertically Oriented Heat Sinks – Triangular Fins

10. HSA: Fin Height……. 28
11. HSA: Fin Thickness…… 29
12. HSA: Fin Thickness Vs. Efficiency…… 30
13. HSA: Fin Spacing……. 31
14. HSA: Combined Fin Spacing…… 32
15. HSA: Combined Fin Heights…… 34
16. Combined Effects…… 35

Horizontally Oriented Heat Sinks – Rectangular Fins

17. HSA: Fin Height……. 37
18. HSA: Fin Height Vs. Heat Transfer Coefficient……. 38

19. HSA: Fin Thickness……. 39

20. HSA: Fin Thickness Vs. Efficiency……. 40

21. HSA: Fin Spacing……. 41

22. Combined Effects……. 42

23. Fin Spacing Vs. Thermal Resistance – 3 Configs……. 43

24. Heat Transfer Coefficient – 3 Configs…….. 43

25. Lee and Song et al. Spreading Resistance……. 53

26. Spreading Resistance Divergence……. 53

27. Heat Sink Experment Diagram…….. 55

28. 3D Heat Diffusion Solution – *Conduction3DTransient.m*……. 56

29. 3D Heat Diffusion Solution – Fluent…….. 57

30. Case 1: Single Eccentric Plate…… 57

31. Case 1: Temperature Distribution…… 57

32. Case 2: Single Centered Plate…….. 58

33. Case 2: Temperatur Distribution……. 58

34. Case 3: Four Horizontal Plates…… 58

35. Case 3: Temperature Distribution…… 58

36. Case 4: Four Vertical Plates…… 58

37. Case 4: Temperature Distribution…… 58

38. 3D Experimental Temp. Distribution…… 62

39. Contour – Experimental…… 62

40. Analytical Vs. Experimental……. 62

41. Peterson et al. Model…… 65

42. Heat Pipe Cycle……. 66

43. Thermal Test Vehicle (TTV)……. 69

44. Condenser Lengths……. 70

45. Heat Pipe – Heat Sink Assembly…… 70

46. Thermocouple placement…… 71

47. Condenser Geometries…… 71

48. Temperature Profile – VED……. 73

49. Temperature Profile – Horizontal……. 73

50. Temperature Profile – VEU……. 74

51. Resistance – VED…… 77

52. Resistance – Horizontal…… 77

53. Resistance – VEU…… 77

54. Resistance – 160 mm…… 78

55. Resistance – 260 mm…… 78

56. Resistance – 360 mm…… 79

57. Resistance – 160 mm Round/Flat…… 80

58. Resistance – 260 mm Round/Flat…… 81

59. Resistance – 360 mm Round/Flat…… 81

List of Tables

Table Page

1. Literature Review…….....…… 2
2. Parametric Analysis of all 3 heat sink configurations…… 45
3. Comparitive Data: Analytical Vs. Numerical……. 59
4. Analytical Vs. Experimental Thermal Resistance……. 60
5. Heat Pipe Investigation Independent Variables…… 68
6. Heat Pipe Guideline Table……. 83
7. Applied Correlations and Limitations…… 98

Abstract

The purpose of this research is to fundamentally explore the limitations of natural convection as it pertains to the cooling of desktop personal computers (PCs) and, in particular, maximize total thermal loads while minimizing the volume of the complete package. This research is directed towards the ultimate goal of finding the optimum design of a sealed, Fanless personal computer conforming to the Ultra Small Form Factor (USFF). The work presented herein has developed the foundational tools and knowledge base required to accomplish the stated goal from a thermal perspective. This was realized in three unique investigations: heat sink optimization, thermal spreading analysis, and heat pipe implementation study. A program was developed utilizing a cumulative empirical correlation database to output optimized heat sink designs. A look at lumped capacitance, as well as numerical, analytical, and experimental comparisons for spreading resistance revealed good results for simple analytical approximations as a design tool. Finally, heat pipe implementation was looked at from several common design assumption angles allowing for several valuable conclusions to be made on heat pipe placement in any future Fanless PC design.

Introduction

In cooling any heat producing device, it is necessary to first characterize the impedances to thermal energy transport known as thermal resistances. To begin this process, a heat source must be identified. The nature of this research is focused upon the personal computer, and ultimately a fully functional, sealed unit that is cooled entirely by free convection. Within the personal computer, there exists various heat producing devices of diverse thermal energy outputs, however, the largest producer of heat is the Central Processing Unit (CPU). It is by this token that the CPU has been explicitly defined as the heat source with the ultimate intention of applying the tools gained throughout the research to other heat producing devices within the system. The next step was to define the thermal energy sink in which all of the heat generated at the source would finally be ejected, in this case, the ambient air. Throughout the history of the electronic computer, great amounts of research have been focused upon enhancing the transport of thermal energy from the CPU to the ambient air. Devices such as liquid cooling blocks and multi-phase heat pipes have been developed allowing for heat to efficiently travel from a CPU to a larger heat exchanger than could be effectively utilized at the base of the heat source. The summation of thermal resistances from the generation of heat located at the CPU to the final dissipation of heat in the ambient air comprises the total thermal resistance network shown below (Fig 1). Figure 1 will frequently be referred back to for clarification.

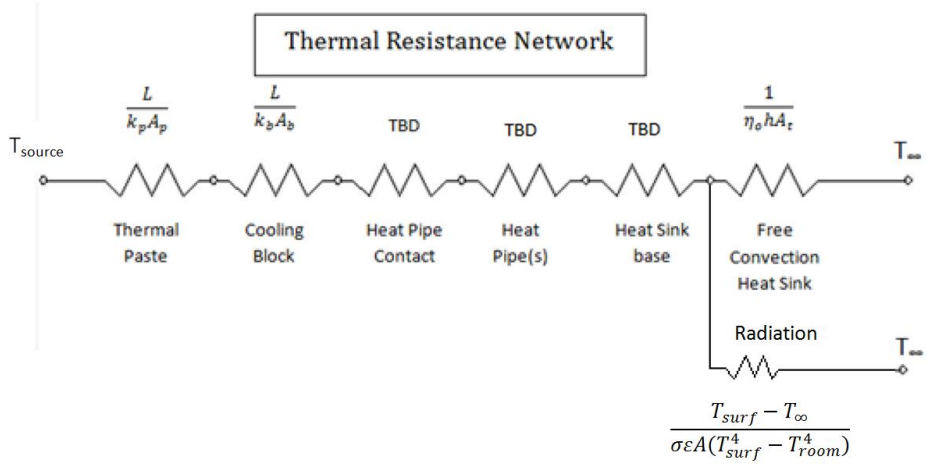

Fig. 1. Thermal resistance network depicting the individual thermal transport impedances

The "Heat Pipe Contact" resistance is a function of the evaporator and condenser contact areas and profiles (i.e. round-groove, flattened, or embedded). "Heat Pipe" resistance is dependent upon a number of factors including orientation, condenser length, and thermal load. The "Heat Sink base" resistance is inclusive of 1-D heat transfer through the base and any potential spreading resistance that may exist. TBD resistances are those that are discussed in greater detail later in this paper. Information in regards to the thermal resistances from the contact of thermal paste through the cooling block is both wealthy and credible, and for the purposes of this research will not be considered. That leaves three fundamental resistances that require attention and provide the most opportunity for improvement: conductive spreading throughout the heat sink base, free convection/radiation out of the heat sink (heat sink will henceforth refer to the final heat exchanger between the ambient air and thermal energy produced at the source), and the strategic implementation of heat pipes. As stated in the research objective, the fundamental goal is to maximize total heat transfer while minimizing (or at the very least staying within a specified value) the size of the total package. The first area of opportunity to be considered is the optimization of the free convection heat sink. This

will be accomplished via two distinct routes: the first will be to perform literature research in order to culminate fundamental existing laws that govern heat sink performance and the second will be to investigate theoretically and experimentally various enhancement techniques that could potentially prove valuable in reducing thermal resistance.

Heat Sink Fundamentals

The term ‘heat sink’ has recently become a commonplace reference to a passive heat spreader that ultimately enhances transport of thermal energy from a heating source or CPU by an increase in convection surface area. Convection heat transfer occurs when a fluid is in contact with a surface of a differing temperature resulting a in a local temperature gradient. This phenomenon can occur naturally when a fluid’s temperature in contact with a surface changes with respect to neighboring fluid that is not in direct contact with the surface, resulting in temperature and, consequently, density gradients throughout the fluid. The density gradients give rise to bulk fluid motion that is driven by buoyancy forces within the fluid and thus convective heat transfer becomes active. From physics, it is known that the total energy transportable via convection is directly proportional to the surface area in contact with the fluid. A heat sink is simply a device that maximizes the total surface area available for heat transfer, typically with the addition of fins or other extended surfaces off of a heating source. This process is not at all arbitrary, however, as it has been found that incorrect application of fins to a surface may actually reduce the total heat transfer to a value below that of the base alone [1].

While countless sizes, geometries, and profiles exist for heat sinks used today, we will, for this research, limit ourselves to plate-fin heat sinks, as they provide the most consistent cooling solution for the size and cosmetic constraints imposed upon such. Figure 2 below shows a generic sketch of a typical heat sink.

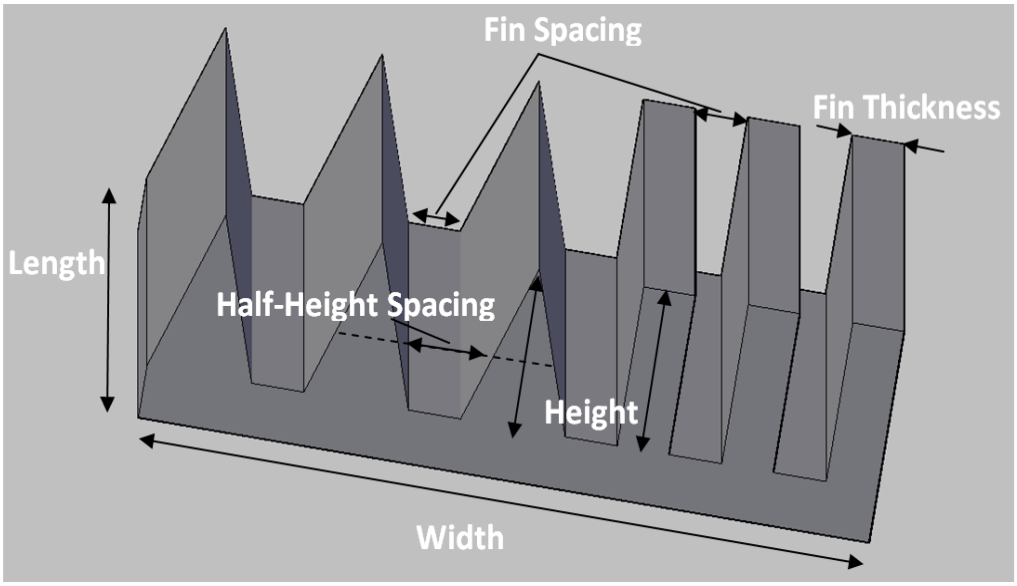

Fig. 2. Illustrates the various geometric features of a typical heat sink

As depicted in the figure, there are five explicitly defined geometric features of the plate-fin heat sink; the length, width, fin spacing, fin thickness, and fin height (for triangular fins shown left, half-height spacing, *b*, is often considered). There are other considerations that comprise the heat sink including fin profile, gravitational orientation, and the implicit calculation of fin number.

Buoyancy Driven Heat Transfer

As mentioned in the previous section, natural convection occurs when local temperature gradients create variations in density throughout a fluid that ultimately induce motion. The study of this process is essential in understanding and optimizing the natural convection heat sink. The first step in characterizing the induced motion across the heat sink is to examine orientation of the surface with respect to gravity. Basic thermodynamics stipulates that as the temperature of a fluid increases its density

decreases; thus warmer fluids will rise. It is then known that by Conservation of Mass, this warmer fluid will be replaced by incoming cooler, denser fluid.

Horizontal Surfaces

Fig. 3 presents an excellent illustration of the buoyancy driven currents on a horizontally oriented heat sink.

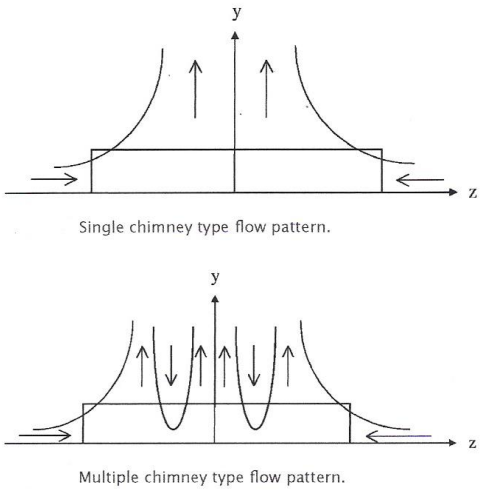

Fig. 3. Illustration of natural convection currents on a horizontally oriented heat sink [1].

The effectiveness of this type of cooling can be influenced by the distance incoming fluid must flow before finally being pushed off of the surface and the flow resistance. Smaller fin spacing and longer fin lengths (see Fig. 2) can both negatively affect the convection heat transfer coefficient. As seen in Fig. 3, warm air rises in the middle of the heat sink drawing in cooler air from the sides creating a plume type flow also known as a chimney. As the fin length increases, this chimney predictably transitions into multiple chimneys in which cool air is not only drawn from the sides, but is also pulled down from above the heat sink. These multiple chimneys can create large flow disturbances as shown in Fig. 3. It was observed that single chimneys are far more efficient in the removal of heat than multiple chimneys and the overall value for the convection heat transfer coefficient reduces with fin length [1].

Inclined/Vertical Surfaces

Positioning the heated surface at an angle complicates the analysis further. Rather than strictly maintaining a parallel component, the buoyancy force now has both a normal and a parallel component with respect to gravity. Fig. 4 below shows an illustration of a heated inclined surface.

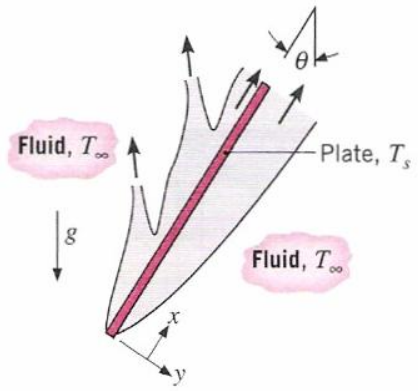

Fig. 4. Buoyancy driven currents on a heated inclined surface [2].

The bottom side of plate in Figure 4 shows typical boundary layer development on a convective surface. The development of the curve on the boundary layer is representative of the change in fluid temperature as it moves along the heated surface and when the angle θ is equal to 90º (vertical orientation) would be present on both sides of the plate. It should be assumed that as $x \rightarrow \infty$, the temperature of the fluid will equal that of the surface and the largest temperature gradients will exist when x equals zero. It is for this last bit of reasoning that boundary layer development, in thermal engineering, is typically regarded as a negative consequence in convection that should be minimized. The top side of the plate in Fig. 4 (being inclined in orientation), however, shows multiple boundary layer disruptions caused by the buoyancy force acting in the y-direction ejecting warmer particles of fluid. This type of boundary layer disruption has been found to significantly

enhance convection, but the flows created by such are strictly three-dimensional and are unable to be characterized by traditional analytical correlations [3].

Fin Channels

As viewed in Fig. 2, heat sinks typically contain a combination of horizontal, inclined, and vertical plate attributes, and thus a combination of flow types. For most cases, as this research, it is acceptable to assume the fins on a heat sink as being isothermal with respect to one another. This assumption may be poor for heat sinks with larger fin heights and low thermal conductivity materials; however, it simplifies the characterization of fluid flow between the fins. Fig. 5 shows a depiction of natural convection from within parallel plate heat sink fins (channels). W. Elenbaas was the first to characterize flow of this type and the correlations he developed are still utilized today [4]. Elenbaas essentially postulated that heat transfer between two isotheral plates (fins) could be quantified by a relationship between the spacing and length of the plates. These correlations have undergone only slight modification and are very widely accepted [1].

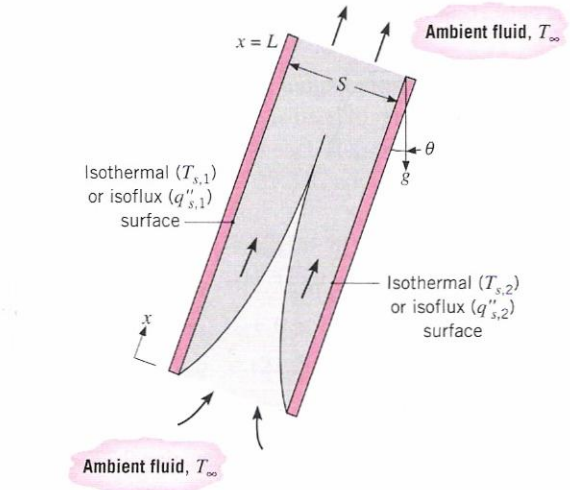

Fig. 5. Illustration of the boundary layer flow between two heated parallel plates [3].

Results of Literature Research – Natural Convection Heat Sink

Fundamental Literary Works

The first step in beginning to optimize the free convection heat sink was to compile the foundational ground breaking work contributed by engineers and researchers in previous studies. While by no means comprehensive and all inclusive, a tabularized literature review is shown below in Table 1. Also shown in the literature review are some of the other notable works aligned with the goal of designing a Fanless PC system that will be discussed in later sections of the thesis including convection enhancement and thermal spreading related work.

Literary Work	Purpose/Goal	Findings	Correlations
Elenbaas [4]	Studied the effects of natural convection heat transfer taking place between two isothermal plates. *(Fin Array Heat Transfer)*	- The heat transfer coefficient between parallel plates is directly dependent upon the plate spacing. - As s → 0, the heat transfer coefficient approaches its maximum value associated with isolated plates.	Elenbass Number: $El = \frac{g\beta\theta_b \Pr s^4}{L\nu^2}$
Bar-Cohen, et al. [5]	Extended the pioneering work of Elenbass to a variety of boundary conditions. *(Fin Array Heat Transfer)*	- Developed a composite Nusselt number correlation for nonisothermal parallel plates such as those encountered in rectangular plate-fin arrays.	$Nu_{fin} = \frac{h_{fin}s}{k_{fluid}} = \left[\frac{576}{(\eta_{fin}El)^2} + \frac{2.873}{(\eta_{fin}El)^{1/2}}\right]^{-1/2}$
Karagiozis, et al. [7]	Characterized the performance of triangular fin arrays in vertical orientation	- Developed Nusselt correlation for vertically oriented triangular fin arrays. - Addressed the **non-existent nature of horizontally oriented triangular fin correlations.**	Vertically Oriented Triangular Fin arrays: $Nu_{fin} = \left[0.515(\eta_{fin}Ra_b)^{1/4}\right]\left[1 + \left(\frac{3.26}{(\eta_{fin}Ra_b)^{0.21}}\right)^3\right]^{-1/3}$

Literary Work	Purpose/Goal	Findings	Correlations
Bar-Cohen, et al. [6]	Used existing empirical correlations to optimize natural convection heat transfer with pin, triangular, and plate fin structures using least-material as the optimization metric. *(Fin Array Heat Transfer)* *(Vertical Orientation)*	- Based upon computational evaluation of existing empirical correlations, triangular fins were found to be thermally superior to pin and plate fin types for max heat transfer. - Pin-Fin arrays, however, were found to be the most volumetrically efficient configuration with regards to material used and mass.	- Developed the array heat transfer coefficient h_a to capture the effectiveness of the heat sink area being used $$h_a = \frac{q_{total}}{LW\theta_b}$$
Bar-Cohen, et al. [3]	Used existing empirical correlations to optimize natural convection heat transfer for plate-fin arrays using thermal resistance as the optimization metric. *(Fin Array Heat Transfer)* *(Vertical Orientation)*	- Study yielded several empirically based, analytical optimization expressions for heat sink optimization.	- Optimum Spacing $$s_{opt} = 2.66\left(\frac{L\nu^2}{g\beta\eta_{fin}\theta_b \Pr}\right)^{1/4}$$ - Least-material Thickness $$t = \frac{0.993 h_{fin} H^2}{k_{fluid}}$$

Literary Work	Purpose/Goal	Findings	Correlations
Baskaya, et al. [1]	Used CFD to perform a parametric study on the effects of fin spacing, height, length, and temperature difference between fins and surrounding air natural convection heat sinks with rectangular plate fins. Analyzed fin (entrance) length effect on plume flow behavior. *(Fin Array Heat Transfer) (Horizontal Orientation)*	- Showed that it is not possible to obtain optimum performance in terms of overall heat transfer by only concentrating on one or two parameters. Rather, the interactions among all design parameters must be considered. - Found that as the fin (entrance) length increases, the buoyancy driven flows transition from single plume to multiple plume type flow which decreases the value of the heat transfer coefficient. - Redefined correlation constants for proposed expression by Harahap and McManus [#].	$$Nu_L = a\left[Ra_L \frac{S}{H}\right]^d \left(\frac{S}{L}\right)^{0.656} \left(\frac{H}{L}\right)^{0.412}$$ - Where *a* and *d* were, for the present study, found as *a* = 0.00071561 and *d* = 0.6576. - Original correlation developed by Harahap and McManus [#].
Fisher, et al. [7]	- Studied the effects of porosity and chimneys on pin-fin heat sinks in natural convection from a theoretical viewpoint. *(Chimney Effect on Pin-Fin Arrays)*	- Developed non-dimensional correlations for fluid flow and heat transfer within chimneys shrouding pin-fin arrays that were, found to be accurate. - Showed that the chimney effect can enhance local heat transfer such that the minimum temperature rise remains approximately invariant while the height of the heat-sink relative to the total system height is reduced; thus allowing for reduced heat sink volume. - Predicted optimal heat sink porosity to be greater than 90%.	- Dimensionless draft equation: $$\frac{RaD^{*3}(1-H_H^*/2)}{W^*L^*\,\mathrm{Pr}^2} = F\frac{H_H^*}{D^*S^{*2}}\mathrm{Re}^2 + \frac{1}{2}\Gamma^2\,\mathrm{Re}^3$$ - Where $$Ra = \frac{g\beta Q_{tot}H^2}{\nu\alpha k_{fluid}}$$ $$H_H^* = \frac{H_H}{H}, W^* = \frac{W}{H}, L^* = \frac{L}{H}, D^* = \frac{D}{H}, S^* = \frac{S}{D}$$ - Drag model $$F = Ak_o(\phi) + B\frac{k_o(\phi)}{1-\phi}\mathrm{Re}$$

Literary Work	Purpose/Goal	Findings	Correlations
Thrasher, et al. [8]	Experimentally analyzed the effects of chimney-aided free convection on vertically oriented pin-fin heat sinks. Compared experimental results with theoretical correlations proposed in previous work [1]. *(Chimney Effect on Pin-Fin Arrays)*	- In general, chimneys provide significant heat transfer enhancement to free-convection heat sinks. - Reduction to heat sink temperature by as much as 30% are possible with the studied pin-fin heat sinks. - Optimal Porosity $\phi \approx 90\%$	- Correlations produced in previous work [1] were validated experimentally in this study with typical deviations less than 5%. - Determined that cold inflow into the chimney exit was the most significant contributor to theoretical/ experimental divergence and is still largely uncharacterized.
Kitamura, et al. [9]	Studied the chimney effect on natural convection heat transfer for a flat heated plate with varying porosity coefficients and inclination angle. *(Chimney Effect on Inclined Flat Plate)*	- Increasing the inclination angle and porosity coefficient of the outlet openings enhances natural convection and leads to an increase in airflow throughout the chimney. - When the porosity coefficient of the outlet opening, β_o = 0.011, further increases in porosity will result in negligible gains. - Proposed a modified reference length to be used in the design of thin chimneys.	- Porosity Coefficient, β, is the ratio between open area and surface area in the open face abutting on air. $$\eta = \frac{1-\beta}{\beta^2}$$ - Modified reference length x^* $$\frac{1}{x^*} = \frac{\eta_i V_{heater}}{\eta_o V_{ca\sin g}}\left(\frac{1}{horizontal} + \frac{1}{2}\frac{1}{vertical}\right)$$

Literary Work	Purpose/Goal	Findings	Correlations
Lee, S., Song, S, et al. [12]	- Used cylindrical coordinate transform to produce a simple closed-form approximation to the Laplace Equation governing heat spreading in a heat sink with convection on one face. *(Simple Approximation of thermal spreading resistance)*	- By the method of separation of variables, the heat equation was solved in polar coordinates and reduced to an explicit approximation expression. - Solution employs a circular substrate assumption.	$$R_s = \frac{\sqrt{A_p} - \sqrt{A_s}}{k\sqrt{\pi A_p A_p}} \times \frac{\lambda k A_p R_o + \tanh(\lambda t)}{1 + \lambda k A_p R_o \tanh(\lambda t)}$$ Where $$\lambda = \frac{\pi^{3/2}}{\sqrt{A_p}} + \frac{1}{\sqrt{As}}$$
Ellison, et al. [13]	Solved the 3-D heat equation using non dimensional analysis and infinite Fourier Series. *(Highly accurate but complicated solution to thermal spreading resistance)*	Equation shown in heat diffusion section	

Theory Development

Because of the great explosion of personal computing in the late 1980's into the 1990's, a tremendous amount of pressure was placed upon thermal engineers to develop methods of cooling all of the new types of processors. This pressure resulted in a great quantity of empirical and analytical correlations for the heat transfer on natural convection fin arrays of horizontal, vertical, and, to a lesser extent, inclined orientations. As discussed in the fundamentals segment of this research, free convection relies on an inherent balance between viscous dissipation and buoyant potential rather than on pump or blower specifications and as such it can be anticipated that as the channel width or plate spacing is reduced, the heat transfer coefficient will decrease below the value associated with an isolated plate.

Application of Theory – Heat Sink Investigation

The primary metric being employed to optimize the natural convection heat sink in this research is thermal resistance. For this segment of the research, thermal resistance will only refer to the convective resistance of the heat sink given by

$$R_{th} = \left[\frac{1}{h_{base} A_{base}} + \frac{1}{\eta_{fin} h_{fin} A_{fin}} \right]^{-1} \tag{1}$$

The secondary metric, used to constrain the first, is volume. To reiterate what has already been stated, the purpose of this research is to find the maximum amount of thermal energy that can be dissipated via free convection in a given volume constraint, which for the present has been established as 4.5 liters. Using these two metrics and the correlations presented above, a series of plots were generated to aid in the visualization of theoretical trends and ultimately guide optimization. To start this process, a base area of Length = 40cm by Width = 20cm was chosen for the heat sink with a fixed thermal load. Because the surface area of the heat sink is held constant, parameters such as fin thickness and fin spacing become the independent variables and the number of fins for a given thickness and spacing is a dependent variable that changes accordingly. In order to evaluate several thermophysical properties, as well as the convection correlations, surface temperature is always iteratively converged upon based upon the relationship of surface temperature, heat transfer coefficient, and total power dissipation (see Appendix *HSAnalysis.m*). This approach dictates that the entire heat sink surface be isothermal; an assumption that will be removed later in the research.

Three configurations were considered in the analysis: vertically oriented rectangular-profile fins, vertically oriented triangular-profile fins, and horizontally

oriented rectangular-profile fins. These three configurations were chosen for several reasons. All of the configurations mentioned are likely implementations for any future Fanless PC designs. Pin-profile fins are routinely implemented in heat sinks today, however, their strength is in radiation heat transport and are more costly than the other two fin profiles to manufacture. The absence of a triangular-profile fin array in the horizontal orientation is due to the real lack of literature concerning the topic. Either by virtue of always performing worse than other fin profiles in the horizontal orientation or some other factor, there is a gap in the readily available literature for horizontally oriented triangular fin arrays.

Vertically Oriented Heat Sink

- *Rectangular Fin Array*

The first set of optimization trends were conducted on the vertically oriented rectangular fin array heat sink. For purposes of this research, vertical orientation always refers to the length vector of the heat sink being parallel with gravity. While many papers and techniques have been published on the subject, nearly all technical discussions on natural convection heat sinks draw from the aforementioned work of Elenbaas in 1942. Elenbaas determined than an optimum spacing between parallel isothermal plates along with an optimized Nusselt number could be quantified by setting the channel Rayleigh number (dubbed the *Elenbaas number*) equal to 50 [5]. Where the Elenbaas number is given by

$$El = \frac{(g\beta\theta_b \Pr s^4)}{L\upsilon^2} \tag{2}$$

and the variables are as defined in the Nomenclature section. Bar-Cohen expanded this relationship for rectangular fins/channels in the vertical orientation as

$$Nu_{fin} = \frac{h_{fin}s}{k_f} = \left[\frac{576}{(\eta_{fin}El)^2} + \frac{2.873}{(\eta_{fin}El)^{1/2}} \right]^{-1/2} \tag{3}$$

and determined that the optimum fin array Nusselt number value is equal to 1.25. Using this value, optimum fin spacing can be derived from equation (3) yielding the relationship:

$$s_{opt} = 2.66 \left(\frac{L\upsilon^2}{g\beta\eta_{fin}\theta_b \Pr} \right)^{1/4} \tag{4}$$

For both equations (3) and (4), the rectangular fin efficiency is calculated using

$$\eta_{fin} = \frac{\tanh(mH)}{mH} \tag{5}$$

and the fin parameter m is defined by the relationship:

$$m = \left(\frac{2h_{fin}}{k_{f\ \mathrm{int}}} \right)^{1/2} \tag{6}$$

Bar-Cohen took a least-material approach to optimizing the plate fin heat sink and was able to develop a final correlation that relates an optimum fin thickness value to the heat transfer coefficient and the fin height [1]:

$$t_{opt} = \frac{0.993h_{fin}H^2}{k_{fin}} \tag{7}$$

It should here be noted that the correlations derived for the heat transfer coefficient across the rectangular fin array in the vertical orientation do not contain an explicit dependence upon the fin height *H*. This is not the case, however, for the strictly horizontal orientation, for which well supported correlations have been developed that consider fin spacing, length, and fin height. In each plotted trend, the total number of fins in the array is

implicitly calculated based upon the values for fin thickness, fin spacing, and the pre-set dimensions of the heat sink width, *W*.

Using the Bar-Cohen analytical correlation in Eqn. (3), a full trend analysis was conducted for the vertically oriented rectangular fin array. The first performance trend analyzed was the effect of fin height upon thermal resistance for the heat sink prescribed in the preceding section. Figs. 6a and 6b show the relationship between fin height and thermal resistance for varying fin spacing at 0.5 mm and 2 mm fin thickness respectively.

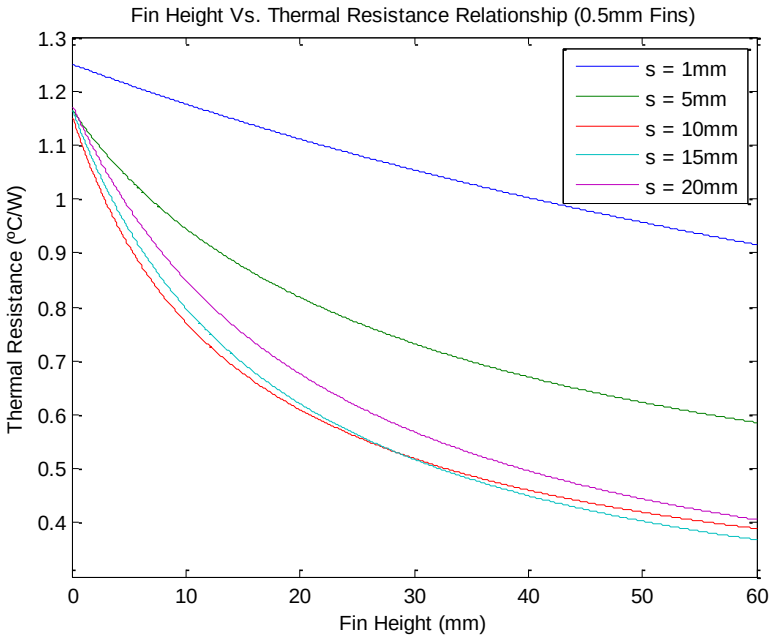

Fig. 6a. Plot of thermal resistance verses fin height for several fin spacings at 0.5mm thick fins.

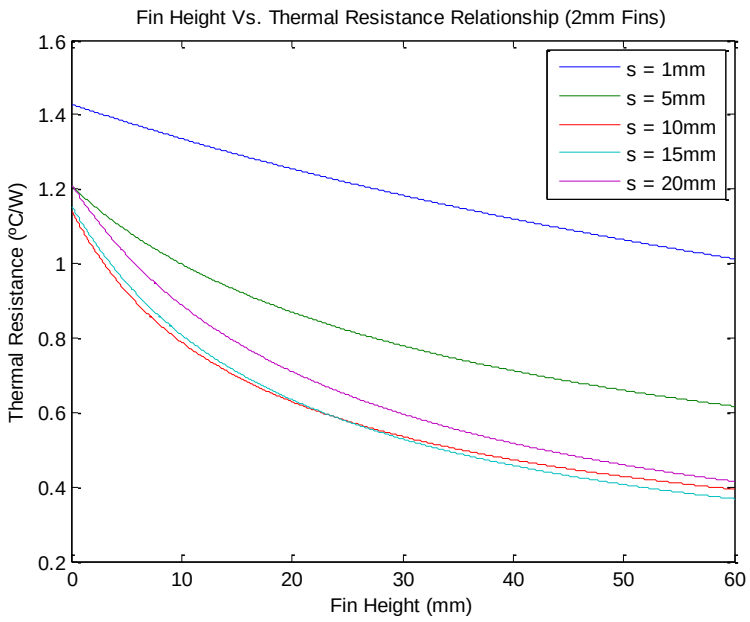

Fig. 6b. Plot of thermal resistance verses fin height for several fin spacings at 2 mm thick fins.

As the above plot clearly shows, thermal resistance only continues to improve as fin height is increased for a given fin spacing. However, this does come with some diminished returns as the improvements in thermal resistance tend to level off due to the fin efficiency term taking over. Another noticeable trend in the two preceding figures is the depiction of fin spacing and fin thickness's impact on thermal resistance. Fin spacing significantly influences the thermal resistance a great deal more than thickness appears to. This is shown more clearly in the next two sets of plots.

The next trend examined was the relationship between fin thickness and thermal resistance shown in Fig. 7. The analytical correlations in this trend are pointing towards thinner fins for improved performance. This is due to an increased number of fins that can now be placed on the heat sink and what is possibly an underrepresented fin conduction term. Because the fin conduction only appears in the fin efficiency term, it is possibly underweighted in that the vastly reduced cross sectional area of the fin now poses a non-negligible thermal resistance. The original correlation proposed by Elenbaas

in 1942 [4] characterized the natural convection flow between isothermal flat plates. Bar-Cohen's correlation seems to appeal to this isothermal assumption and performs with moderate indifference towards what should be a decaying isothermal condition in the fin array for these ultra-small fin thicknesses.

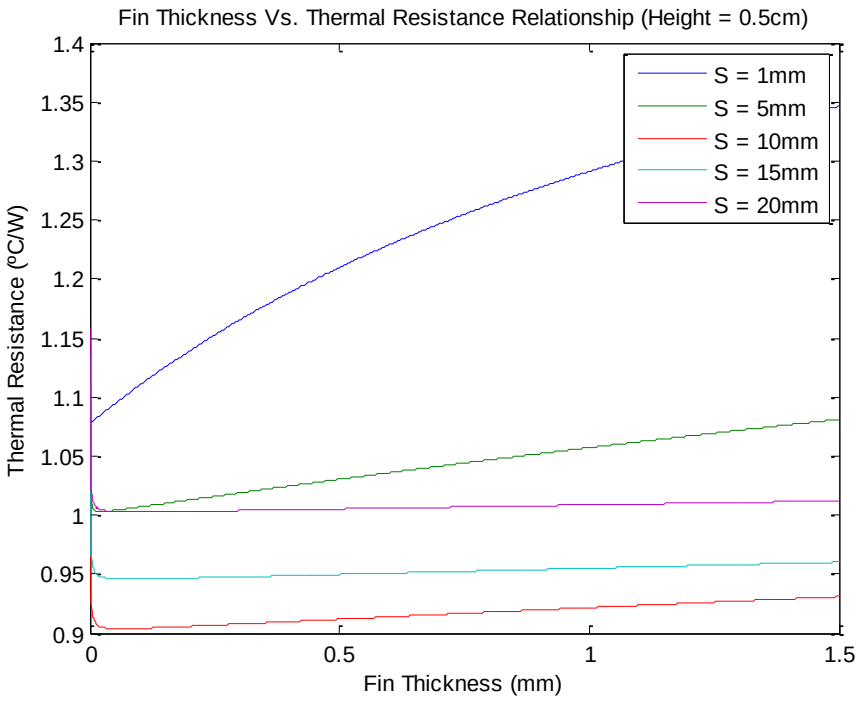

Fig. 7a. Plot of the relationship between fin thickness and thermal resistance for 0.5cm fin height.

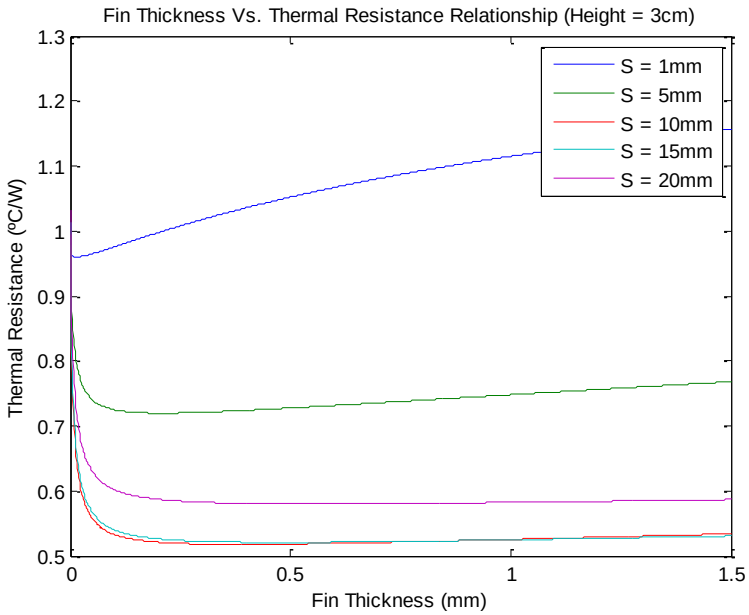

Fig. 7b. Plot of the relationship between fin thickness and thermal resistance for 3cm fin height.

The above stated, it is also known that, in natural convection, lumped capacitance plays a significant role in heat transfer. Due to relatively low heat transfer coefficients, the geometry of the fin range tested may not permit large temperature fluctuations to occur throughout the fins, as evidenced by the fin efficiency graph shown below in Figs. 7c and 7d for 0.5cm and 3cm fin heights respectively. The fin efficiency term is essentially a modified derivation of the Biot number, *Bi*. Lumped capacitance theory hold that for small *Bi* (and conversely a high η), temperature distribution across a solid should be nearly isothermal. While lumped capacitance will be discussed in greater detail in a later section, Figures 7c and 7d tend to support the notion that for the range of fin thicknesses tested, there may not exist a strong divergence from lumped capacitance, and thus the fins may, indeed, continue to perform isothermally for the small fin thickness range tested.

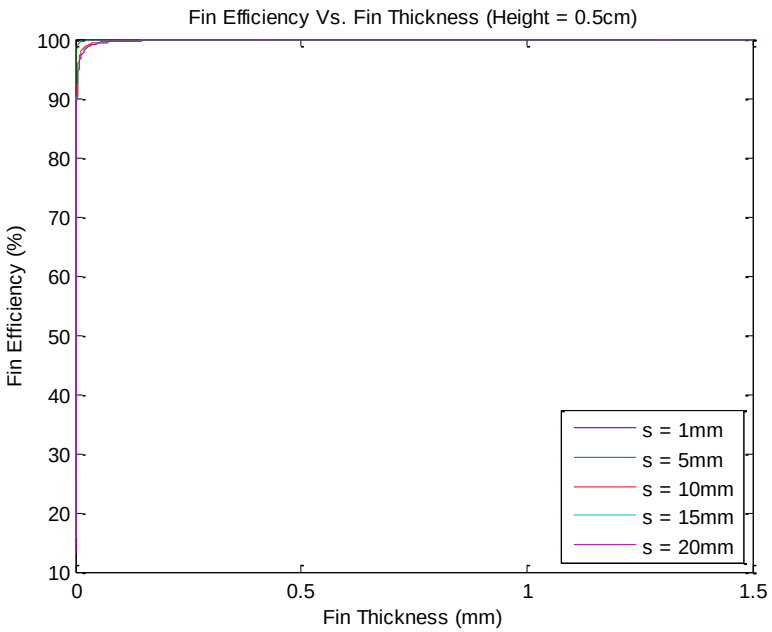

Fig. 7c. Plot of the relationship between fin thickness and fin efficiency for 3cm fin height.

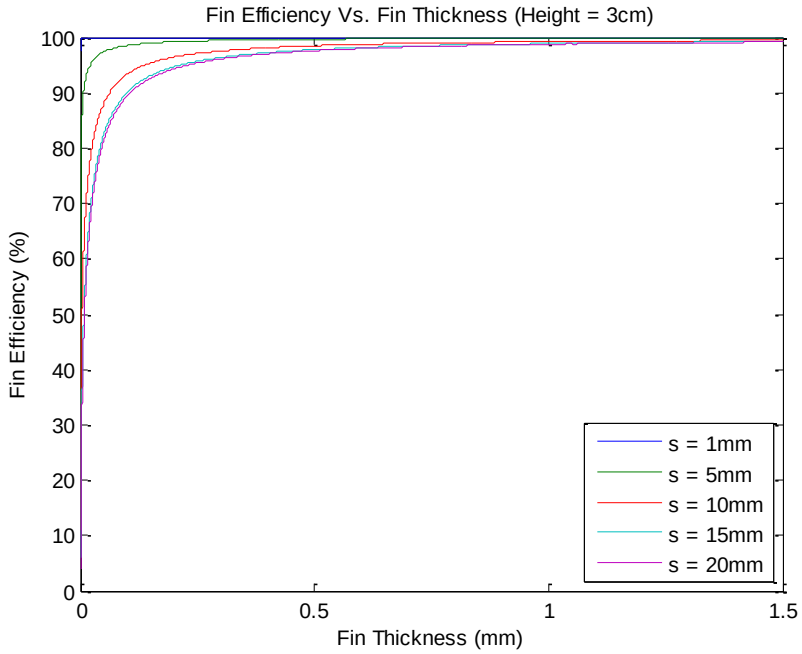

Fig. 7d. Plot of the relationship between fin thickness and fin efficiency for 3cm fin height.

The final trend examined individually was the relationship of fin spacing verses thermal resistance shown in Figs. 8a and 8b for 0.5mm and 2 mm fin thickness respectively.

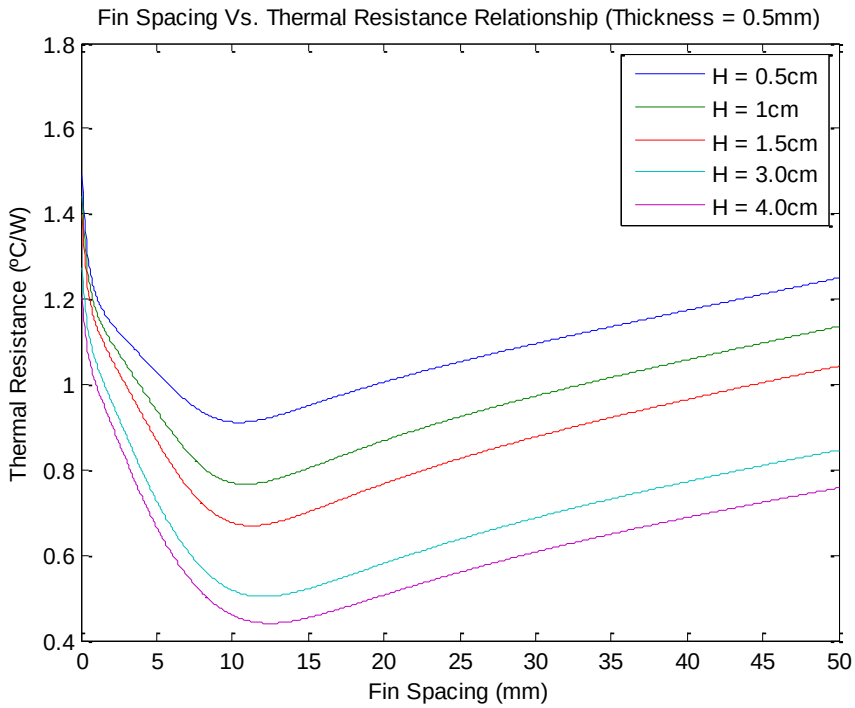

Fig. 8a. Plot of fin spacing verses thermal resistance for 0.5mm fin thickness.

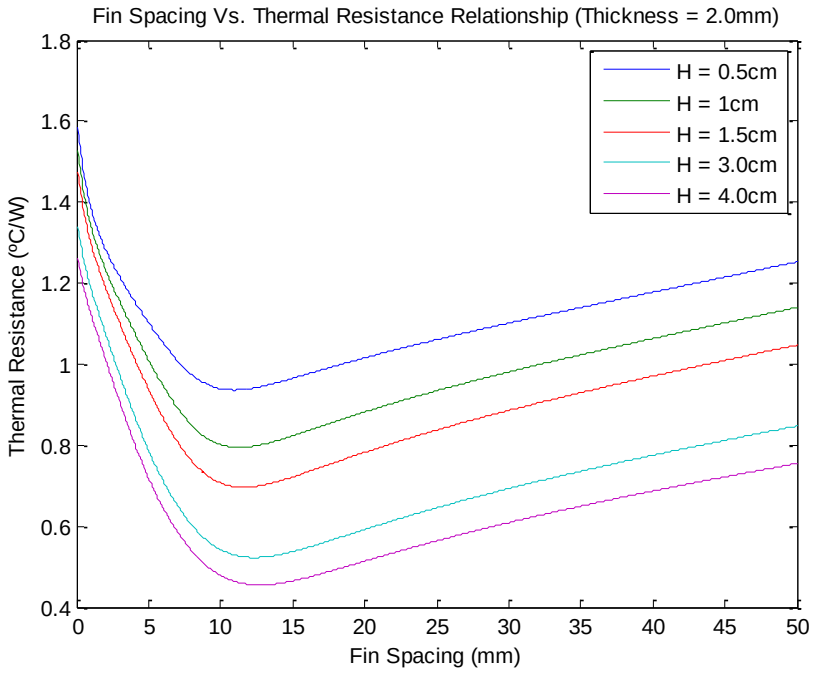

Fig. 8b. Plot of fin spacing verses thermal resistance for 2mm fin thickness.

The plots visual depiction of an alleged minimum is consistent with Bar-Cohen's representation of an optimum spacing. This is a consequence of the balance between the

heat transfer coefficient's direct dependence on flow impedance (i.e. channel spacing) and the reduction in the number of fins and thereby heat transfer area. From a fluid dynamic perspective, larger fin spacing provides less pressure loss for a given length of travel. Skin friction, viscous imbalances, and density gradients are all consequences of flow across a plate or fin and ultimately drive the existence of the boundary layer. Narrow fin spacing causes the boundary layers from both sides of a flow channel to intersect one another and present additional flow constriction along with a reduced local temperature gradient at the fin surface. Larger fin spacing is a means to prolong the entering distance before this boundary layer intersection takes place.

It also seems prudent to note here the means by which total fin number *N* was calculated shown below. The value of *N* was not rounded to prevent the existence of one fractioned fin. This yields obvious errors in exact fin count by +/- 1 fin but ultimately allowed for faster, higher resolution optimization trend illustration.

$$N = \frac{W}{(s+t)} \tag{8}$$

Examining the above plots allows for several conclusions to be made about the direction for optimization of the natural convection heat sink. The first conclusion is that increasing fin height will always return lower thermal resistances and thus higher performance at the cost of volume. A cost-benefit analysis must then be conducted to determine the ideal design point on the heat sink. The last conclusion is that, as proposed by Bar-Cohen and Elenbaas, there exist finite optimums for both fin spacing and fin thickness. Fig. 9 below shows a three-dimensional plot of the relationships for both fin spacing and thickness at a given fin height and its conclusions are, again, very consistent with the results presented by Bar-Cohen [1]. (Thermal Resistance in Fig. 9 has been

inverted for visualization of a minimum). The results are for the same 40cm X 20cm heat sink area that the other trends have been produced for. The benefit of a three dimensional trend analysis is that maximums and minimums from the combined fin spacing and thickness effects become apparent.

For the aforementioned heat sink area, fixed fin height of 4 cm, and a thermal load of 50 Watts, the empirically correlated optimum values are show below:

$$s_{opt} = 11.6347 \text{ mm}$$

$$t_{opt} = 0.4864 \text{ mm}$$

$$R_{min} = 0.3799 \text{ }^{o}\text{C/W}$$

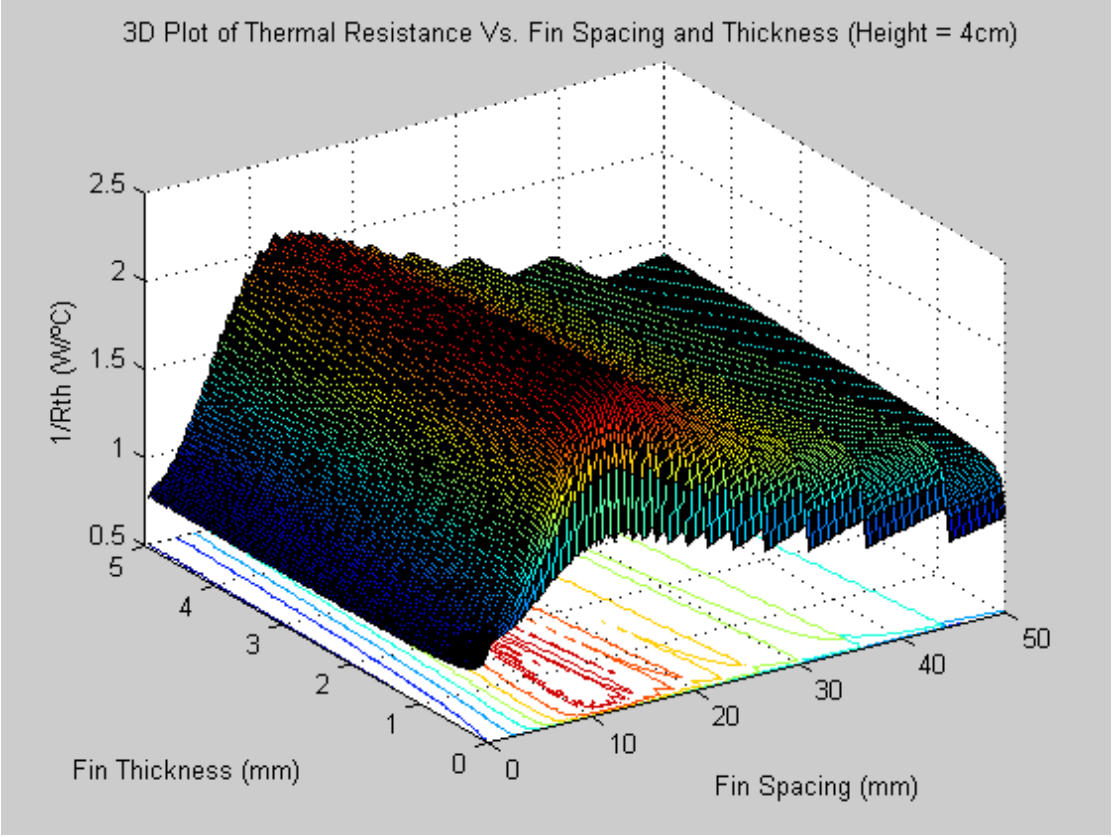

Fig. 9. Plot of fin thickness and fin spacing verses thermal resistance for a 4cm fin height.

- *Triangular Fin Array*

After rectangular fins were analyzed in the vertical orientation, triangular fins were investigated. For vertically oriented natural convection heat transfer, Bar-Cohen et al. showed the triangular fin array to be thermally superior to plate and pin fin arrays [6]. Nusselt correlations for triangular fin arrays were first published by Karagiozis et al. [7] based off of the early work of Elenbaas [1].

$$Nu_{fin} = \left[0.515\left(\eta_{fin} Ra_b\right)^{1/4}\right]\left[1+\left(\frac{3.26}{\left(\eta_{fin} Ra_b\right)^{0.21}}\right)^3\right]^{-1/3} \tag{9}$$

Ra_b is the modied Raleigh number based upon the mid-height fin spacing b shown below.

$$Ra_b = \frac{g\beta\Delta T\left(b^4/L\right)}{\nu\alpha} \tag{10}$$

η_{fin} is the triangular fin efficiency shown below where I_0 and I_1 are modified Bessel functions of the first and second kinds.

$$\eta_{fin} = \frac{1}{mL}\frac{I_1(2mL)}{I_0(2mL)} \tag{11}$$

As for rectangular fins, the first trend analyzed for triangular fins was the effect of fin height. Figures 10a and 10b show the effect of fin height upon thermal resistance for 0.5 mm and 2 mm fin thickness respectively. Not surprisingly, the trend, superficially, appears quite comparable to that of the rectangular fins. The key difference lies in the system response to varied fin spacing. For the same base dimensions, the triangular fin optimum spacing is approximately 1mm while the optimum spacing for rectangular was nearly 12 mm. This will be explored in greater detail in the next few pages.

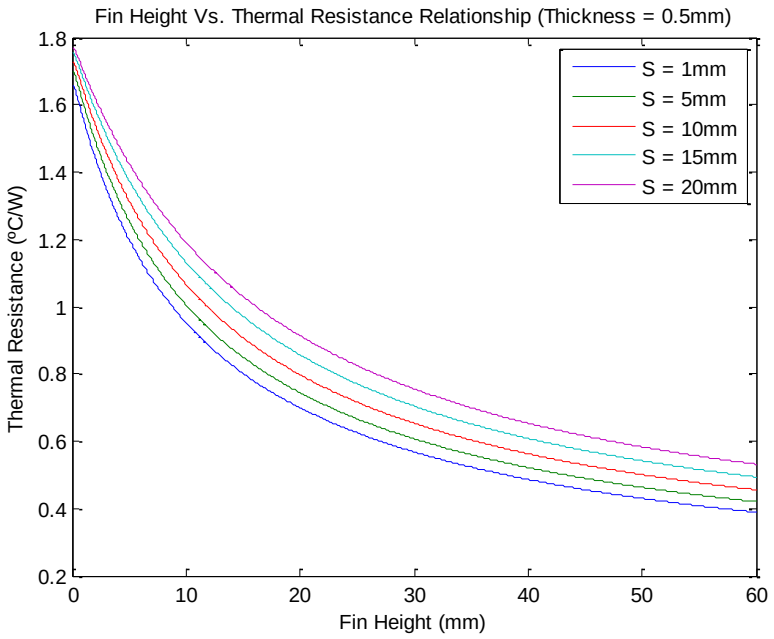

Fig. 10a. Plot of thermal resistance verses fin height for several fin spacings at 0.5mm thick fins.

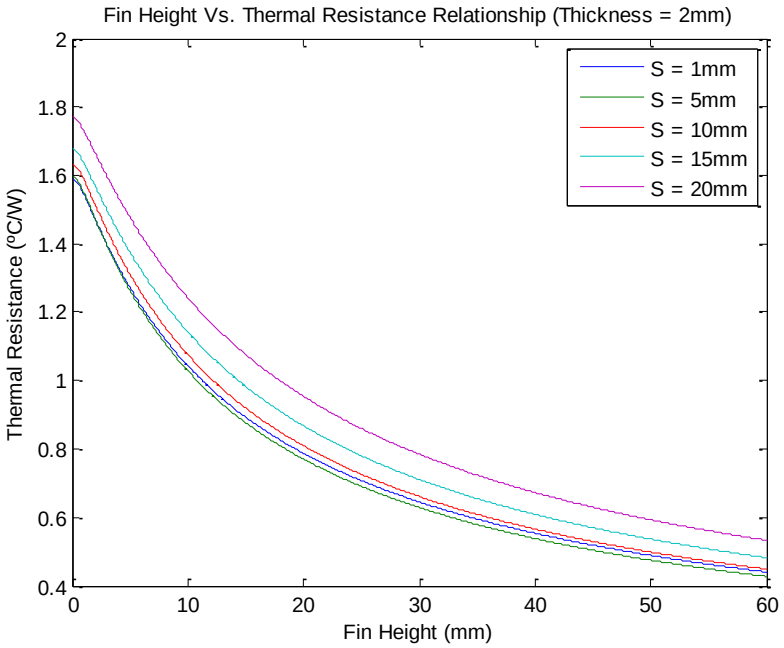

Fig. 10b. Plot of thermal resistance verses fin height for several fin spacings at 2 mm thick fins.

After fin height was explored, fin thickness was explored. Similarly to rectangular fins, performance appears to improve with small fin thicknesses allowing for a greater number of fins and convective surface area. Figures 11 and 12 show the trends for thermal

resistance and fin efficiency for varied fin thickness respectively. Again, fin efficiency is not hugely impacted over the range of fin thicknesses and heights due to the relatively low heat transfer coefficients.

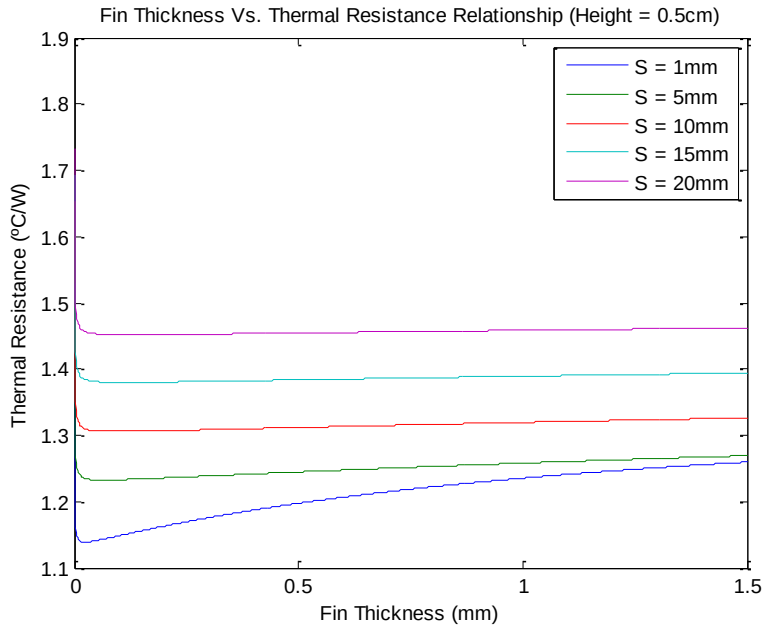

Fig. 11a. Plot of the relationship between fin thickness and thermal resistance for 0.5cm fin height.

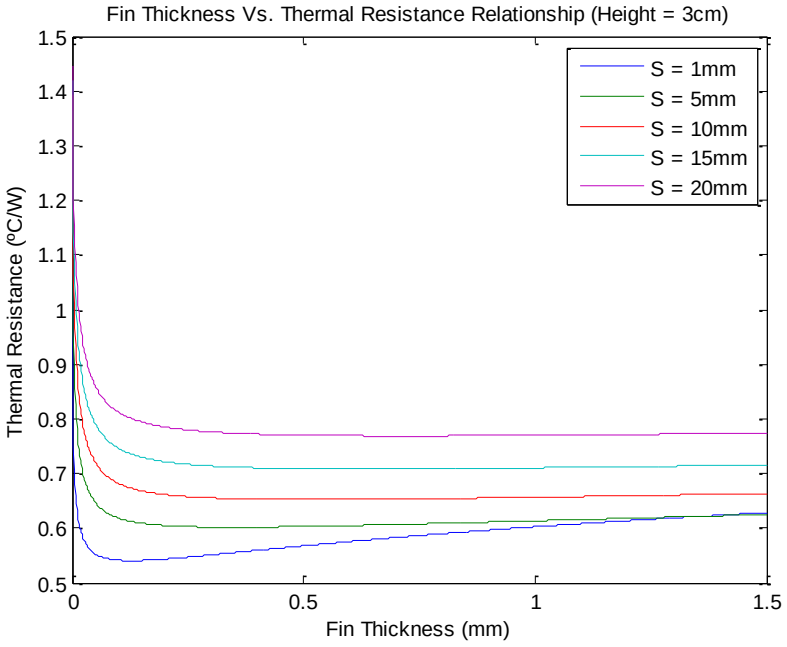

Fig. 11b. Plot of the relationship between fin thickness and thermal resistance for 3cm fin height.

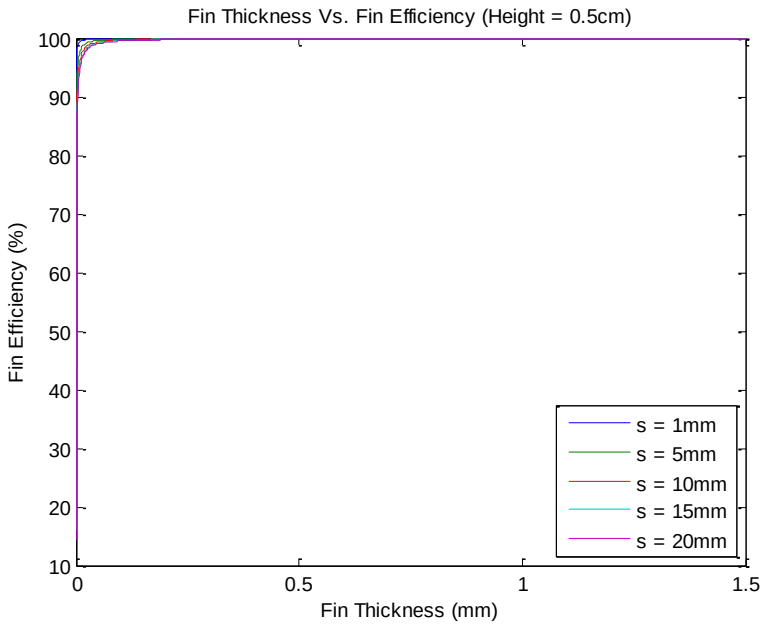

Fig. 12a. Plot of the relationship between fin thickness and fin efficiency for 0.5cm fin height.

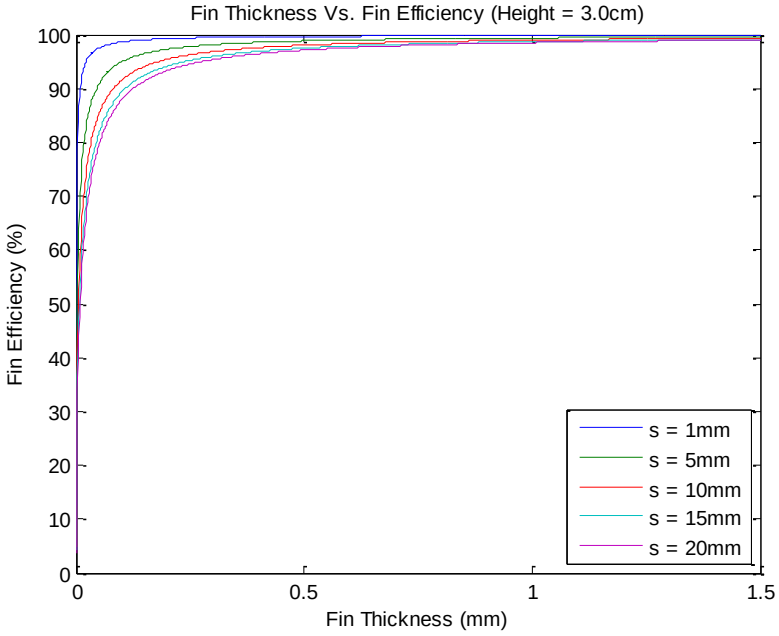

Fig. 12b. Plot of the relationship between fin thickness and fin efficiency for 3cm fin height.

For fin spacing, the trends, while similar to rectangular fins in the presence of a minimum, differ in the small amount of spacing required to achieve that minimum. Figs.

13a and 13b show the effect of fin spacing on thermal resistance for 0.5mm and 2mm thick fins respectively. To more fully understand the reasons why the thermal resistance behaves differently with respect to fin spacing between rectangular and triangular fin profiles, the thermal resistance and fin heat transfer coefficients for both profiles were plotted next to one another in Figs 14a and 14b shown below

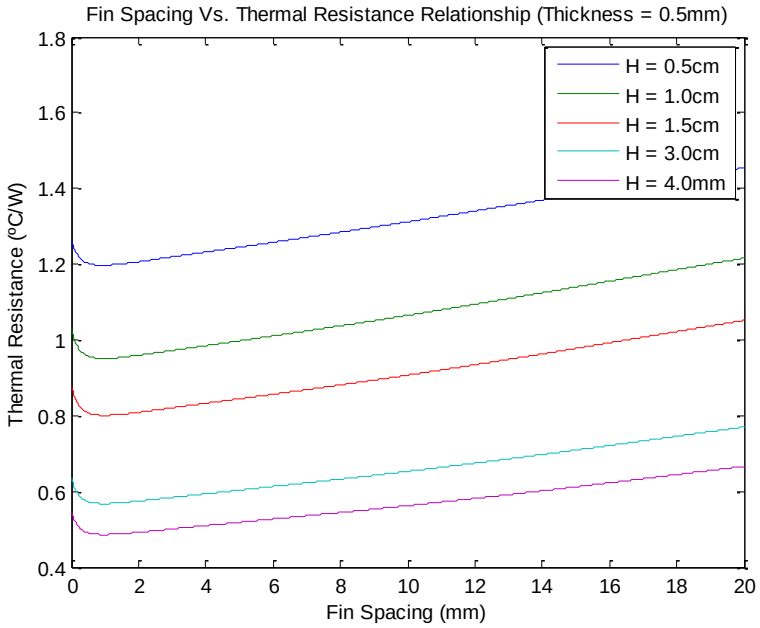

Fig. 13a. Plot of fin spacing verses thermal resistance for 0.5mm fin thickness.

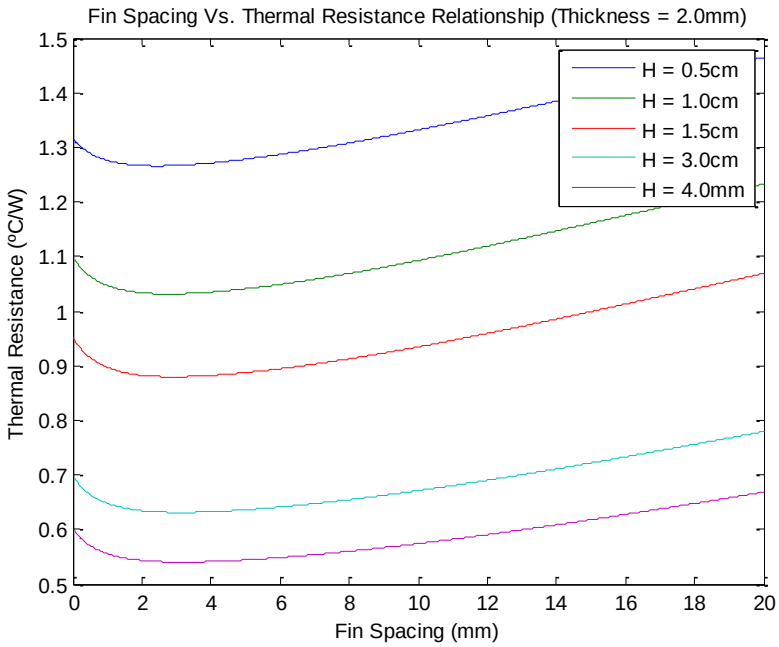

Fig. 13b. Plot of fin spacing verses thermal resistance for 2mm fin thickness.

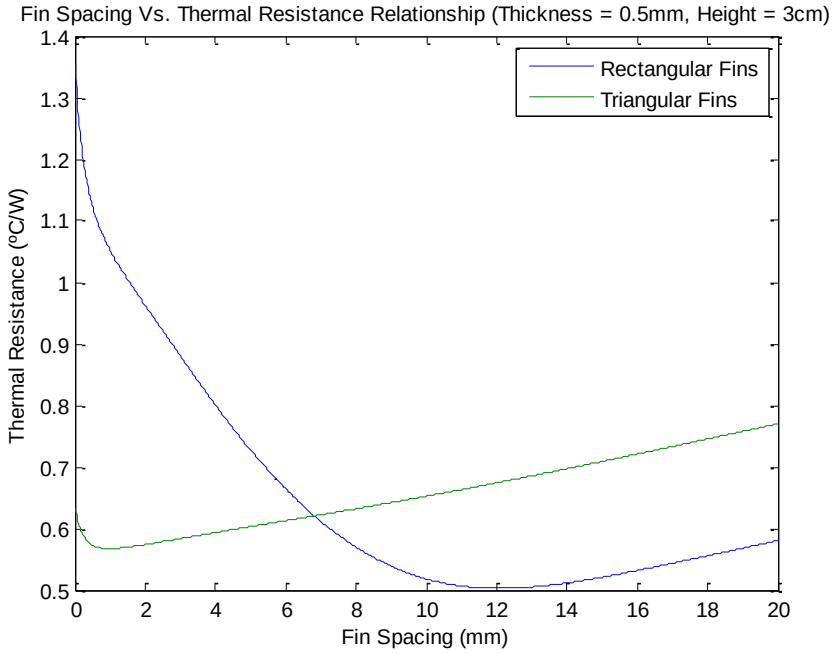

Fig. 14a. Plot of fin spacing verses thermal resistance for both rectangular and triangular fins.

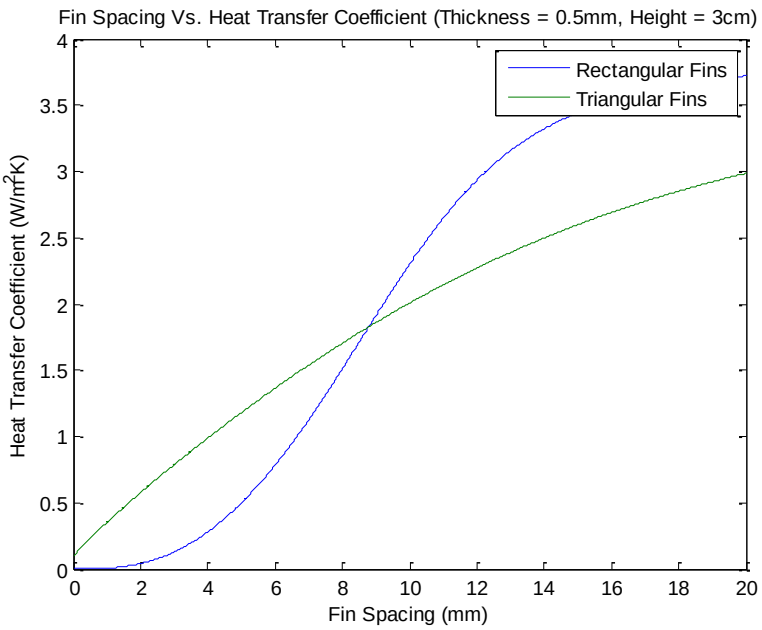

Fig. 14b. Plot of fin spacing verses fin heat transfer coefficient for both rectangular and triangular fins.

Evidenced by Fig. 14b, rectangular and triangular fin profiles have very unique trends for fin spacing's impact on heat transfer coefficient. Perhaps unsurprisingly, at smaller fin spacing, the heat transfer coefficient for the triangular fin array is considerably larger than that of the rectangular fin array. While the discussion on flow impedence for natural convection currents in the rectangular fin array portion of this study still applies, it is obvious that the non-constant wall spacing promoted by the sloped profile of the triangular fins promotes less boundary layer intersection than that of rectangular fins. This means, as shown in Fig. 14b, that until some limit is reached (possibly the flat plate limitation) triangular fin arrays will always have a superior heat transfer coefficient. However, this gain in heat transfer coefficient is offset by a reduced surface area per fin relative to rectangular fin arrays. Simple geometry attests to the fact that for a given fin thickness and height, a rectangular fin will have greater surface area and thus superior heat transfer contact surface than a triangular fin.

To make one last direct comparison between rectangular and triangular fin arrays in the vertical orientation, Fig. 15 shows fin efficiency verses fin height for the two profiles.

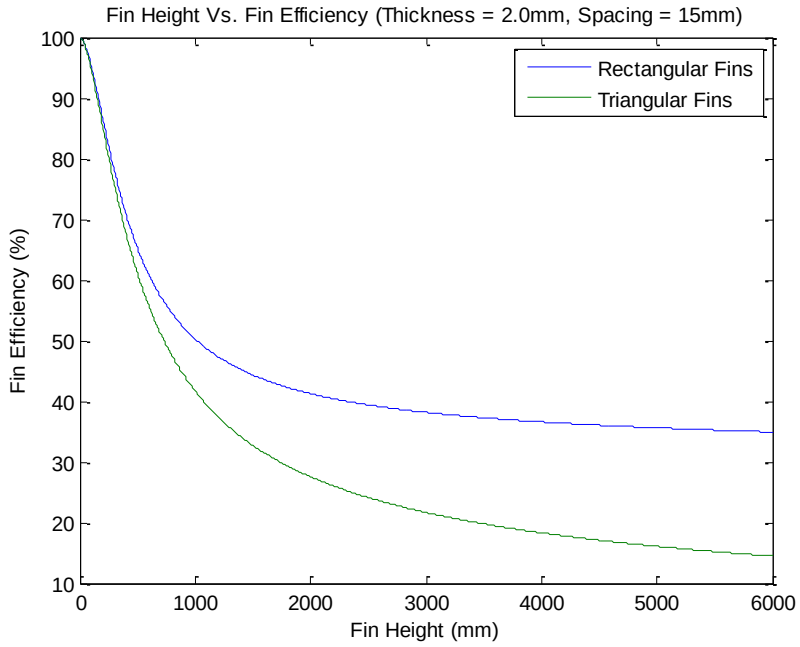

Fig 15. Plot showing the effect of fin height upon fin efficiency for both fin types

As expected, a great fin heights, the triangular fin efficiency decays faster than that of the rectangular fin array by virtue of a decreasing cross-sectional heat transfer area in the triangular fins. What is interesting in reference to previous trends shown in this section, however, is that it appears to require some very large fin heights before fin efficiency will decrease appreciably.

The final investigation on vertically oriented triangular fin heat sinks was the combined effects of fin thickness and fin spacing shown in Fig. 16 below. This was, again, done for base area of 40cm X 20cm, thermal load of 50 Watts, and a fixed fin height of 4cm. The combination resulting in the smallest thermal resistance was

$$s_{opt} = 0.1015 \text{ mm}$$

$$t_{opt} = 0.0462 \text{ mm}$$

$$R_{min} = 0.388 \text{ ºC/W}$$

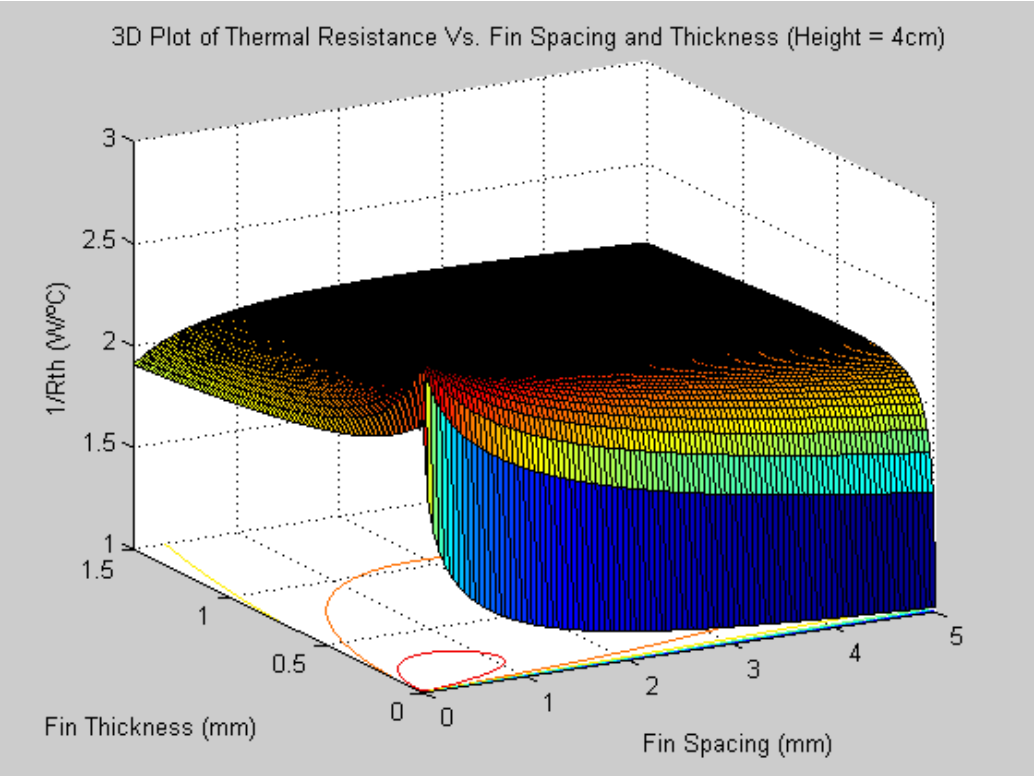

Fig. 16. Plot of fin thickness and fin spacing verses thermal resistance for a 4cm fin height.

Horizontally Oriented Heat Sink

- *Rectangular Fin Arrays*

While horizontal convection is typically inferior to vertical, there exists value in understanding how much the performance changes from one orientation to another. This is particularly useful in the design of Fanless PCs when one considers the potential for end-user implementation of a system. While a designer may specify a required system orientation, a heat sink that cannot operate in orientation independence may become a failure liability.

The first correlations for quantifying the performance of horizontal rectangular fin arrays was published by Harahap and McManus et al. shown below

$$Nu_L = a\left[Ra_L \frac{s}{H}\right]^d \left(\frac{s}{L}\right)^{0.656} \left(\frac{H}{L}\right)^{0.412} \tag{12}$$

where *a* and *d* are empirically determined correlation constants [8]. Using equation (12) with values of *a* and *d* set to 0.00071561 and 0.6576 respectively [2], a similar trend analysis was conducted for horizontally oriented heat sinks. Fig. 17 below shows that the trend for thermal resistance as a function of fin height is very similar to that displayed by vertically oriented heat sinks. There again appears to be some 'optimal' value associate with the fin spacing. Fig. 18 shows the effect of fin height and spacing upon heat transfer coefficient. As expected, the *h*, value decays with both height and spacing. This is indicative that for, some regions, increases in fin area (i.e. number of fins) are more valuable in terms of thermal transport than increases in heat transfer coefficient for the prescribed heat sink. This is not, however, without caveat. Baskaya et al. determined a significant impact of heat sink length, *L*, on heat transfer coefficient. While not presented here, values for heat sink length outside of those tested would be expected to show up as

an affected heat transfer coefficient. Figs. 19 through 22 show the remainder of the heat sink trends analyzed in this study including effects of changing fin thickness and fin spacing on thermal resistance, fin efficiency, and heat transfer coefficient. The trends did not spark any noteworthy discussion but do help idealize how the horizontal rectangular fin array might be optimized in design. A more detailed discussion of these findings is presented at the end of this section.

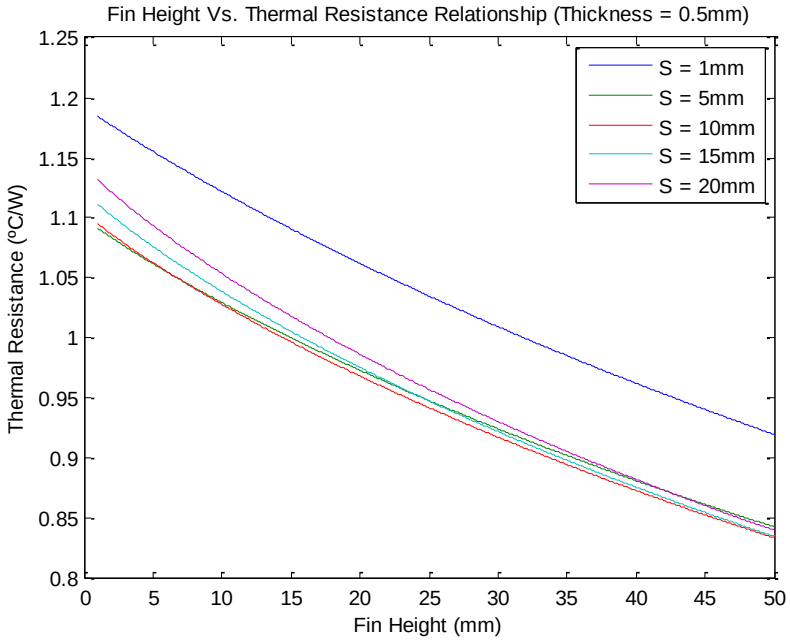

Fig. 17a. Plot of fin height verses thermal resistance for fin thickness of 0.5mm.

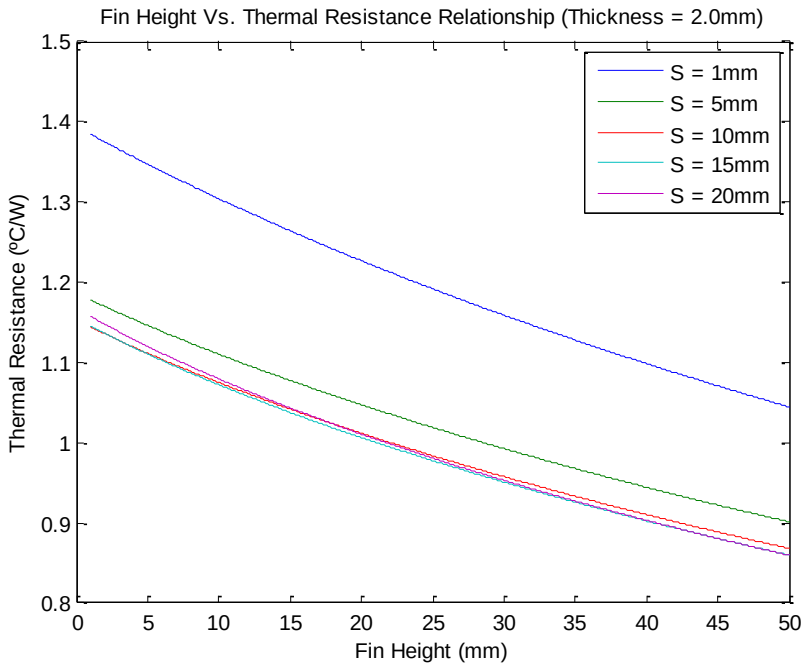

Fig. 17b. Plot of fin height verses thermal resistance for fin thickness of 2.0mm.

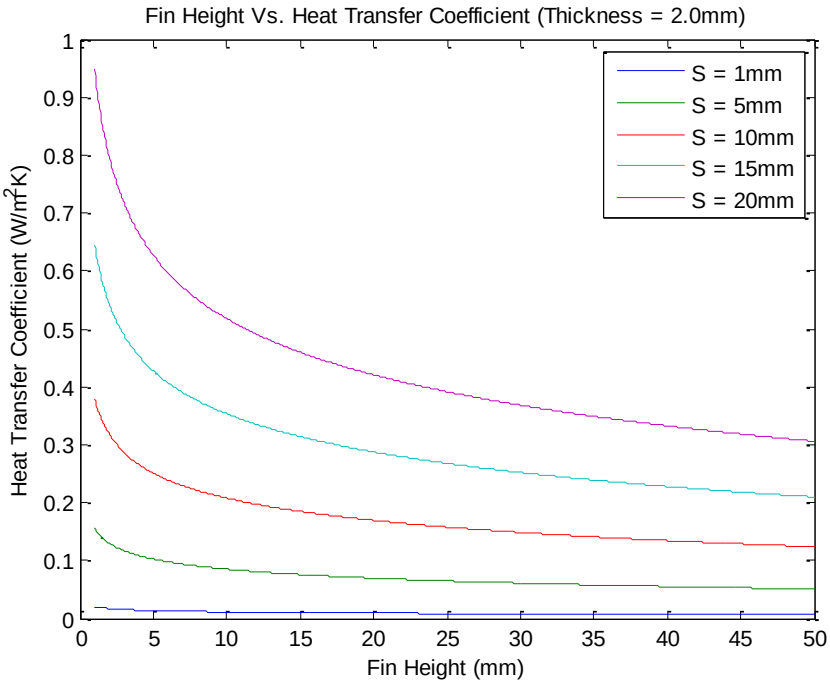

Fig. 18. Plot of fin height verses heat transfer coefficient for fin thickness of 2mm.

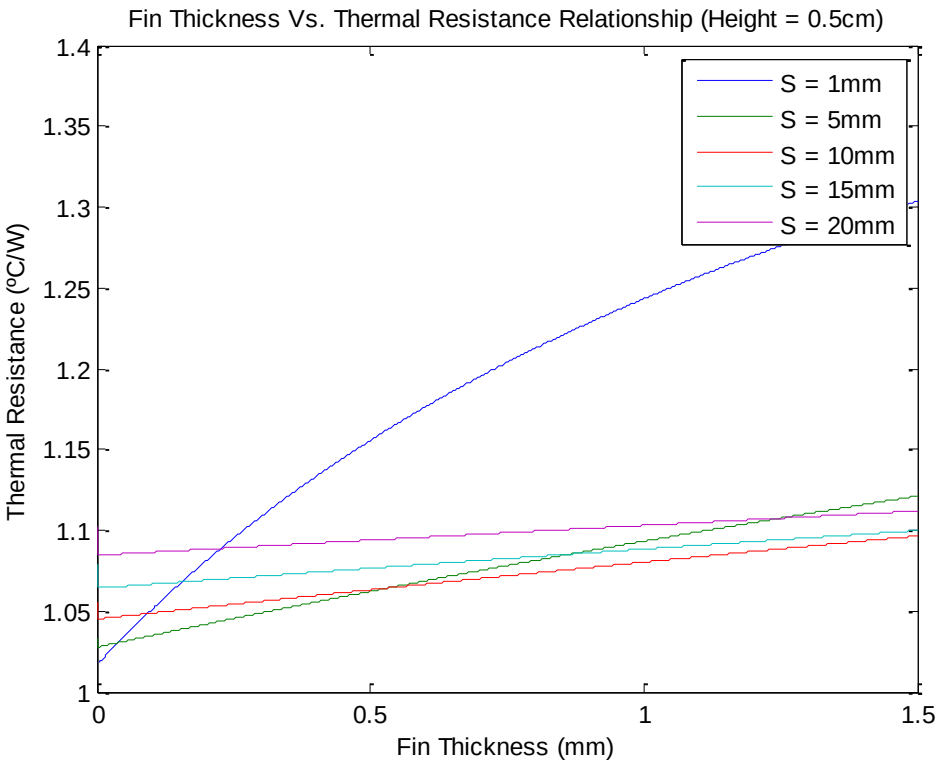

Fig. 19a. Plot of the relationship between fin thickness and thermal resistance for 0.5cm fin height.

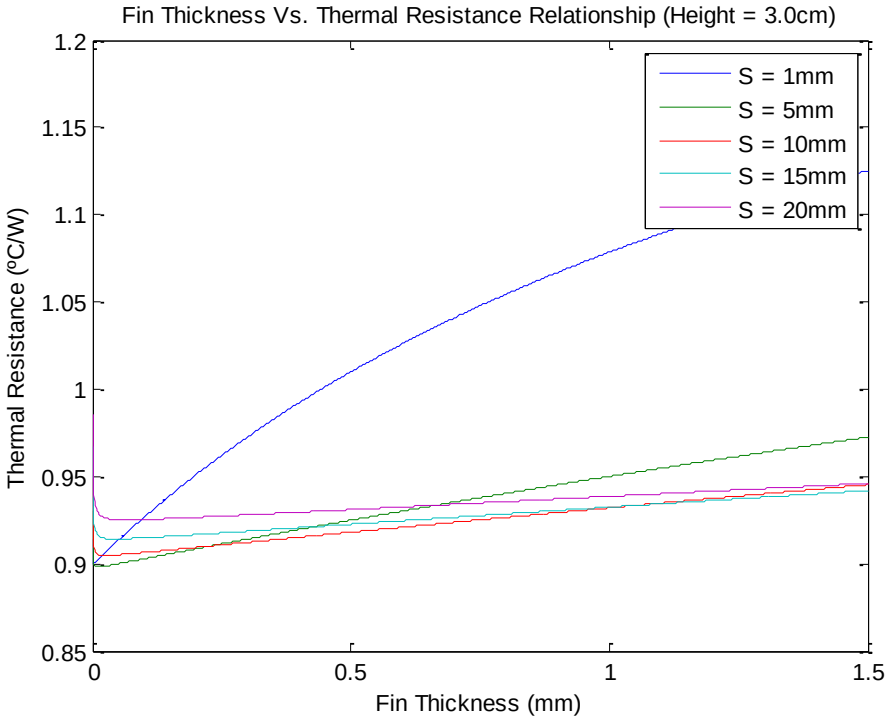

Fig. 19b. Plot of the relationship between fin thickness and thermal resistance for 3.0cm fin height

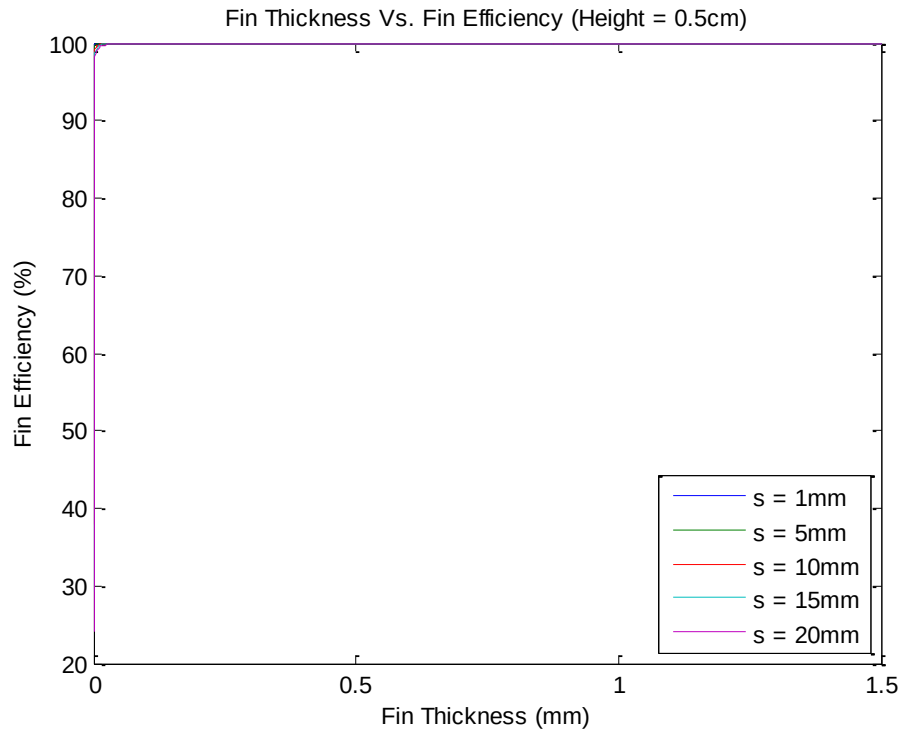

Fig. 20a. Plot of the relationship between fin thickness and fin efficiency for 0.5cm fin height.

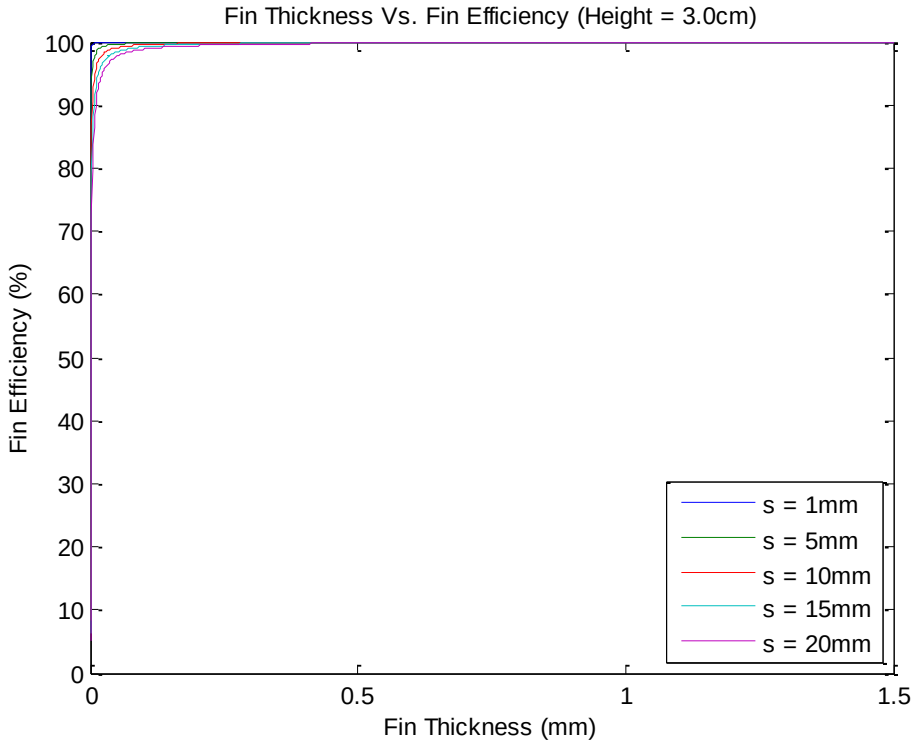

Fig. 20b. Plot of the relationship between fin thickness and fin efficiency for 3cm fin height.

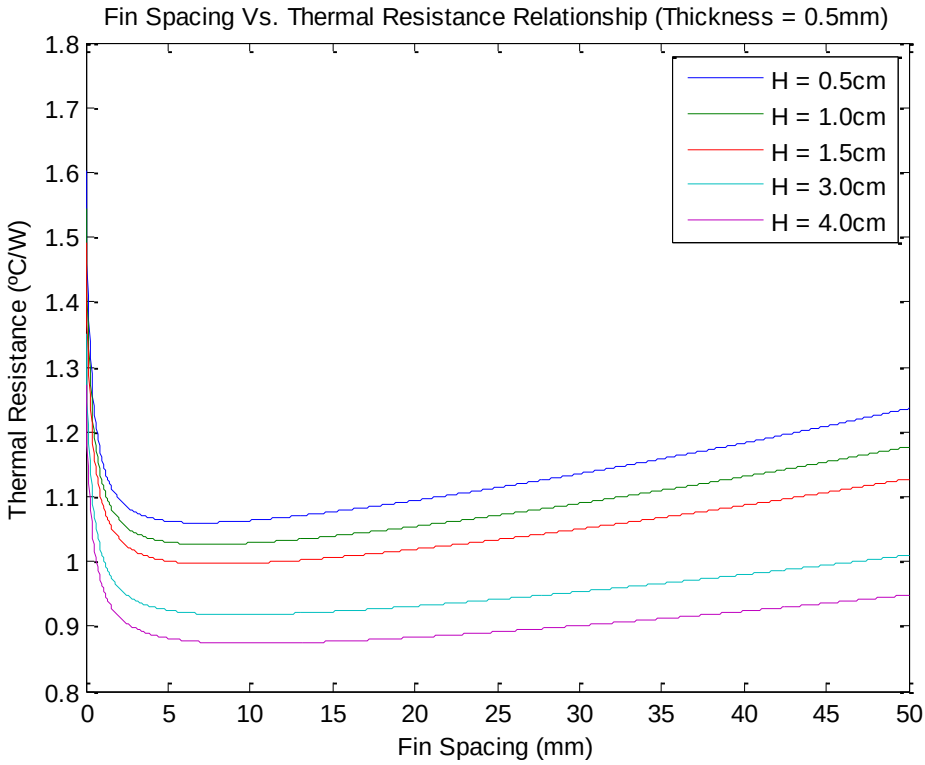

Fig. 21a. Plot of fin spacing effect upon thermal resistance for 0.5mm fin thickness.

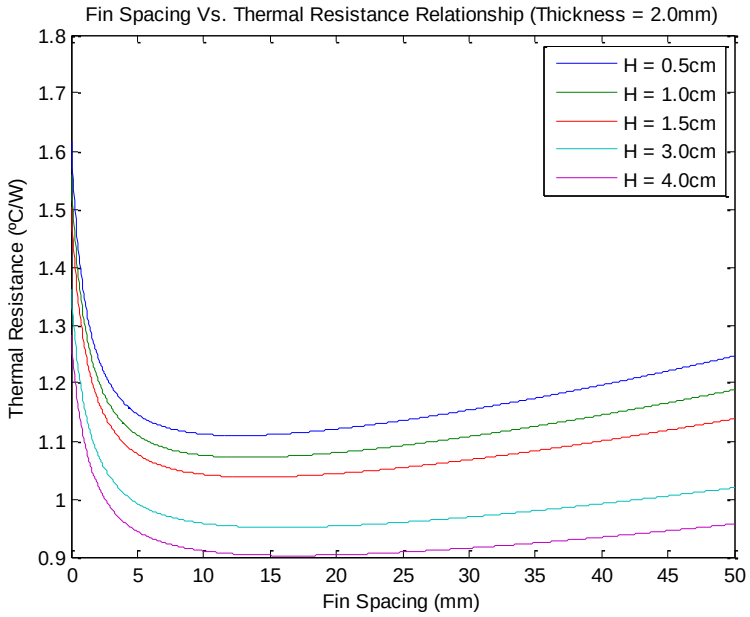

Fig. 21a. Plot of fin spacing effect upon thermal resistance for 2.0mm fin thickness.

Fig. 22 below shows the combined effects of fin thickness and fin spacing for the horizontally oriented rectangular fin array.

$$s_{opt} = 5.026 \text{ mm}$$

$$t_{opt} = 0.0161 \text{ mm}$$

$$R_{min} = 0.7792 \text{ ºC/W}$$

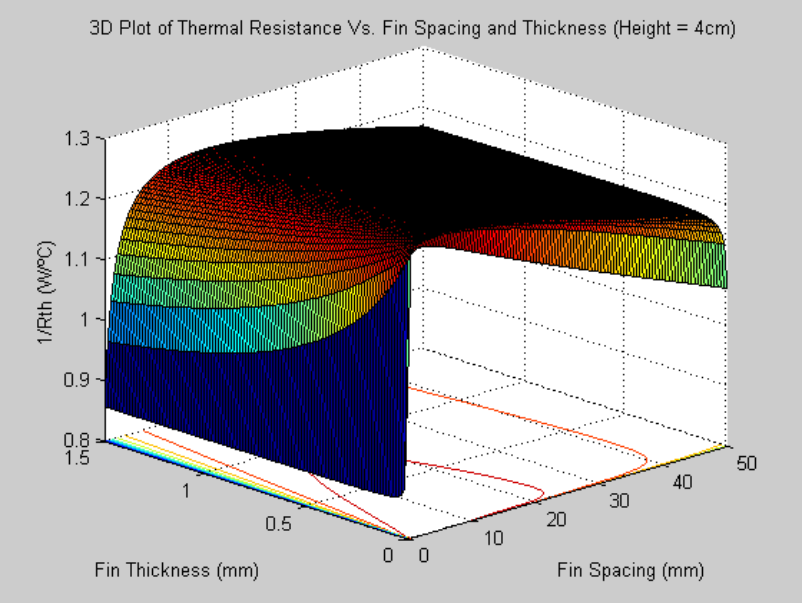

Fig. 22. Plot of the combined relationship of fin spacing and thickness verses inverted thermal resistance.

Compiled Results

A final look was given to the difference in how fin spacing impacts the performance of the natural convection heat sink in terms of thermal resistance and heat transfer coefficient for all three configurations shown in Figures 23 and 24 respectively.

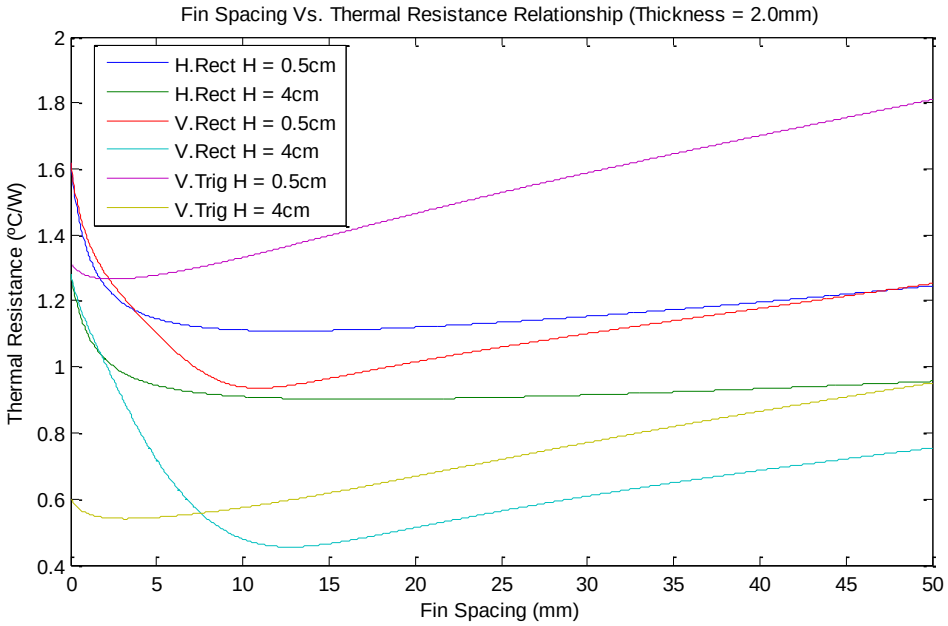

Fig. 23. Plot of thermal resistance as a function of fin spacing for all three configurations at 0.5cm and 4cm fin heights.

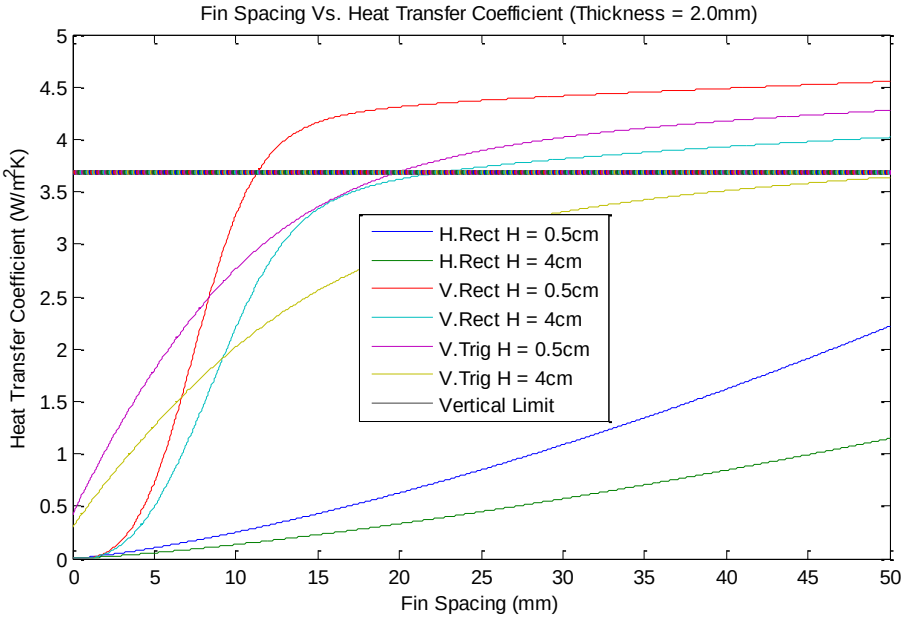

Fig. 24. Plot of heat transfer coefficient as a function of fin spacing for all three configurations at 0.5cm and 4cm fin heights.

Examining the trends shown in the above plots brings to light the importance of fin spacing in free convection heat sink design. The horizontal line shown in Fig. 24 marks the vertical flat-plate limit for heat transfer coefficient. There are a couple of interesting remarks concerning this limitation. First both the vertical rectangular and vertical triangular correlations used, while they do show some convergence near the line, this limitation is exceeded by the predicted heat transfer coefficient value as spacing increases suggesting some corollary error. Next, the optimum fin spacing for the vertical rectangular heat sink analyzed in this study was nearly 12 mm; not surprisingly this is almost the exact point where fin array heat transfer coefficient intersects the flat-plate limitation. Conversely, the maximum spacing for the vertical triangular heat sink was just over 0.1mm. This is indicative of the relatively high importance of heat transfer coefficient for rectangular fin arrays whereas the triangular fin array correlations are more dependent upon surface area via high fin count. Also, as mentioned in the triangular discussion, heat transfer coefficient for triangular fins is much higher than the rectangular counterpart at small fin spacing. The point at which the heat transfer coefficients for the two vertical profiles intersect is quite near the vertical flat plate limit, which is somewhat expected by virtue of boundary layer interaction. This is a clear indication of the advantages triangular fin arrays have over rectangular fin arrays in promoting less boundary layer interaction at small plate spacing giving them superior heat transfer coefficients. This is, however, again, offset by a reduced surface area experienced by triangular fins relative to rectangular arrays.

Optimization schemes were executed for all three fin array configurations and are shown below in Table 2. Analyzing the table allows for comparison of the independent

variables associated with heat sink design. As noted for the final graphs of each of the three preceding sections, a program was written based upon the aforementioned empirical correlations to characterize the performance of natural convection heat sinks. The beauty of the program is that it allows for a user to choose an orientation and/or fin profile and, in turn, receive the optimum heat sink values for fin thickness, spacing, and height tailored to unique physical constraints. (See the Appendix for a detailed examination of the code used for this study – *HSAnalysis.m, Trendscript.m, OptScript.m,* and which correlations were used in *Table of Applied Correlations and Limitations*)

Table 2. Parametric analysis of all three heat sink configurations investigated.

Q (Watts)	*L* (cm)	W (cm)	H (cm)	Horizontal Rectangular			Vertical Rectangular			Vertical Triangular		
				s_{opt} (mm)	t_{opt} (mm)	R_{min} (ºC/W)	s_{opt} (mm)	t_{opt} (mm)	R_{min} (ºC/W)	s_{opt} (mm)	t_{opt} (mm)	R_{min} (ºC/W)
15	40	20	0.5	3.228	0.100	1.160	11.410	0.100	1.035	0.233	0.100	1.269
15	40	20	4.0	5.291	0.100	0.963	14.077	0.570	0.520	0.233	0.100	0.521
30	40	20	0.5	3.400	0.100	1.033	10.200	0.100	0.904	0.200	0.100	1.116
30	40	20	4.0	6.400	0.100	0.861	12.500	0.568	0.440	0.200	0.100	0.445
50	40	20	0.5	3.500	0.100	0.936	9.500	0.100	0.811	0.200	0.100	1.001
50	40	20	4.0	7.200	0.100	0.782	11.500	0.577	0.388	0.200	0.100	0.394
75	40	20	0.5	3.600	0.100	0.856	9.000	0.100	0.739	0.200	0.100	0.907
75	40	20	4.0	7.700	0.100	0.717	10.800	0.577	0.350	0.200	0.100	0.358
15	20	40	0.5	5.237	0.152	1.188	10.200	0.100	0.943	0.200	0.100	1.173
15	20	40	4.0	11.862	0.100	1.047	12.362	0.568	0.455	0.225	0.100	0.459
30	20	40	0.5	5.480	0.100	1.040	8.984	0.100	0.821	0.225	0.100	1.024
30	20	40	4.0	14.489	0.100	0.913	10.986	0.568	0.381	0.225	0.100	0.387
50	20	40	0.5	5.731	0.100	0.941	8.358	0.100	0.736	0.225	0.100	0.915
50	20	40	4.0	16.366	0.100	0.823	10.110	0.577	0.334	0.225	0.100	0.340
75	20	40	0.5	5.981	0.100	0.860	7.858	0.100	0.671	0.225	0.100	0.831
75	20	40	4.0	17.868	0.110	0.752	9.484	0.577	0.300	0.225	0.100	0.307

* Minimum values for fin thickness and spacing constrained to 0.1mm

Discussion

Several key conclusions can be drawn from the heat sink investigation. Despite the remarks of Bar-Cohen [6], rectangular fins out performed triangular fins in every configuration investigated. Vertically oriented heat sinks have lower thermal resistances than their horizontal counterparts. A program was written in MATLAB based off of the analytical correlations mentioned in the preceding investigation. Using physical constraints of length, width, height, and power load as input, an iterative minimization scheme is executed to find the combination of fin spacing and thickness that yields the 'best', or lowest thermal resistance, natural convection heat sink design. The constraint of heat sink width in the code input allows for fin number to be implicitly calculated based upon the summed values of fin spacing and fin thickness. For all fin array profiles and orientations, the heat transfer coefficient is highly dependent upon the spacing between individual fins and less so on the thickness of each fin. Reasons for the later include a potentially underrepresented fin efficiency term and the overall presence of lumped capacitance and isothermal fin conditions. Triangular fins benefit from a sloped profile that enables them to experience less boundary layer intersection between fins at small spacing giving them an advantage in heat transfer coefficient over rectangular counter parts, but suffer from reduced heat transfer surface area. Furthermore, the horizontal orientation produced, across the board, lower heat transfer coefficients than the vertically oriented arrays. This is not to say that vertical orientation is always superior (in fact, for many cases heat transfer coefficients are superior in horizontal orientation than vertical for flat plates) for heat transfer, but as mentioned by Baskaya, et al. [1], the effects of fin height and entrance length impede natural convection flow to a far greater extend in the

horizontal orientation and cause disruptions to the plume type flow described in a previous section. Because of the relatively small heat transfer coefficients seen in the horizontal orientation, the fin efficiency term doesn't deviate from unity any significant amount leading to very small fin thicknesses being the optimal value. To this point, the optimization trends displayed for the differing profiles and orientations are logically dissimilar. It is thus the fine tuning between heat transfer coefficient and surface area that produces the optimum values for fin spacing and thickness shown in the above table.

Free Convection Enhancement

Beyond fin geometry optimization, there are several other methods for enhancing free convection heat transfer on a heat sink. Two such methods being considered are chimney effect enhancement, and fin inclination. The latter only pertaining to vertically oriented heat sinks.

Chimney Effect Enhancement

Chimneys, in natural convection, are physical ducts that surround the fins or surface of a heat sink. By increasing the average density differential of the free stream fluid, chimneys actually increase the bulk fluid motion, driving larger velocities. These higher velocities ultimately yield increased heat transfer coefficients. One particular study on this effect yielded correlations that propose up to a 200% increase in the average heat transfer coefficient using chimneys in natural convection [9]. This study was conducted on an isothermally heated flat plate and lacks significant theory development publication. Another study by Fisher et al. proposed several dimensionless equations for characterizing the fluidic motion within chimneys for both pin and rectangular fin arrangements [7]. They later conducted a series of experiments that validated their previous theoretical work with typical deviations less than 5% [8]. In this work, it was concluded that chimneys can reduce the surface temperature of the heat sink by as much as 30% and that it is also possible to use a heat sink-chimney combination with equal performance and smaller height than heat sinks alone. There still exists a great need to understand chimneys and develop more accurate and usable empirical correlations to describe their performance. One of the largest obstacles in the study of chimneys is the presence of a cold inflow at the chimney exit. This flow is extremely difficult to

characterize and is the most significant contributor to the divergence of theoretical predictions and experimentally obtained data.

Fin Inclination

Perhaps the most difficult to model, are inclined fins. As shown in Fig. 4, for vertically oriented heat sinks, fin inclination can result in improved convection heat transfer via boundary layer disruption on the upper surface of the fin (with respect to gravity). However, this comes with a hit to heat transfer on the lower surface of the fin, as bulk fluid motion along the fin is now being slowed. As aforementioned, flow fields of this type are quite difficult to characterize [4]. However, a series of empirical experiments were conducted to show that a net improvement to overall heat transfer can be obtained using fin inclination when the heat sink length to width ratio is greater than 2 (Fig. 2) [8]. This again, requires further empirical investigation to be analyzed properly.

Heat Diffusion within the Heat Sink

As noted in preceding sections, the amount of energy that can be removed via convection is ultimately dependent on the surface temperature gradient. To be more accurate, however, the total energy that can be dissipated via free convection is actually equal to the summation of local heat transfer coefficients multiplied by the local temperature gradients. Until now, this was considered trivial by use of an isothermal surface condition assumption. Yet, to refine the approach by which the heat sink is truly optimized, it is necessary to now consider the distribution of temperature across the heat sink surface.

Determining the temperature distribution across a heat sink is beneficial in several ways. First, as mentioned above, it allows for a more accurate analysis of the heat transfer coefficient. In addition to this, it also allows for the characterization of the Heat Sink Effective Area (which will be referred to henceforth as HSEA). The HSEA is a parameter that seeks to define the extremities of heat diffusion within a heat sink, or in other words, the distances from a heating source at which the temperature gradient between the heat sink surface and ambient air is insufficient to drive significant heat transfer. The latter part of this definition is an excellent point of optimization. Another significant issue with the HSEA is that it is a parameter in literature that has not been greatly addressed. The third and final benefit to determining the temperature distribution within the heat sink is that it allows for the depiction of the heat sink spreading resistance, which is assumed negligible in one-dimensional analytical correlations. Thermal spreading resistance becomes critically important to quantify as the ratio of surface area of heat sink to heat source increases.

Many previous studies have been conducted on heated solids in convective environments in regards to their temperature distribution. The most popular technique for determining how large the temperature gradient will be within a solid is the Lumped Capacitance Method, or Biot Method. The Biot Number (Bi) represents the ratio of conductive to convective resistance for a solid undergoing convective heat transfer.

$$Bi = \frac{R_{conduction}}{R_{convection}} = \frac{hL_c}{k} \tag{13}$$

where L_c is the characteristic length and is defined as

$$L_c = \frac{V}{A_s} \tag{14}$$

Theory holds that when *Bi* is significantly less than 0.1, assuming an isothermal temperature distribution across a solid is valid and thus the error in Lumped Capacitance is small [3]. Thus in optimizing the heat sink, for situations in which *Bi* is quite small, the temperature distribution throughout the heat sink can be considered uniform from a design perspective. However, this does not necessarily negate the presence of a spreading resistance.

Methods for solving Heat Diffusion

Determining the temperature distribution throughout a three-dimensional body, such as the heat sink in question is not an uncomplicated matter. There are two fundamental techniques for solving three-dimensional heat diffusion: analytical and numerical. The analytical solution for this problem in three dimensions requires the simultaneous solving of a coupled second-order partial differential equation which can, with great effort, be completed using a variety of Fourier Transforms.

$$\frac{\partial^2 T}{\partial x^2} + \frac{\partial^2 T}{\partial y^2} + \frac{\partial^2 T}{\partial z^2} = S \tag{15}$$

This has been done by Song et al. through the approximation of a square on square substrate as a circle on circle substrate and a cylindrical coordinate transformation [10].

$$R_s = \frac{\sqrt{A_p} - \sqrt{A_s}}{k\sqrt{\pi A_p A_p}} \times \frac{\lambda k A_p R_o + \tanh(\lambda t)}{1 + \lambda k A_p R_o \tanh(\lambda t)} \tag{16}$$

$$\lambda = \frac{\pi^{3/2}}{\sqrt{A_p}} + \frac{1}{\sqrt{As}} \tag{17}$$

Fig. 25 shows an illustration of this approximation. As can be quickly inferred, this approximation becomes less accurate the more the geometry of the source on substrate diverges from the profile of a circle; i.e. for rectangular or elliptic contact surfaces the error for this approximation should be quite high – as in the case of heat pipe embedded in a heat sink shown in Fig. 26.

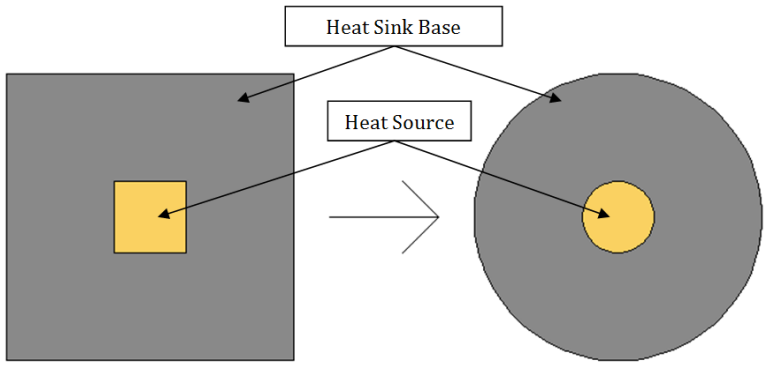

Fig. 25. Illustration of spreading resistance approximation conducted by Lee and Song et al.

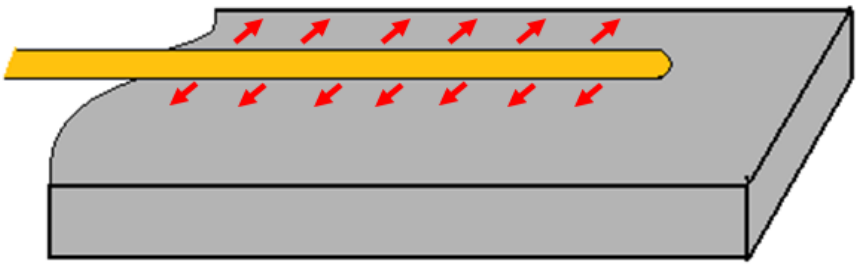

Fig. 26. Portrayal of how the Lee and Song [10] solution may diverge for heat pipes embedded in heat sinks.

A much more comprehensive analysis was later conducted by Ellison et al in which the rectangular source on rectangular substrate spreading resistance problem was solved using indexed Fourier Series [11]. Ellison's approach solved the 3-D heat equation analytically, but is dependent upon the approximation of infinite series convergence making it a cumbersome tool for use in quick design optimization, yet, an excellent resource for checking final results.

$$\psi_{spreading} = \left(\frac{\rho}{\pi^3\alpha}\right)\sqrt{\frac{\beta}{\alpha}}\sum_{l=1}^{\infty}\frac{1}{l^3}\sin^2(l\pi\alpha)\left[\frac{1+\left(\frac{Bi\cdot\tau}{2l\pi\tau}\right)\tanh(2l\pi\tau)}{\left(\frac{Bi\cdot\tau}{2l\pi\tau}\right)+\tanh(2l\pi\tau)}\right]$$

$$+\left(\frac{1}{\pi^3\rho^2\beta}\right)\sqrt{\frac{\alpha}{\beta}}\sum_{m=1}^{\infty}\frac{1}{m^3}\sin^2(m\pi\beta\rho)\left[\frac{1+\left(\frac{Bi\cdot\tau}{2m\pi\rho\tau}\right)\tanh(2m\pi\rho\tau)}{\left(\frac{Bi\cdot\tau}{2m\pi\rho\tau}\right)+\tanh(2m\pi\rho\tau)}\right]$$

$$+\left(\frac{4}{\pi^4\rho\alpha\beta\sqrt{\alpha\beta}}\right)\sum_{l=1}^{\infty}\sum_{m=1}^{\infty}\frac{1}{l^2m^2}\sin^2(l\pi\alpha)\sin^2(m\pi\beta\rho)$$

$$\cdot\left\{\frac{1+\left(\frac{Bi\cdot\tau}{2\pi\tau\sqrt{l^2+m^2\rho^2}}\right)\tanh\left(2\pi\tau\sqrt{l^2+m^2\rho^2}\right)}{2\pi\sqrt{l^2+m^2\rho^2}\left[\frac{Bi\cdot\tau 2\pi\tau}{\sqrt{l^2+m^2\rho^2}}+\tanh\left(2\pi\tau\sqrt{l^2+m^2\rho^2}\right)\right]}\right\} \qquad (18)$$

Ellison's work also reported criteria for determining the proper number of Fourier terms to achieve significant convergence.

Numerical methods provide an alternative means to determine the temperature distribution of a heat sink. Numerically solving heat diffusion requires one to break a control body into a finite number of smaller control volumes known as meshing. Once the body is properly meshed, boundary conditions can be applied along with a solution algorithm. The beauty of numeric solving is that the greater burden lies on a computer which must iteratively determine the solution, while the user must only apply working theory to the solution algorithm. Patankar [9] developed one such method for writing relatively simple algorithms to solve complex differential equations that involve diffusion, advection, source generation, and transient behaviors numerically. Patankar and several students of his later went on to develop the well known thermal fluid solver

Fluent. Both Patankar's numerical method and Fluent were used to compare the validity of analytical tools for optimization.

As mentioned above, an experiment has been setup using off-the-shelf components to verify any models validity. The experiment consists of a 39X23X1.0 cm heat sink with an eccentric heat load shown in the diagram below (Fig.27).

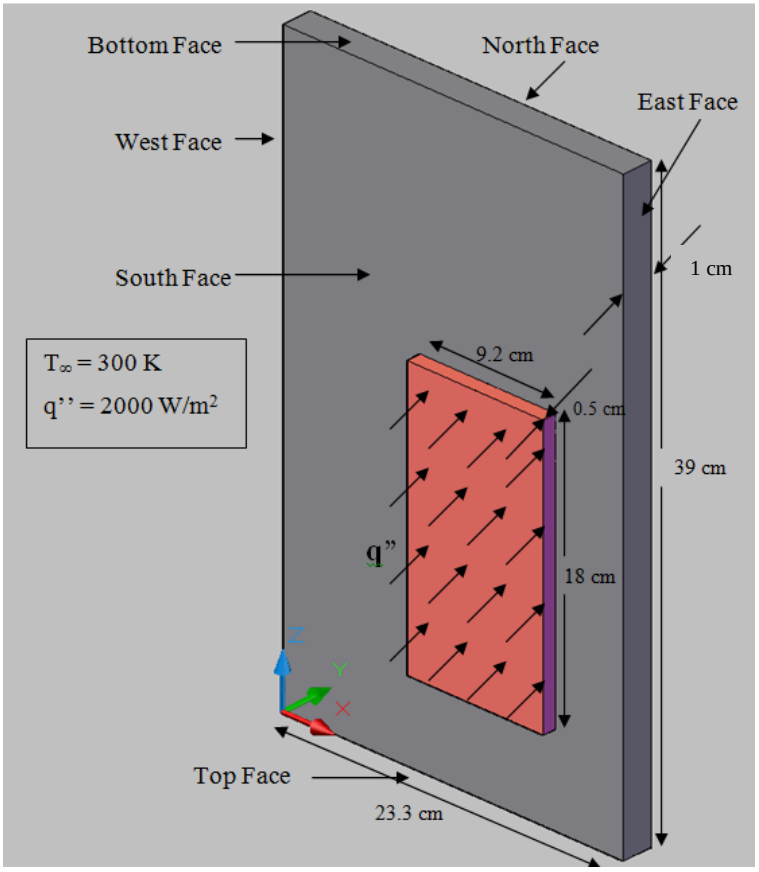

Fig. 27. Diagram depicting the heat sink and heat load used for experimental and numerical comparison.

The first look at temperature distribution was accomplished by the writing of a numerical heat diffusion program within MATLAB using the Patankar Method [9]. Using a total thermal load of 30W, the temperature distribution across each face is shown in Fig. 28. This same scenario was also analyzed in Fluent yielding the temperature distribution shown below in Fig 29. The self written 3-Dimensional numerical code was found to be a

cumbersome tool prone to error and was thus dropped for the industry accepted FLUENT software (See Appendix *Conduction3DTransient.m* for a more detailed examination of the code discussed herein).

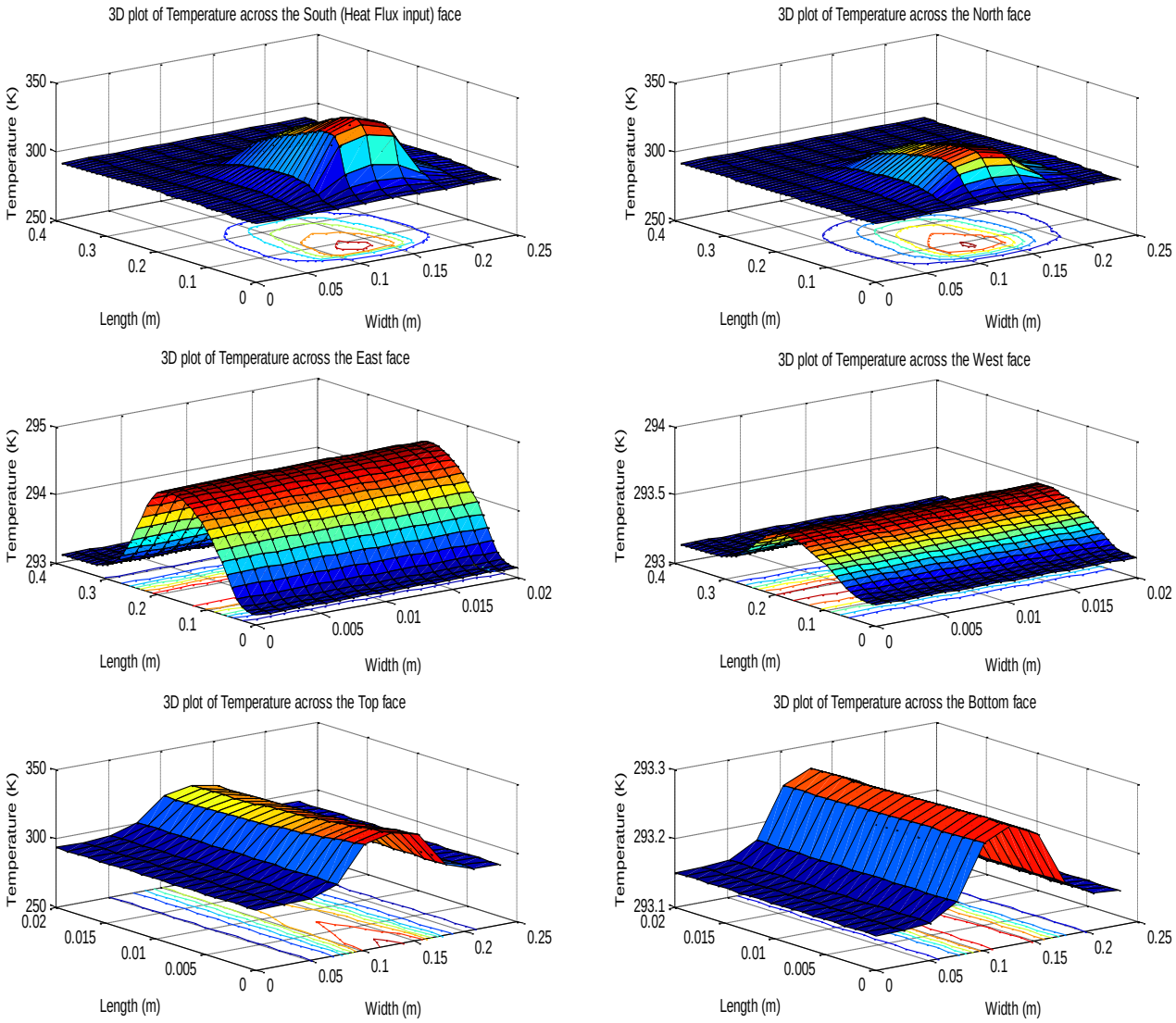

Fig. 28. Plots showing the temperature distribution across each face using Patankar's Method.

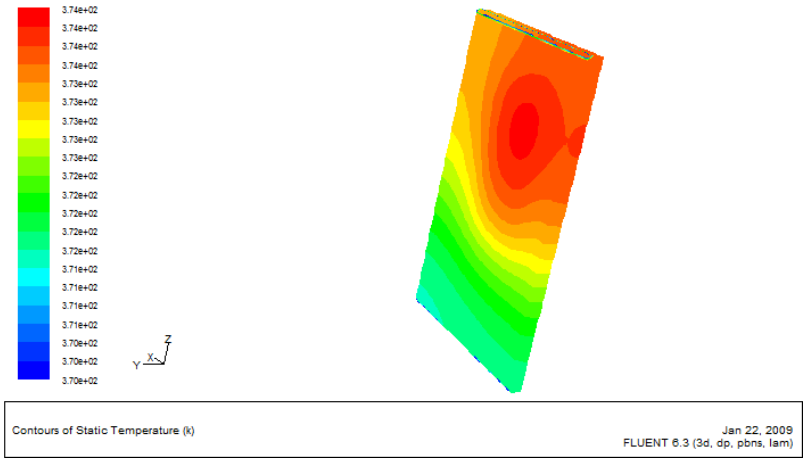

Fig. 29. Temperature distribution solved using Fluent.

As shown in the above illustrations, Patankar's method and the Fluent results differ by as much as 50 K in some circumstances. This is most likely due to a significant coding error. The self written code was thus dropped for Fluent.

Further investigation was done in Fluent to study the effect of spreading the heat source across the heat sink base on surface temperature distribution. Using a full natural convection simulation, four different cases were studied. Figures 30-37 illustrate the different positions of the heat input to the sink in which heat flux and total area were conserved. Table 2 compares the results with analytical predictions.

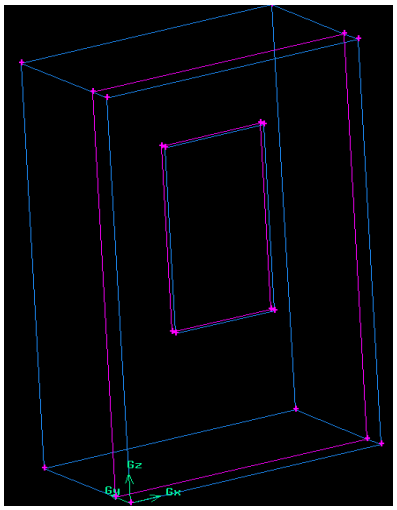

Fig. 30. Case 1 – Single eccentric plate.

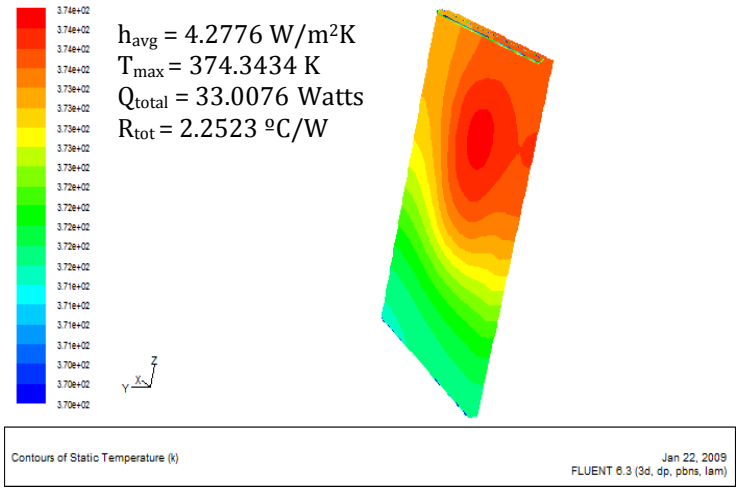

Fig. 31. Case 1 Temperature distribution.

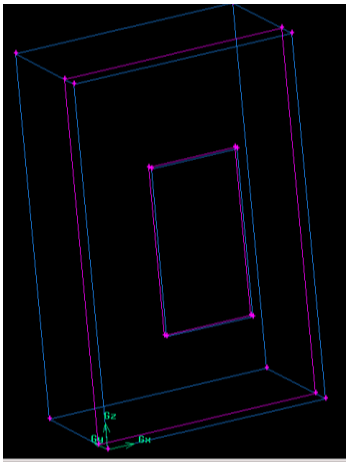

Fig. 32. Case 2 – Single centered plate.

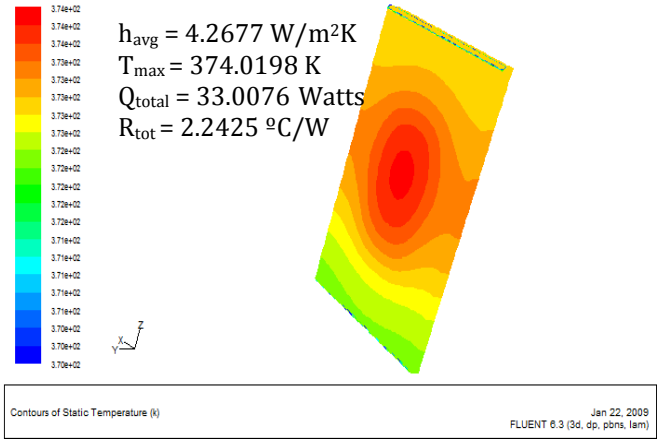

Fig. 33. Case 2 Temperature distribution.

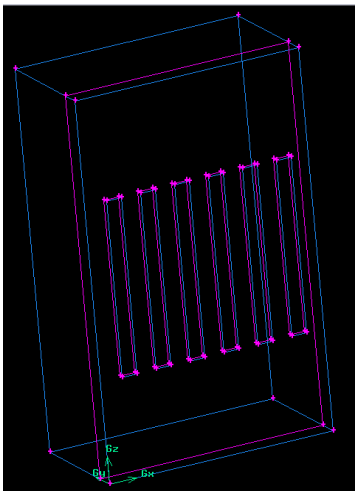

Fig. 34. Case 3 – Four horiz plates.

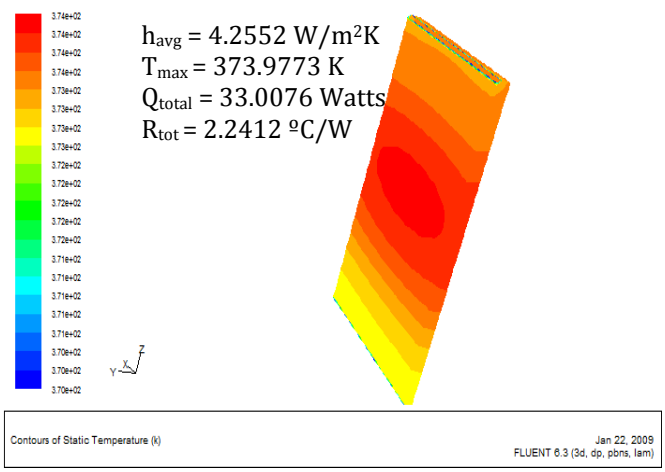

Fig. 35. Case 3 Temperature distribution.

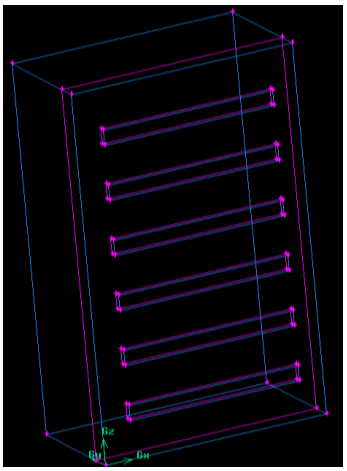

Fig. 36. Case 4 – Four vertical plates.

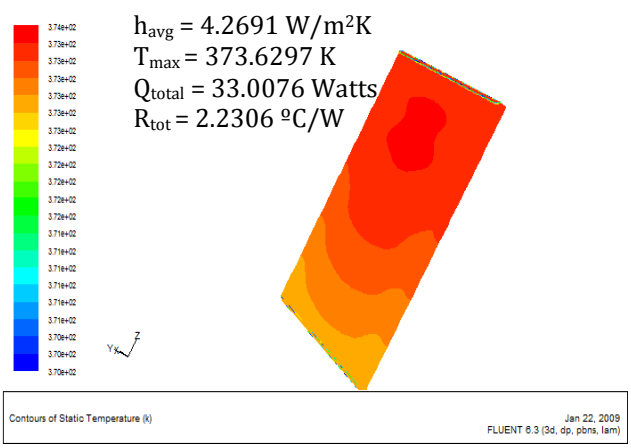

Fig. 37. Case 4 Temperature distribution.

Table 3. Comparitive data for the four numerical cases and the 1-D analytical solution

	h_{avg} (W/m^2K)	T_{max} (Kelvin)	R_{total} (ºC/W)
Analytical	3.7170	377.8360	2.3581
Case 1	4.2776	374.3434	2.2523
Case 2	4.2677	374.0198	2.2425
Case 3	4.2552	373.9773	2.2412
Case 4	4.2691	373.6257	2.2305

There are several observations worth pointing out in regards to the preceeding Fluent diagrams. The first is that for the aluminum heat sink base having thickness of 1 cm, there exists very little benefit to spreading the heat source across the surface. The maximum temperatures and total thermal resistance from source to sink is within a few percentage points for all four cases analyzed and the largest temperature gradients were within just a few Kelvin. The Biot number (*Bi*) for this particular combination was ~0.00886 for each of the cases leading to the conclusion that the Lumped Capacitance Method was quite valid in predicting the temperature distribution in this circumstance. Another aspect worth discussing is the proximity of the analytical correlation's representation of heat transfer coefficient verses that shown for each of the numerical cases. When thermal spreading becomes a significant effect, temperature gradients will cause the local heat transfer coefficient to diverge from what is predicted analytically based on an isothermal surface. The above four cases seem to suggest that as long as the Biot number is maintained below 0.1, lumped capacitance can justify analytical correlations for heat transfer coefficient. Another observation that should be noted is the colored temeprature trends shown in the plots. While the gradients represented by those trends are small, they are accurate representations of the heat flow one would expect to see in each configuration. The final comment is based upon the thickness of the plate

itself. Conductive resistance is directly linked to the thickness of the medium in which heat is transfering. It is thus expected that as the heat sink base thickness decreases from 1 cm, the temperature gradients should become increasingly significant as the Lumped Capacitance Method would predict.

Experimental Comparison

After time had been spent developing the tools needed to study the heat sink both analytically and numerically, experimental tests were conducted on one heat sink to compare the accuracy of the techniques. The dimensions of the heat sink tested are identical to those outlined in Fig. 27 with the exception of the base thickness being 5.3 mm and the presence of a triangular fin array having fin height of 3.9 mm, spacing 1.54 mm, and thickness of 1.50 mm (More information on the experimental test setup can be found in the Appendix – *Heat Sink Spreading Experiment*). Using the analytical correlations outlined in equations 9 and 10 for vertically-oriented, triangular fin arrays [6], the temperature difference from source to sink was calculated and is shown below in Table 4. Fig. 1 is also shown again below for conveniene in visualizing the individual

Table 4. Shows the comparison between analytical and experimental results for thermal resistance values.

Thermal Resistance	R (°C/W) Analytic	ΔT (ºC) Analytic	T (ºC) Experimental	R (°C/W) Experimental	ΔT (ºC)-Experimental
CPU	0.000	0.000	48.0	0.00	0.0
CB/TP Interface	0.060	1.801		0.00	
Cooling Block	0.010	0.297	43.1	0.16	4.9
Heat Pipe	0.100	3.001	39.2	0.13	3.9
Heat Sink base	0.000	0.007	39.1	0.00	0.1
Spreading Resistance	0.118	3.535	34.5	0.15	4.6
Ambient Air	0.440	13.195	24.9	0.48	14.3
Total:	0.728	21.836		0.77	23.1

thermal resistances. The analytical spreading resistance depicted in the table was solved using the Song et al. cylindrical coordinate transformation approximation [16]. The Heat Pipe resistance shown as 0.100 ºC/W was a somewhat arbitrary chosen value based upon previously obtained industrial information on heat pipe performance and does not represent a true analytical model. True heat pipe performance is a function of a number of independent variables including gravitational orientation, condenser length, power level, and condenser geometry which will be investigated in much more detail in the upcoming section. Radiation was considered, but based off of a somewhat loose approximation correlation shown below

$$q_{rad} = \{(N-1)\varepsilon S + \varepsilon[Nt + 2(H+B)]\}L\sigma(T_s^4 - T_\infty^4) \tag{19}$$

The other analytical thermal resistances were calculated from the well documented correlations depicted in Fig. 1. As seen in the Tables 3 and 4, the analytical approximations for thermal performance are quite reasonable.

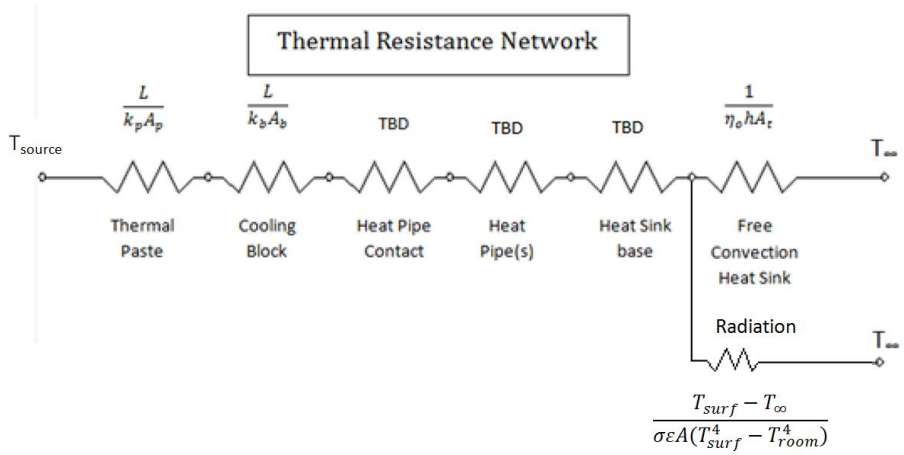

Fig. 1. Thermal resistance network depicting the individual thermal transport impedances

Figs. 38 and 39 below show the experimentally obtained surface temperature distribution across the heat sink.

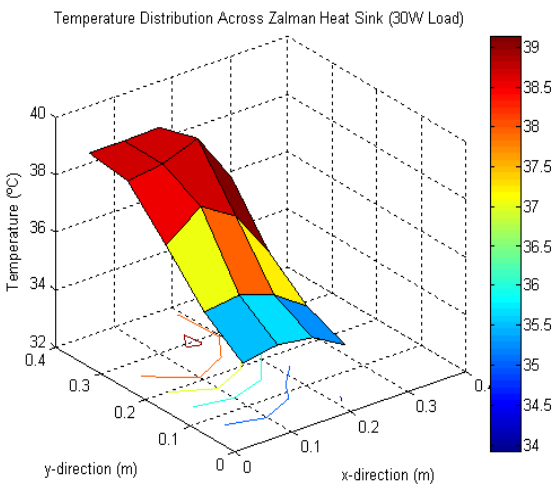

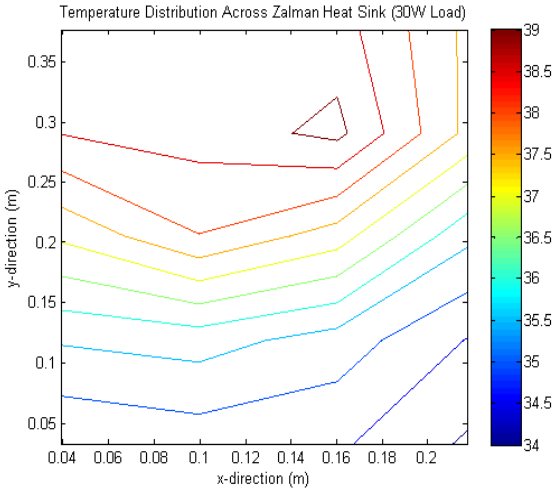

Fig. 38. 3-D surface plot of temperature on heat sink. Fig. 39. Contour plot of temperature on heatsink.

Referring to Figures 27 and 28 of Case 1, the trends shown experimentally are not unlike those shown numerically. This temperature distribution was also compared to an analytical solution of the 1-D heat equation shown below in Fig. 40.

$$\frac{d^2T}{dx^2} - \frac{hP}{kA_c}(T - T_\infty) = 0$$

$$\frac{\theta(x)}{\theta_b} = \frac{\cosh m(L-x) + (h/mk)\sinh m(L-x)}{\cosh mL + (h/mk)\sinh mL} \tag{19}$$

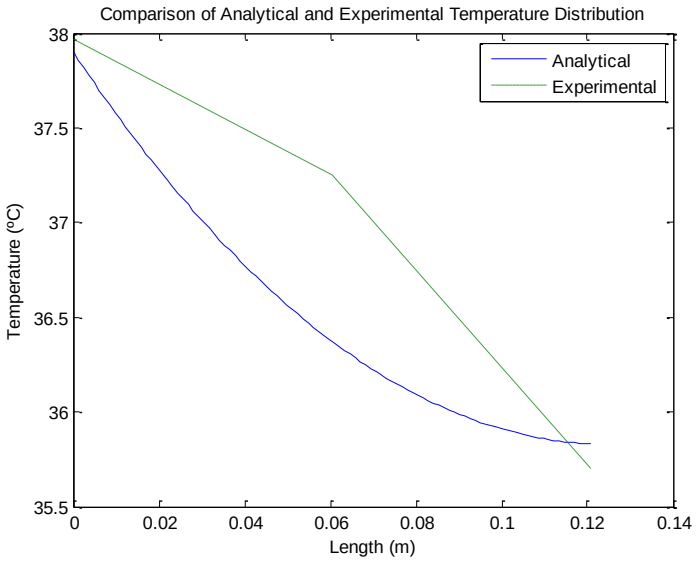

Fig. 40. Comparison of 1-D analytical solution and experimental data.

The one dimensional path shown in the above plot is from the center of the heat pipe contact plate to the western face of the heat sink shown in Fig. 13 and represents one of an infinite number of temperature distribution paths. The Biot number (*Bi)* of the experimental heat sink was calculated to be 0.01267 attesting to its small temperature gradient as a consequence of Lumped Capacitance. While the experimental heat sink's conductive thickness was nearly 1 cm, this is not typical of what is most commonly used in industry. Common PC frames are constructed from 1-2 mm thick aluminum walls which changes the Biot number value significantly. Following the same logic conductive to convection resistance ratio, changing the base thickness from 1 cm to 1 mm increases the Biot number to 0.1267. This now crosses this suggestive $Bi < 0.1$ guideline that is associated with lumped capacitance and it would be expected that a similarly equipped heat sink with this thinner base plate would be subject to increased spreading resistance temperature gradients.

Final Spreading Thoughts

As shown in the above section on heat diffusion throughout a solid with a natural convection boundary, thermal spreading is not a negligible factor when optimizing heat sinks. It is, however, an effect that can be quantified to reasonable accuracy by using simple analytic solution methods. Other, more complicated, techniques exist using numerical solution algorithms or by approximating infinite Fourier series that can improve upon the accuracy of a chosen design. It is here suggested that 1-D analytical techniques be the driver for design optimization and that the more complicated techniques be used as a final design verification.

Furthermore, applying the principles of lumped capacitance appears to be a very lucrative technique in increasing heat sink area utilization. By examining the nature of the conductive to convective thermal resistance ratios and orchestrating thermal transport contact surfaces such that the Biot number is always less than 0.1, full surface to air convection area can be taken advantage of. The other task of ensuring that large temperature gradients across a heat sink surface don't cause large deviation in the analytical correlation's prediction of heat sink performance is handled well by applying the Biot number as a sanity check. Small Biot number designs will, for all practical purposes, conform well to the analytical heat transfer predictions discussed in a previous section of this research.

Empirical Heat Pipe Investigation

The final area for consideration in this study is the strategic implementation of heat pipes. Heat pipes are well understood to efficiently transfer thermal energy from one point to another via latent energy absorption and expulsion. Other attractive features of heat pipes include that they are capable of fitting into a large spectrum of heat transfer applications, can vary greatly in geometry, and are quite cost effective. However, well used as heat pipes may be, industry still relies greatly on empirical data for quantifying the performance of these devices and assumptions are often used. It seems that there is great difficulty encompassing the nearly infinite orientation, gravitational, and cross-sectional variation that accompany heat pipe implementation and thus there is still a great dependence upon experimental design verification. It should be noted that this is not to say that heat pipe performance models do not exist but rather that the models that do exist require an intimate knowledge of the working fluid, heat pipe structure, and porous media constituting the wicking structure. Figure 41 below shows the steady-state model predicted axial temperature variation presented by Peterson et al [15]. Comparing this trend with the data presented later in this section will allow for a good validation of the model.

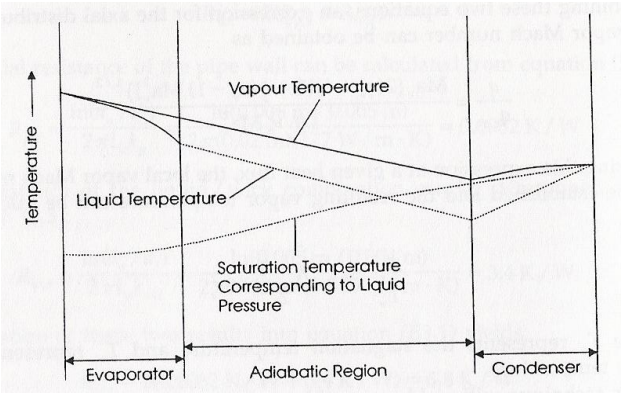

Fig. 41 Plot of temperature profile along the heat pipe length from the Peterson model [18].

Common design assumptions associated with heat pipes include, but are not limited to: relatively low temperature gradient throughout length, an isothermal condenser condition, and a relatively small gravitational dependence. To further clarify the existence of these assumptions, a brief heat pipe fundamentals section is provided.

Heat Pipe Fundamentals

The inner workings of what are called 'traditional' heat pipes are somewhat complicated, but can be explained relatively simplistically. Essentially, a heat pipe is a sealed, hollow, tube of a metal (typically copper or aluminum) with a wicking structure and saturated fluid inside the tube. Fig. 42 shows a good diagram of a heat pipe operation cycle. Fluid at its saturation point, as inside the heat pipe, can exist in liquid, vapor, or a mixture of both phases of matter. The ratio of liquid to vapor is known as the *quality* of the fluid.

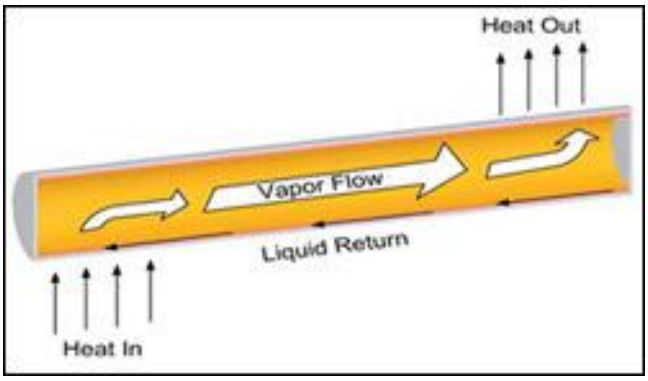

Fig. 42. Illustration of heat pipe operation cycle [19].

Increasing the temperature of the saturated fluid above its saturation point will cause additional liquid to change phases into vapor. The energy required to start this process is known as latent energy and typically results in very low temperature increases during the phase change period. Heat pipes thrive off of latent energy exchanges. Energy gets transported to the fluid at the evaporator portion of the heat pipe. Liquid at the liquid-vapor interface receives this latent energy and evaporates into vapor. The density of

vapor is substantially less than that of the liquid and thus there is a large pressure increase due to higher vapor content. This high pressure vapor pushes towards the opposite end of the heat pipe where latent energy is again extracted and the vapor condenses upon the heat pipe walls, returning to its liquid state. This liquid is then pulled back to the evaporator via a wicking structure. The wick inside a heat pipe is porous media, often metallic or felt, that absorbs liquid causing a capillary pumping of fluid. The liquid is retunred to the evaporator via this capillary action and the process is repeated. When plenty of liquid surrounds the evaporator, the heat pipe will function with a very small temperature gradient from evaporator to condenser as a result of the thin film evaporation thickness – which basically allows fluidic exchange between the liquid and vapor interface at a very low temperature difference. This temperature difference is far lower than the super heat required for boiling processes (often 1 to 8 ºC for water) occurring between a solid and liquid. However, it is by this last bit of logic that heat pipe performance can be significantly hindered under certain operating conditions. When there ceases to be enough liquid in the evaporator for thin film evaporation to occur, the heat pipe will first experience boiling fluid at a relatively large ΔT followed by a complete dryout condition, where liquid is no longer found near the evaporator and all heat input is going to sensible temperature gains and not latent. This 'dryout' condition can be onset by several factors including: gravitional opposition to capillary motion, very large heat inputs that cause vaporization to occur faster than condensation and capillary motive force can react, pressure head loss attributed to long condenser lengths, and many other types of vapor and liquid flow impedances that may arise.

By this logic of the Fanless PC study, it was determined that four independent variables of heat pipes would be experimentally studied; length, gravitational orientation, condenser geometry, and heat load. (See Table 5 for details.)

Table 5. Experimental test setup: Definition and range of variables.

Independent Variable	Tested Range or Value(s)
Condenser Length	• 160 mm • 260 mm • 360 mm
Gravitational Orientation	• Horizontal Condenser with Vertical Evaporator - neutral gravity - (Horizontal) • Vertical Condenser Evaporator Down - gravity assist - (VED) • Vertical Condenser Evaporator Up - gravity opposed - (VEU)
Condenser Geometry (see Figure 47)	• Round • Flattened
Thermal Load	• 0-50 Watts
Ambient Temperature (Chamber Controlled)	• 27 ºC

To these independent variables the total temperature difference from evaporator to condenser and temperature gradient along condenser length were established as the two dependent variables allowing performance quantification and the implicit calculation of thermal resistance.

Experimental Setup

In order to characterize the significance of each independent variable chosen, a well controlled experimental setup was designed and implemented. A total of six unique heat pipe-heat sink test specimens were erected. Each specimen was heated using identical Thermal Test Vehicles (TTV) which are designed to simulate the heating and

physical structure of a Central Processing Unit (CPU). A picture of one TTV used as a part of a test specimen is shown in Fig. 43.

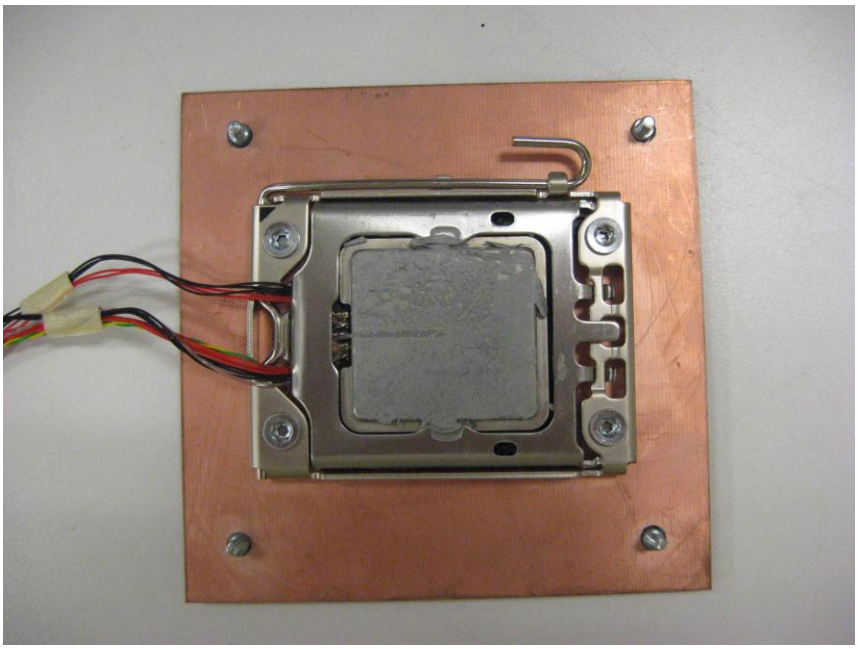

Fig. 43. Picture of one of the Thermal Test Vehicles (TTV) used to supply thermal loading to the heat pipes

Mounted to each TTV was a heat pipe embedded copper slug serving as a base for the heat sink apparatus. Each heat pipe was bent at a 90º angle just past the 50 mm evaporator region with an exposed adiabatic length of about 20 mm. Three different condenser lengths were then mated to corresponding heat sinks with proportional lengths shown in Figure 44.

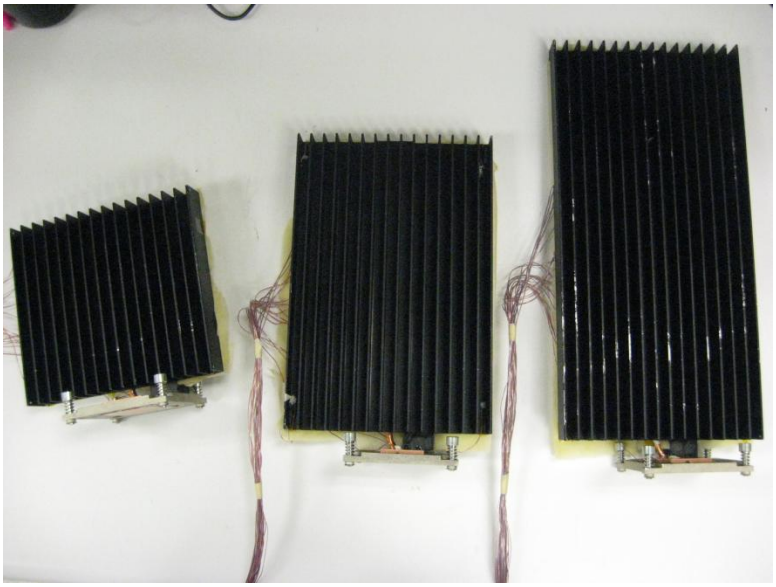

Fig. 44. Side by side view of the three different condenser-heat sink length used. (160, 260, 360mm)

Each heat sink was identical in width, fin spacing, fin thickness, and fin height with the only difference being in the length (being 160 mm, 260 mm, and 360 mm). Figure 45 shows an entire heat pipe-heat sink assembly.

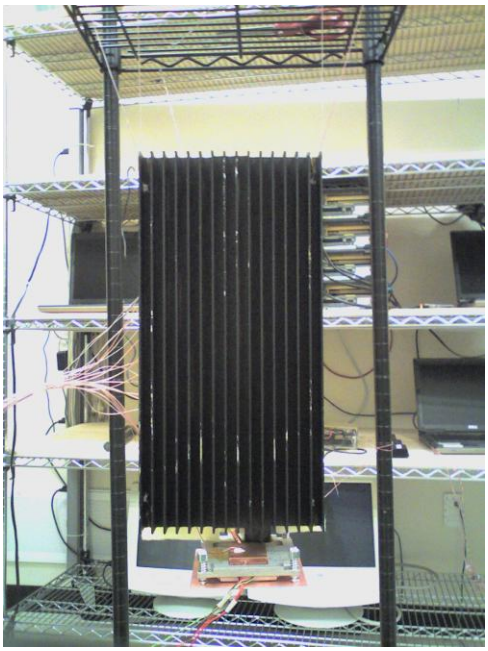

Fig. 45. Picture of a heat pipe-heat sink assembly in test apparatus with instrumentation.

Each test was conducted in a specially designed environmentally controlled room at the Dell facilities in Austin, TX which allows room temperature to be set and controlled without any compromising ventilation currents to affect data collection (see *Dell Support Acknowledgments* in Appendix). The heat sinks were also suspended via thin wire to negate any potential edge effects or flow obstructions. Type T thermocouples were attached at the midpoint of the evaporator, midpoint of the adiabatic region, at the beginning and end of the condenser, and approximately every 25 mm in between shown in Figure 46.

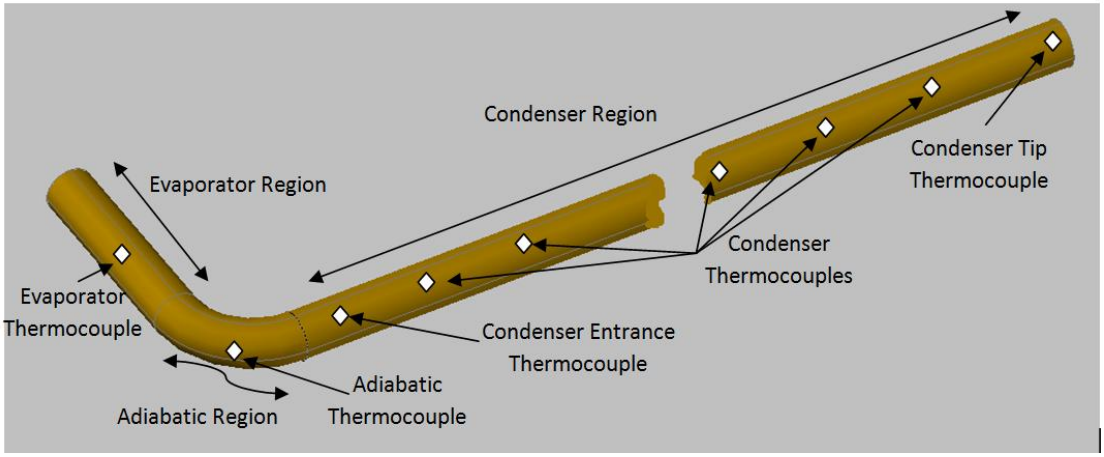

Fig. 46. Illustration of thermocouple attachment to each heat pipe test specimen.

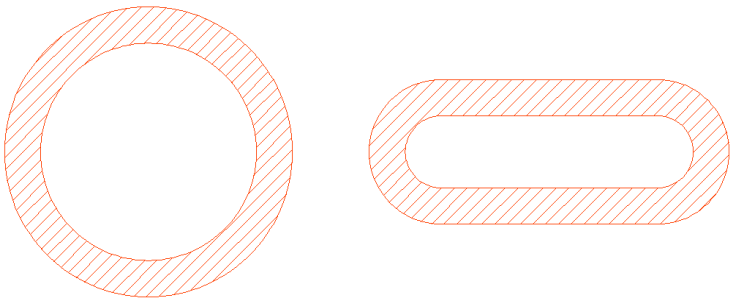

Fig. 47. Cross-sectional view of a round condenser (left) and a flattened condenser (right).

Investigation Results

As this study was parametric in nature, in seems pertinent to review that all four established independent variables can affect the significance of one another. This will become evident with the presentation of the data that follows, but suffice it to say that significance is relative and behaviors exhibited by changing one independent variable become more or less exaggerated with the presence of change in other independent variables.

Condenser Length

The first independent variable studied was the effect of changing condenser length. Often in industry, it is assumed that regardless of the length of the heat pipe condensing region, the temperature profile will always be isothermal along that length. This assumption translates into isoflux conditions and convenient heat spreading calculations. However, basic insight would suggest that heat pipe diameter, wicking structure, working fluid properties, total heat pipe length, gravitational orientation, and heat load should all contribute to the effective conductivity of the condenser length. Rather than assuming an isothermal profile, it could be argued that changing any of those contributing factors may lead to dryout or liquid-vapor stagnation affecting the heat pipe's transport capabilities. To this end, length was studied while holding the other aforementioned factors constant. Three different lengths were selected for the test specimen condensers: 160 mm, 260 mm, and 360 mm. This range was deemed appropriate for any potential implementation within a Fanless PC chassis. Figure 43 shows all three of the condenser configurations side by side. Figures 48-50 show the temperature profiles for the three tested condenser lengths at

Vertical Condenser Evaporator Down (VED), Horizontal Condenser (Horizontal), and Vertical Condenser Evaporator Up (VEU) orientations respectively.

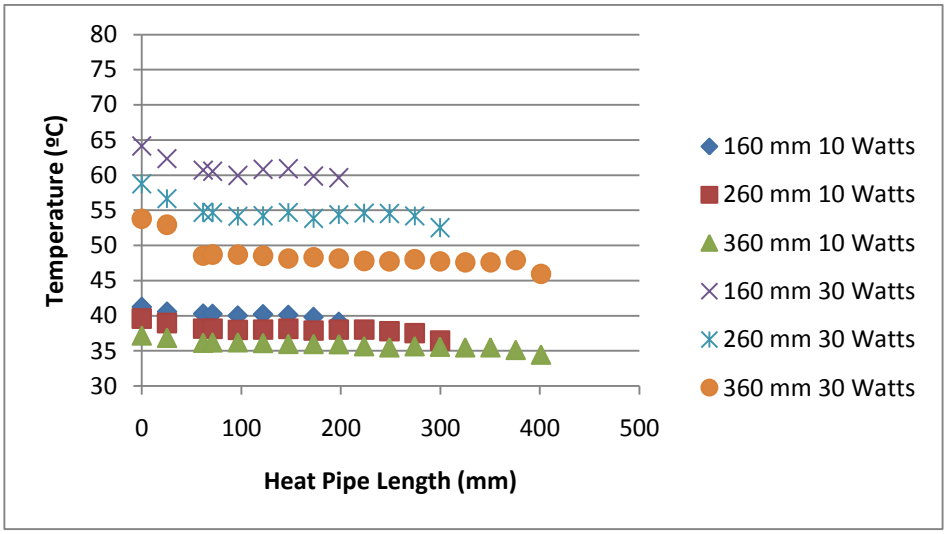

Figure 48. Illustration of length effect for the VED orientation for 10 and 30 Watts.

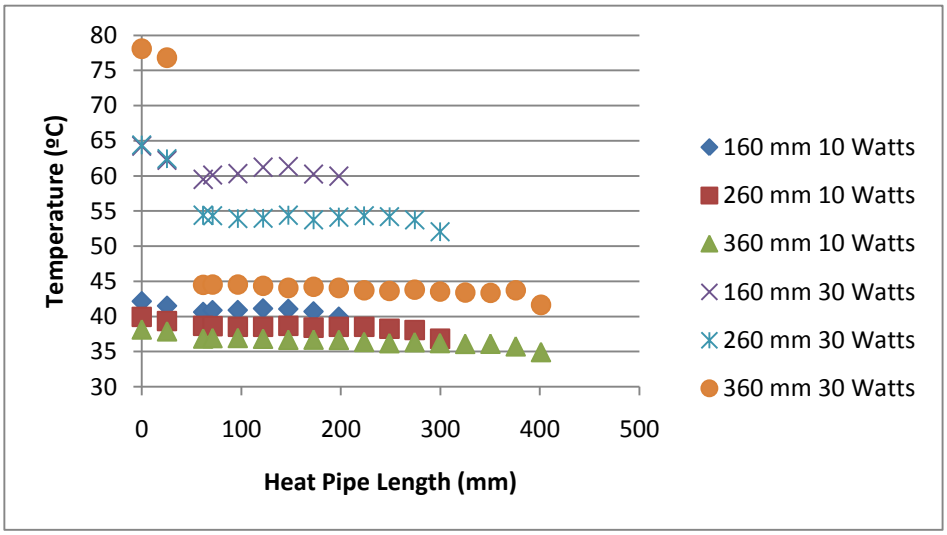

Figure 49. Illustration of length effect for the horizontal orientation for 10 and 30 Watts.

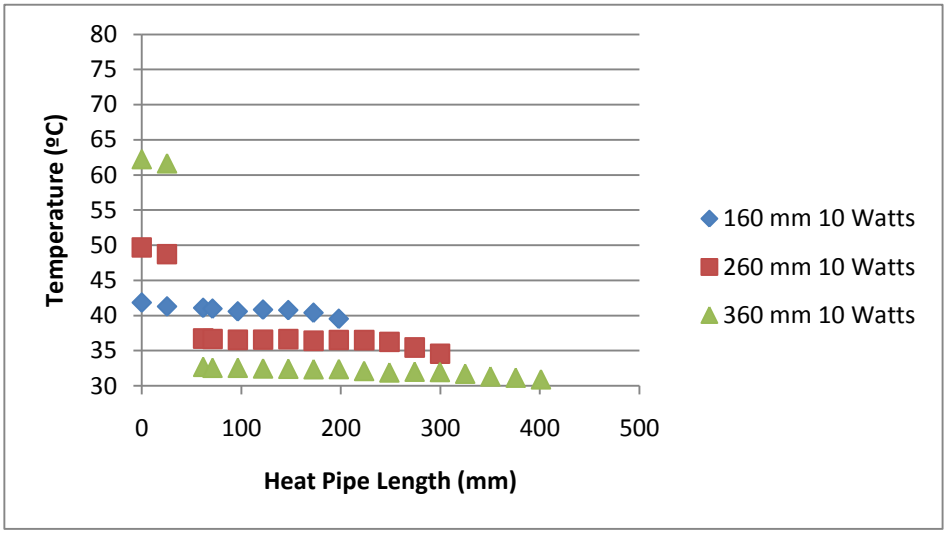

Figure 50. Illustration of length effect for the VEU orientation for 10 Watt thermal load.

The data in the preceeding graphs allows for a couple of conclusions about condenser length and simultaneously about power and orientation to be made. First, for all three specimen lengths and orientations, the temperature profile along the condenser region was nearly isothermal. For most test samples this was a condenser entrance to condenser tip temperature difference of less than 1.5 ºC and a maximum diference of 4.1 ºC. This does not suggest that there exists no maximum transport length at which conductivity decays due to inherent limitation but rather that for the domain of lengths constrained by original design specifications the condenser can arguably be assumed as isothermal. The next conclusion that can be made is in reference to the temperature gradient between the evaporator and condenser entrance. Representing the largest temperature gradient along the entire heat pipe, the temperature drop from evaporator to condenser invariably increases with condenser length. The ratio of condenser length to condenser diameter is a likely culprit for this phenomenon. While knowledge the nature of the wicking structure in the heat pipes tested was unavailable, fluidic pressure drop is a direct function of length. 90º tubing bends are also cause for substantial fluidic pressure

head loss and the large temperature difference across this bend (being the adiabatic section) seems to suggest that this force balance is lost to entrainment at larger lengths. Furthermore, this steep temperature difference with condenser length is exacerbated by both gravitational orientation and thermal load. As gravitational assist is diminished (as the horizontal and VEU orientations) the temperature gradient increases; similarly with increase in power. The exact charging nature of the heat pipes is unknown, but being of the same vendor, they were likely all filled based upon an interior volume ratio rather than a scientific approach considering capillary and vapor pressure balances that depend upon length and diameter. The difference in condenser length temperatures from size to size is very well accounted for by the increased heat transfer surface area present in the larger heat sinks. Using the analytical methods discussed in a previous section, the 360 mm heat sink would have a 0.7259 ºC/W convection resistance compared to the 160 mm's 1.0762 ºC/W resistance; thus suggesting a 10.51 ºC temperature difference at 30 Watts verses the 13.1 ºC difference observed in Fig. 48.

Beyond temperature profile along the heat pipe, there are other characteristics of value to be discussed when examining the effects of condenser length. For design engineering, it is helpful to define a thermal resistance from the evaporator to condenser of a heat pipe or an effective thermal condutivity of the heat pipe. Recalling that thermal resistance is defined as the temperature rise per unit of power between two points of reference and is shown below in equation 17

$$R = \frac{\Delta T}{q} \tag{20}$$

From Fourier's Law (equation 18), effective thermal conductivity can be defined as shown in equation 19 below

$$q = \frac{k\Delta T}{dx} dydz \tag{21}$$

$$k_{effective} = \frac{qL}{\Delta TA} \tag{22}$$

or

$$k_{effective} = \frac{RL}{A} \tag{23}$$

While defining effective conductivity in this manner can be useful, strictly defining the thermal resistance from evaporator to condenser entrance and tip allows for more practical use of the thermal resistance network shown in Figure 1. To show results more pertinent to the heat pipes and not the surrounding appartus, thermal resistance was taken as the relative temperature difference along points of the heat pipes themselves. Figs. 51-53 show the thermal resistance for the three tested condenser lengths at VED, Horizontal, and VEU orientations respectively (all round condensers). Examining the charted data seems to suggest a parabolic nature for thermal resistance as a function of power for the tested heat pipes. The point where thermal resistance begins to make its large ascent suggests dryout potentially caused by capilary, entrainment, or viscous limitation within the heat pipe. The thermal resistance from evaporator to condenser tip for all three orientations and condenser lengths is shown in Fig. 54 (260 & 360 VEU have been omitted as they are in immediate dryout state).

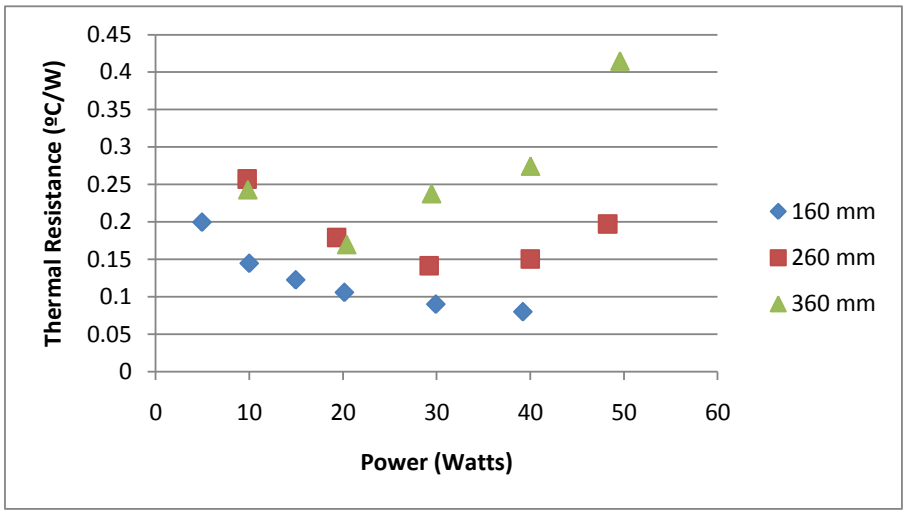

Fig. 51. Plot of thermal resistance from Evaporator to Condenser Tip for VED orientation.

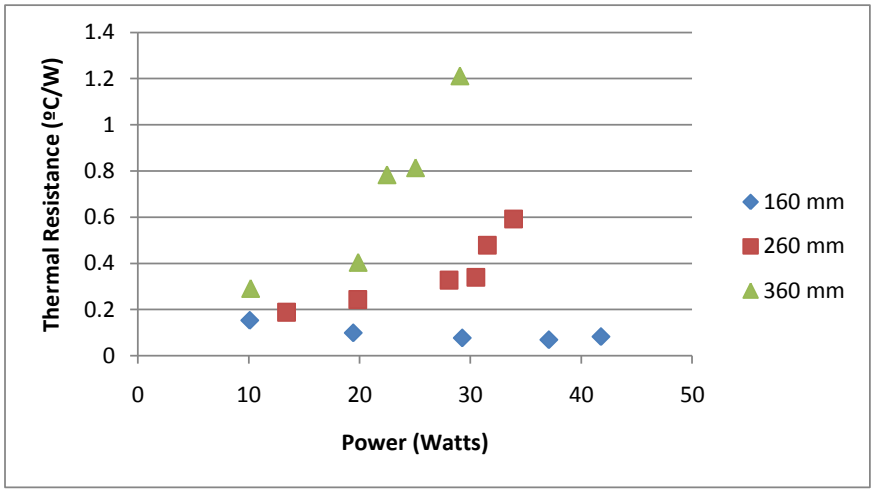

Fig. 52. Plot of thermal resistance from Evaporator to Condenser Tip for Horizontal orientation.

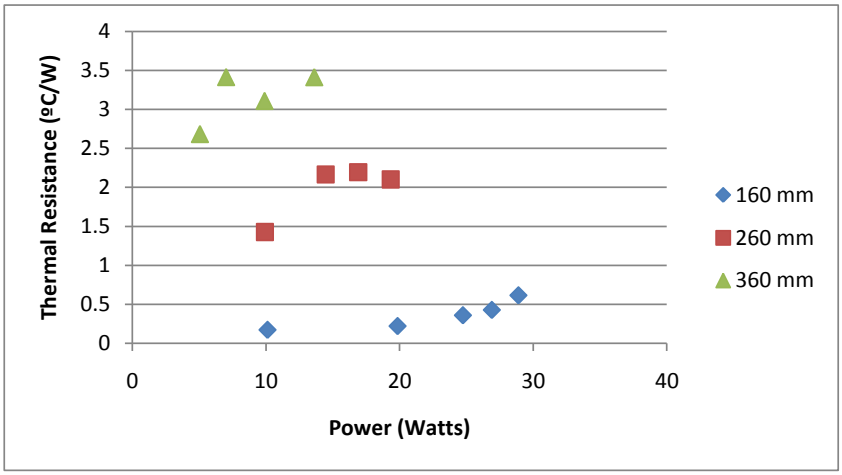

Fig. 53. Plot of thermal resistance from Evaporator to Condenser Tip for VEU orientation.

Orientational Effects

While the effects of varied gravitational assistance can be seen in the preceeding graphs, detecting the noticable effects of such changes is more readily accomplished on a single graph. Figs. 54-56, again, show thermal resistance as a function of power, but are now broken down to illustrate orientational effects for 160, 260, and 360 mm round condensers respectively.

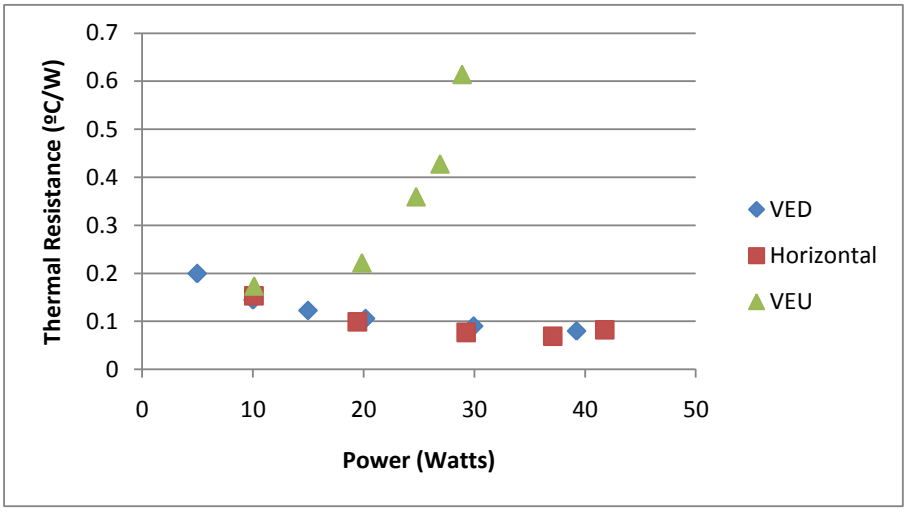

Fig. 54. Plot of thermal resistance verses power at three different orientations for 160 mm condensers.

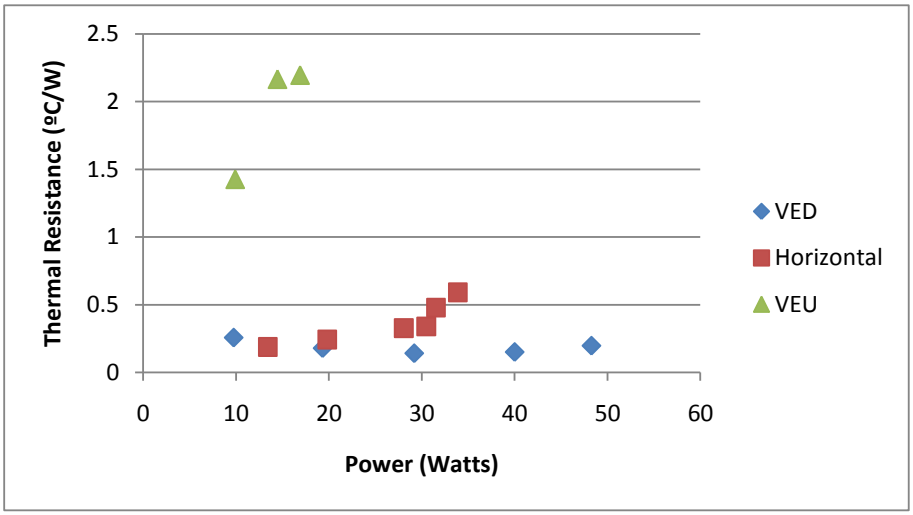

Fig. 55. Plot of thermal resistance verses power at three different orientations for 260 mm condensers.

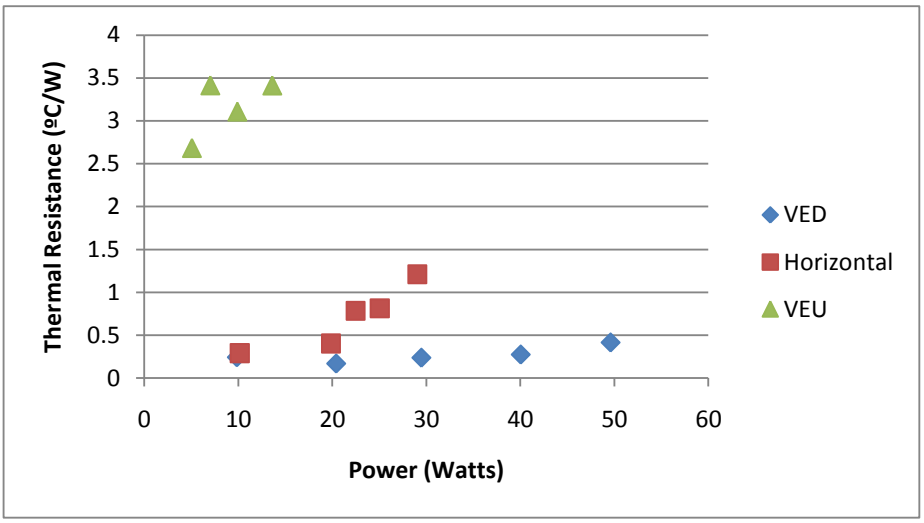

Fig. 56. Plot of thermal resistance verses power at three different orientations for 360 mm condensers.

Seeing the data presented in this manner leads to some possibly unsuprsing conclusions. The power at which dryout occurs decreases with the decrease in gravitational assistance. Thought the test equipment did not allow for such a high powered test (maximum operation temperature of the TTV is limited to 75 ºC), the curves for Horizontal and VED thermal resistance in Fig. 54 would be expected to trend upwards with a further increase in power in a fashion similar to Fig. 55 and 56. The results of these trends will be more clearly discussed in the conclusion of this section.

Condenser Geometry

The final independent variable for consideration was the effect of flattening the condenser portion of the heat pipes. Fig. 47, again, provides a visual tool for what this process actually entails. Flattening the condenser portion of a heat pipe is attractive in the design of Fanless PCs because it allows for improved contact resistance between the heat pipe and heat sink without the additional cost of grooving the surface or manufacturing the condenser into the heat sink. Every test conducted for the round condenser cross section was repeated for the flattened condenser heat pipes. Both condenser types were

provided by the same vendor, using the same wicking structure, and having the same manufacturing process with the exception of the post vaccuum sealing condenser flattening performed by the heat pipe vendor. Results for these tests are shown in Figs. 57-59 with the results from Figs. 54-56 included for comparison. As seen in the graphs, there is a significant amount of overlap between the rounded and flattened condenser types for thermal resistance from evaporator to condenser tip. In fact there are only subtle discernable trending differences between the two condenser geometries. This means that, from a design stand point, the cheaper method of flattening the condenser, verses extra machining upon the heat sink, is a viable design solution.

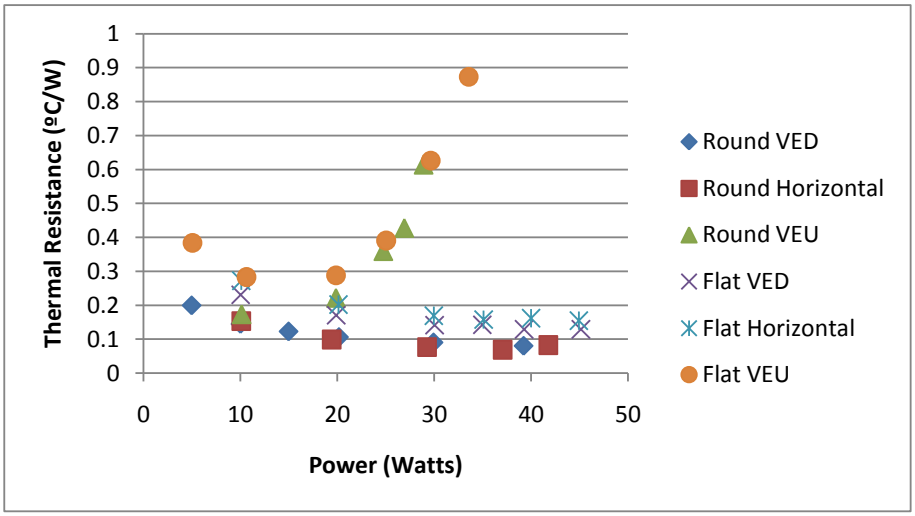

Fig. 57. Plot of thermal resistance verses power at three different orientations for 160 mm condensers.

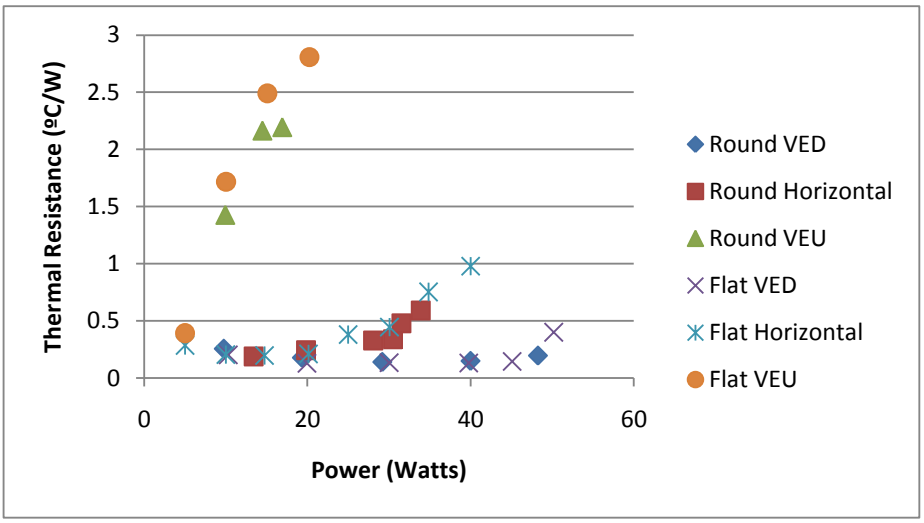

Fig. 58. Plot of thermal resistance verses power at three different orientations for 260 mm condensers.

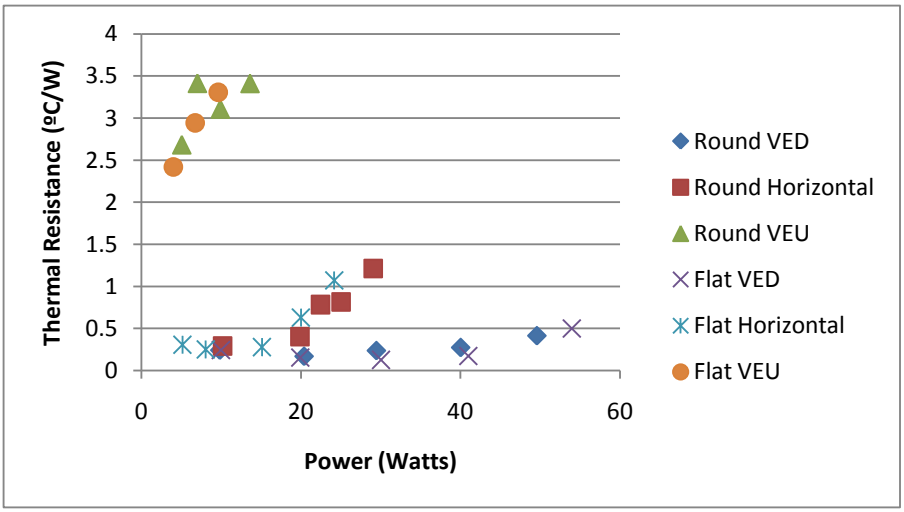

Fig. 59. Plot of thermal resistance verses power at three different orientations for 360 mm condensers.

Heat Pipe Investigation Conclusions

The experimental study presented here is valuable in many ways for the design of future Fanless PC systems. While it is understood that heat pipes are excellent devices for transport of thermal energy, it was important to determine some key design guidelines that should be followed to improve their impementation in a system. The first useful piece of information supported by the data is that for the tested range of condenser

lengths, the temperature profile along the condenser was always nearly isothermal (again, typically less than 1.5 ºC). Regardless of orientation, power input, and condenser geometry, even when the heat pipe ultimately experienced dryout the condenser temperature profile remained fairly constant. This is beneficial to know for design in that heat spreading from the condenser should thus be treated as an isoflux condition, simplifying the nature of analysis. The next useful piece of information gleaned from this study is that dryout reveals itself as increased thermal resistance from the evaporator to condenser entrance. This behavior is provoked by the removal of gravitational assistance and increased power and appears parabolic in nature. It does not, however, appear to have any dependence upon the geometry of the condenser as seen in Fig. 61-63. The power and amount of gravity that can be resisted by a heat pipe is also an inverse function of the condenser length. For a given gravitational resistance, decreasing the condenser length increases the amount of power that can be supported before dryout. Finally, for the smaller two condenser lengths (160 and 260 mm), there exists some orientational independece at low power levels. To be more clear, at a certain power for those two lengths, the heat pipe could feasibly be impemented in any direction with respect to gravity and maintain stable operability. Table 6 below shows some of the guidelines that sum up the results of the heat pipe investigation. Dryout power is the power at which the temperature difference between the evaporator and condenser reaches the specified temperature in the table. While 2 ºC and 5 ºC are somewhat arbitrary, in industry they might often represent the point at which an additional heat pipe is required to keep the overall temperature difference small. Cutoff power was defined as the point where the thermal resistance from evaporator to condenser takes a steep climb representing onset of

a ‘true’ dryout condition. An “N/A” was placed where a configuration could not operate stably at any of the tested power settings.

Table 6. Discernable conclusions from the empirical heat pipe investigation.

Condenser Length (mm)	Orientation	Dryout Power (2 ºC)	Dryout Power (5 ºC)	Cutoff Power Round	Cutoff Power Flat
160	VED	17	53	40+	40+
	Horizontal	15	37	40+	40+
	VEU	6	21	20	20
260	VED	7	47	50	45
	Horizontal	12	20	30	30
	VEU	2	4	N/A	N/A
360	VED	8	24	40+	40+
	Horizontal	7	15	20	15
	VEU	1	2	N/A	N/A

Research Conclusions

The preceding research discourse was focused upon laying the foundational tools, not only for the design, but optimization of future Fanless PC designs. This began with an in-depth analysis of the thermal engineering issues surrounding the topic followed by a topical literature review leading into the present studies. These issues included heat sink optimization, heat sink area effectiveness (thermal spreading), and heat pipe implementation.

The first step in heat sink optimization was accomplished by research into both recent and historical works done in the field of heat sink performance characterization and an evaluation of free convection analytical tools. Information from multiple sources was compiled into a MATLAB based program allowing for every type of useful trend to be analyzed and ultimately the creation of an optimization scheme to determine the best heat sink dimensions for a desired physical constraint, thermal load, and orientation as determined by empirical correlations. The results from this study were parametrically organized in Table 2 and allow for three superficial conclusions: vertical orientation is superior to horizontal orientation, rectangular fins outperformed triangular fins by a small margin, and by reorienting the heat sink such that the width, W, is larger than the length, L, performance improvement can be achieved by virtue of reduced boundary layer effects. Optimum results were found by the fine tuning balance of heat transfer coefficient and surface area. The product of these two quantities is ultimately what drives down the thermal resistance for a fin array and increases in one often meant decreases in the other. The MATLAB subroutine *OptScript.m* in conjunction with *HSAnalysis.m* performed a methodical numerical procedure that outputs the combination of fin spacing

and fin thickness for a given set of physical constraints that yields the best combination of heat transfer coefficient and fin surface area to minimize thermal resistance.

Thermal spreading was studied in three ways: analytical, numerical (CFD), and experimental. There exists a multitude of ways to determine whether or not spreading resistance is a factor for any given design (i.e. analytical approximation, lumped capacitance, and full numerical solutions), but it is not always practical to perform many of the exhaustive methods during the initial design process. Using commercial CFD tool FLUENT in conjunction with a simple experiment, the use of simple analytical tool provided by Lee and Song et al. [12] was largely justified as a design tool by nature of a relatively small volume constraint and the benefit of lumped capacitance. Beyond the sheer magnitude of spreading resistance, the effect it can have on local heat transfer coefficients was also studied. It was found, in a single case study, that for low Biot numbers the results of lumped capacitance justly serve to validate the isothermal quality of a heated surface (heat sink base) ensuring the applicability of analytical heat transfer coefficient correlations used in the fin array analysis.

Finally, the problem surrounding preexisting heat pipe implementation assumptions was given empirical support by a direct experimental investigation. Choosing condenser length, gravitational orientation, power, and condenser cross-sectional geometry as the key independent variables associated with heat pipe implementation in the Fanless PC, a series of tests were executed to negate or give credence to a few of the ideals often used in industry for heat pipe placement. Several key findings arose from this study including: orientation independence diminishes with increases in condenser length and power, flattening a condenser cross-section produced

no significant performance trends, and, finally, the magnitude of power that can be supported by a single heat pipe at a given orientation decreases with an increase in condenser length. These results lead to the development of a general guideline table for heat pipe implementation under the variables most pertinent to the Fanless PC.

Final Thoughts and Suggestions

As mentioned previously, the research conducted for this thesis was largely ground work for Fanless PC design. Many of the thermal obstacles and assumptions associated with that task have been addressed from a variety of angles. Next steps from the work presented here should be aimed at applying the knowledge gained about Fanless PC thermal design to the actual projection and prototyping of a Fanless PC system. Tools such as the fin configuration program and heat pipe guideline table are immediately valuable to Dell or any company seeking to design Fanless desktop PCs. Other tools such as the analytical spreading correlation proposed by Lee and Song et al along with Biot number have been aptly used in a fashion lending itself to easier and more justifiable thermal designs.

Furthermore, future investigations in this area would benefit from a more detailed examination of convection enhancement techniques such as chimney effect and fin inclination. Work done for both of these areas is still somewhat lacking but that which has been published does suggest great potential gains from further investigation.

Works Cited

1. Baskaya, S., Sivrioglu, M., Ozek, M., 2000, "Parametric study of natural convection heat transfer from horizontal rectangular fin arrays," *Int. J. Therm. Sci.*, **39**, 797-805.
2. Incropera, F.P., Dewitt, D.P., Bergman, T.L., Lavine, A.S., 2007, *Introduction to Heat Transfer*, John Wiley & Sons, New York.
3. Bar-Cohen, A., Madhusudan, I., Kraus, A., 2003, "Design of Optimum Plate-Fin Natural Convective Heat Sinks," *Journal of Electronic Packaging*., **125**, 208-216.
4. Elenbaas, W., 1942, "Heat dissipation of parallel plates by free convection," *Physica*, **9**, 1-28.
5. Bar-Cohen, A., Rohsenow, W., 1984, "Thermally Optimum Spacing of Vertical, Natural Convection Cooled, Parallel Plates," *ASME J. Heat Transfer*, **106**, 116-122.
6. Bar-Cohen, A., Madhusudan, 1998, "Least-Material Optimization of Vertical Pin-Fin, Plate-Fin, and Triangular-Fin Heat Sinks in Natural Convective Heat Transfer," *IEEE.*, **ISCTP**, 295-302.
7. Karagiozis, A. Raithby, G.D., Hollands, K.G.T., 1994, "Natural Convection Heat Transfer from arrays of isothermal triangular fins in air," *ASME J. Heat Transfer*, **116**, 105-110.
8. Harahap, F., McManus, H.N., 1967, "Natural Convection heat transfer from horizontal rectangular fin arrays," *J. Heat Transfer*, (February 1967), 32-38.
9. Fisher, T., S., Torrance, K. E., 1998, "Free Convection Limits for Pin-Fin Cooling," ASME J. Heat Transfer, **120**, 633-640.
10. Thrasher, W., W., Fisher, T. S., Torrance, K. E., 2000, "Experiments on Chimney-Enhanced Free Convection from Pin-Fin Heat Sinks," ASME J. Heat Transfer, **122**, 350-355.
11. Kitamura, Y., Ishizuka, M., Nakagawa, S., 2006, "Study on the Chimney Effect in Natural Air-Cooled Electronic Equipment Casings under Inclination: Proposal of a Thermal Design Correlation that Includes the Porosity Coefficient of an Outlet Opening," Heat Transfer—Asian Research, **35**, 122-136.
12. Lee, S., Song, S. and Van Au, "Closed-Form Equation for thermal Constriction/Spreading Resistances with Variable Resistance Boundary Condition", Proceedings of the 1994 International Electronics Packaging Conference, Atlanta, Georgia, pp. 111-121

13. Ellison, G., N., 2003, “Maximum Thermal Spreading Resistance for Rectangular Sources and Plates with Nonunity Aspect Ratios,” IEEE Components and Packaging, **26-2**, 439-454
14. Kraus, A.D., Aziz, A., Welty, J., 2001, *Extended Surface Heat Transfer*, John Wiley & Sons, New York.
15. Starner K.E., McManus Jr.-H.N., 1963, “An experimental investigation of free-convection heat transfer from rectangular-fin arrays,” *Journal of Heat Transfer*, **August**, 273-278.
16. Primore, Frigus, “Natural Convection and Inclined Parallel Plates,” http://www.frigprim.com/articles2/parallel_pl_Inc.html
17. Patankar, Suhas V., 1980, *Numerical Heat Transfer and Fluid Flow*, Taylor & Francis
18. Peterson, G.P., 1994, *An Introduction to Heat Pipes Modeling, Testing and Applications*, John Wiley & Sons, New York.
19. Advanced Cooling Technologies, Inc., “Heat Pipe Technologies,” http://1-act.com/hptech.html

Appendix

- Heat Sink Spreading Experimental Setup
- Heat Pipe Investigation Setup with Dell Acknowledgments
- Table of Applied Correlations and Limitations
- Composed Numerical Coding
    - *HSAnalysis.m*
    - *TrendScript.m*
    - *OptScript.m*
    - *Spreading_Resistance.m*
    - *Conduction3DTransient.m*

Heat Sink Spreading Experimental Setup

In order to validate some of the analytical correlations used in this research, a physical experiment was constructed for comparison. This was initiated by purchasing a Zalman TN300 Fanless PC case shown below in Fig. A. This particular chassis had a very similar

Fig. A. Photo of the Zalman TN300 Fanless PC case.

thermal resistance network to the network proposed in the introductory portion of this paper making it uniquely attractive for validating a few of the design tools employed in this study. To start testing, Type-T thermocouples were strategically instrumented at points allowing for key thermal resistances to be measured. A Dell provided Thermal Test Vehicle(TTV) was used to simulate power from a CPU and is shown in Fig. B below.

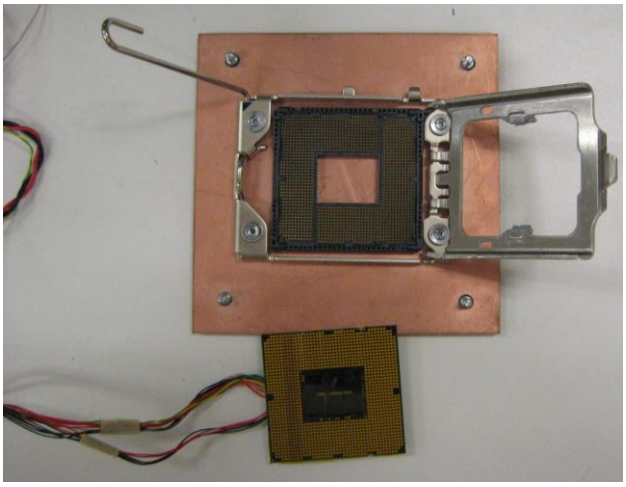

Fig. B. Photo of Thermal Test Vehicle used to simulate CPU thermal loading

A thermocouple slot was carefully end-milled into the top of the TTV case and sealed in place using Loctite 384 adhesive. Mounted to the top of the TTV was a copper CPU block with six heat pipes and heat pipe cap shown in Fig. C. Thermocouple slots were

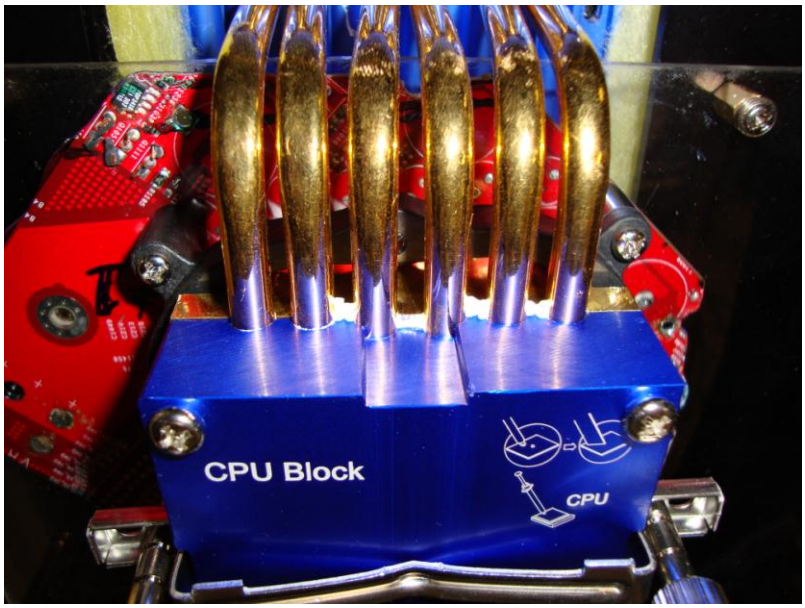

Fig. C. Photo of CPU block and heat pipe apparatus mounted to TTV

milled into the blue heat pipe cap with the tips being located at the evaporator mid point. The six heat pipes transported the thermal energy from the CPU block to the heat pipe

contact plate and heat sink shown in Fig. D. Fiberglass insulation was used to cover the entire assembly to prevent undesirable heat transfer routes from forming.

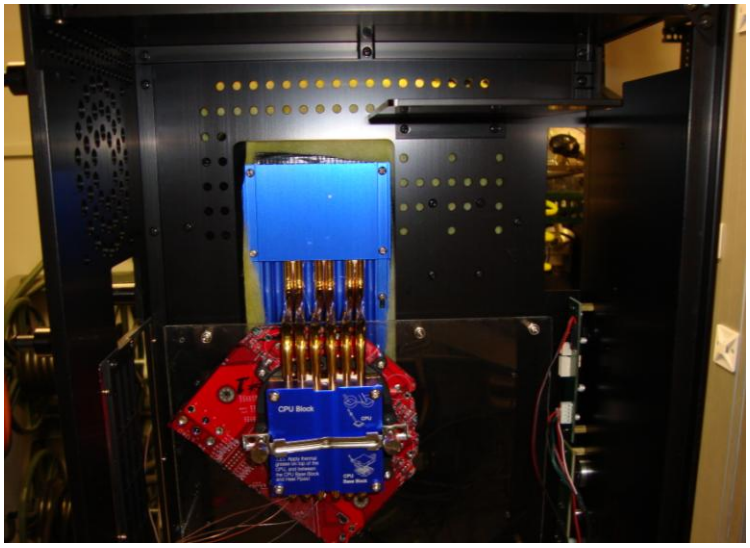

Fig. D. Photo of heat pipes attached to heat pipe contact plate and heat sink.

The heat sink itself, shown below in Fig. E was instrumented with 20 thermocouples in an array shown in Fig. F. This thermocouple array was designed to promote quantification of thermal spreading effects across the heat sink.

Fig. E Photo of heat sink with surrounding insulation

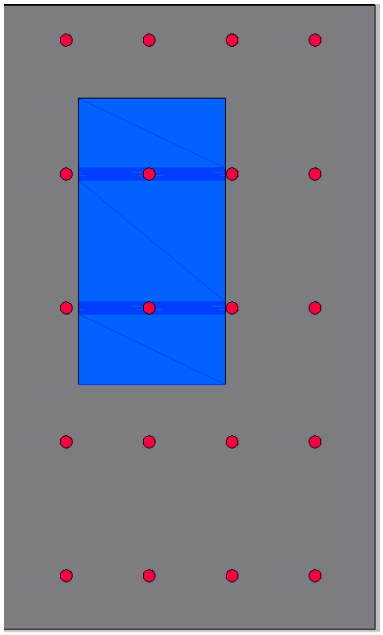

Fig. F. Illustration of thermocouple layout upon heat sink surface (red dots indicate thermocouple loc.)

Power into the TTV was controlled by a DC power supply ranging from 0-60V and 0-20A (not shown). All temperature data collection was performed by a Keithley 2701 Digital Multimeter with a Keithley 7708 Digital Multiplexor with 20 channels and built in Cold-Junction Compensation (CJC) shown in Fig. G. Data acquisition software was Keithley Excellinx.

Fig. G. Photo of Keithly Digital Multimeter used for heat sink temperature measurement.

Heat Pipe Investigation Setup

The empirical heat pipe investigation was conducted at the Parmer South Dell facility in Austin, TX. Many Dell technicians were fundamental in the construction, setup, and execution of the experiment. These efforts were headed up specifically by Robert Prosperi, Dell thermal engineer. Within the machine shop, technicians worked very diligently to fabricate all of the heat sinks used, groove the heat pipe channels, epoxy the TTVs to the heat sink bases, and provide clear, concise guidance for the final preparation of every test specimen. Without their support, the following experiment would have been impossible. The Dell employees' willingness to provide patience, insight, and assistance is a testament to their quality.

To begin the heat pipe investigation, three different heat sinks were hogged out of aluminum at 160, 260, and 360 mm shown below in Fig. A from left to right, respectively.

Fig. A. Photo of 160 mm, 260 mm, and 360 mm heat sinks shown from left to right.

The three tested condenser lengths were then mated to each of the respective heat sink lengths using a Loctite 384 adhesive. Each heat pipe was outfitted with a Type-T thermocouple every 25mm from evaporator to condenser tip as shown in Fig. B.

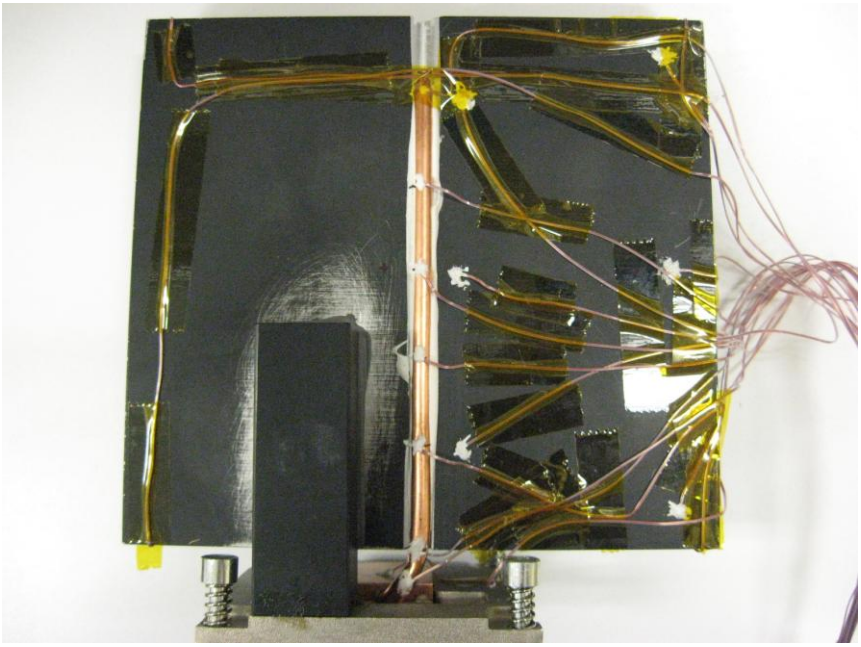

Fig. B. Photo of heat pipe adhered to heat sink with thermocouples attached

Thermal loading was supplied via Thermal Test Vehicle (TTV) shown in Fig. C in uneven increments from 0 to 50 Watts.

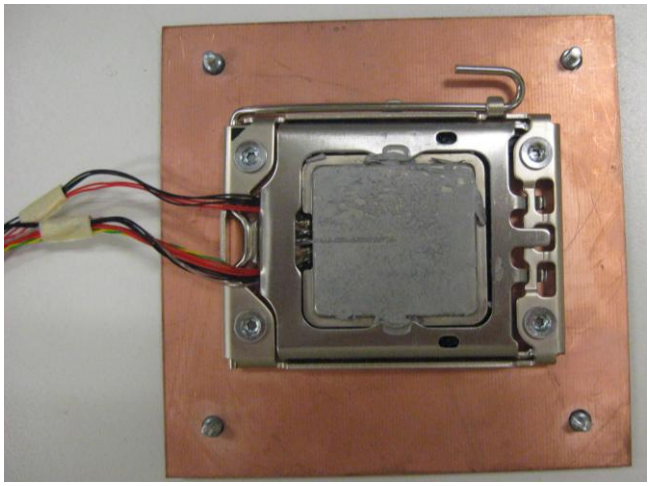

Fig. C. Photo of Thermal Test Vehicle used in heat pipe investigation.

Power to the TTV was provided by an Agilent E3633A DC Power Supply shown in Fig. D.

Fig. D. Photo of Agilent DC power supply used to provide thermal load for TTVs

All temperature and power values were recorded using Fluke Digital Multimeters with built in Cold-Junction Compensation digital multiplexor cards shown in Fig. E.

Fig. E. Photo of two Fluke Digital Multimeters used in heat pipe testing

All thermal testing was conducted in an environmentally controlled room with fixed ambient of 27 ºC shown in Fig. F. This temperature never fluctuated more than +/- one degree during temperature recordings. The impressive design of the room allowed for temperature control without the presence of strong ventilation currents, reducing any forced convective effects upon the heat pipe heat sink assemblies which were insulated and suspended from racks in the room.

Fig. F. Photo of Dell enviormentally controlled room used for heat pipe testing

Table of Applied Correlations and Limitations

Program Name	Corrolary Purpose	Author(s)/Date	Correlation(s) Used	Assumptions/Limitations
HSAnalysis.m	Horizontally Oriented Rectangular fins	Harahap and McManus et al. - *1967* [8]	$Nu_L = a\left[Ra_L \frac{S}{H}\right]^d \left(\frac{S}{L}\right)^{0.656} \left(\frac{H}{L}\right)^{0.412}$	• Assume isothermal fins (no fin efficiency term) • (a,d) = (0.0052,0.57) for low Ra and (0.000278,0.75) for high Ra
	Vertically Oriented Rectangular Fins	Bar-Cohen and Rohsenow et al. - *1984* [5]	$Nu_{fin} = \frac{h_{fin}s}{k_f} = \left[\frac{576}{(\eta_{fin}El)^2} + \frac{2.873}{(\eta_{fin}El)^{1/2}}\right]^{-1/2}$ $El = \frac{(g\beta\theta_b \Pr s^4)}{L\upsilon^2}$	• Usable for any channel spacing • Fins attached to an isothermal heat sink base • assumed insulated fin tip • Nonisothermal fins accounted for in weighting of fin efficiency term
	Vertically Oriented Triangular Fins	Karagiozis, Raithby, and Hollands - *1994* [7]	$Nu_{fin} = \left[0.515\left(\eta_{fin} Ra_b\right)^{1/4}\right]\left[1 + \left(\frac{3.26}{\left(\eta_{fin} Ra_b\right)^{0.21}}\right)^3\right]^{-1/3}$ $Ra_b = \frac{g\beta\Delta T\left(b^4/L\right)}{\nu\alpha}$	• Applying correlations to fin spacing nearing 45 mm considered "risky" – convective conditions quite different for large spacing Vs. small • heat transfer coefficients can adequately account for nonisothermal fins for fin efficiency of 75 and up
Spreading_Resistance.m	Thermal Spreading Resistance	Lee and Song et al. - *1994* [12]	$R_s = \frac{\sqrt{A_p} - \sqrt{A_s}}{k\sqrt{\pi A_p A_p}} \times \frac{\lambda k A_p R_o + \tanh(\lambda t)}{1 + \lambda k A_p R_o \tanh(\lambda t)}$ $\lambda = \frac{\pi^{3/2}}{\sqrt{A_p}} + \frac{1}{\sqrt{As}}$	• Assumes uniform heat flux upon one surface and a thermal boundary condition of the third kind on the other surface

HSAnalysis.m

```
% Function for the determination of thermal resistance for a given heat
sink input

% By: Austin M. Shelnutt
% Last Modified: 27 August 2009


function [R,Nfin,Hbase,Hfin,NHTC] = HSAnalysis(Q,L,W,H,S,t,Orient,Geom)

% Orient = 0 for horizontal; 1 for vertical
% Geom = 0 for rectangular fins, 1 for triangular


in2m = (1/39.370);  % Conversion from inches to meters
L = L;               % Input Given in meters
W = W;
H = H*10^-3;         % Input given in milimeters
S = S*10^-3;
t = t*10^-3;
Bt = 0.002;          % Base Thickness

g = 9.81;

%%%%% Convergence Loop for Surface Temperature %%%%%%%
Tinf = 24;           % Ambient Air Temperature (°C)
Tsurf = Tinf+0.001;    % Surface Temperature first iteration
Titer(1) = Tsurf;
Error1 = 1;
i = 0;
flag = 0;
while Error1 > 0.00000001 % Surface temperature Convergence Loop
i = i+1;
if i > 1000
    Tsurf = 45;     % Divergence Protection
    flag = 1
    if Error1 > 1
        disp('Too Many Errors! I am Paused!')
        cat = 1;
    end
end

% Air properties
Ts = Tsurf;

ThetaB = Ts-Tinf;
Tf = ((Ts+273.15)+(Tinf+273.15))/2;
TfC = (Ts+Tinf)/2;
Beta = 1/Tf;
p = 0.000000000002*TfC^4 - 0.000000005*TfC^3 + 0.000005*TfC^2 -
0.003*TfC + 1.236;
kf = (0.00000001*TfC^3 - 0.00002*TfC^2 + 0.068*TfC + 25.35)*10^-3;
v = (0.00007*TfC^2 + 0.094*TfC + 13.65)*10^-6;
```

```
a = (0*TfC^2 + 0.099*TfC + 25.13)*10^-6;
Pr = v/a;
    % Pr = 0.71;

% Radiation
e = 0.95;
sigma = 5.67E-8;

kfin = 180;
N = (W/(S+t));
if Orient == 0      % Horizontal Orientation
    if Geom == 0    % Rectangular Fins
        Lc = H + (t/2);
        Af = 2*Lc*L;
        Ap = H*t;
        Ac = L*t;
        P = 2*L + 2*t;
        Ab = L*S;
        At = N*Af + (N-1)*Ab;

        % Base Convection (Flat Plate)
        RaL = (g*Beta*(Ts-Tinf)*L^3)/(v*a);
        if RaL <= 10^7
            NuL = 0.54*RaL^(1/4);
        else
            NuL = 0.15*RaL^(1/3);
        end
        hbase = NuL*kf/L;

        % Heat Dissipation from Plate-Fin Arrays
        ac = 0.00071561;
        dc = 0.6576;
        Ra = (g*Beta*(Ts-Tinf)*L^3)/(v*a);
        Nu = ac*(Ra*(S/H))^(dc)*(S/L)^0.656*(H/L)^0.412;
        hfin = Nu*kf/L;
        m = sqrt(2*hfin/(kfin*t));
        nf = tanh(m*H)/(m*H);

        % Thermal Resistance Calcuation
        Rfin = 1/(nf*hfin*N*Af);
        Rbase = 1/(hbase*(N-1)*Ab);
        Rconv = (1/Rfin + 1/Rbase)^(-1);

        % Radiation Transport
        Qrad = ((N-1)*e*S + e*(N*t + 2*(H+Bt)))*L*sigma*((Ts+273.15)^4
- (Tinf+273.15)^4);
        Rrad = (Ts-Tinf)/Qrad;

        R = (1/Rconv + 1/Rrad)^(-1);

        % Natural Convection Heat Transfer Coefficient Check
        RAN = g*Beta*(35-Tinf)*L^3/(v*a);
        NUN = 0.15*RAN^(1/3);
        NHTC = NUN*kf/((L*W)/(2*L+2*W));
    elseif Geom == 1
```

```
        disp('Triangular Correlation in Horizontal Orientation
Unavailable')
    else
        disp('Please Choose a Geometry')
    end
elseif Orient == 1  % Vertical Orientation
    if Geom == 0    % Rectangular Fins
        Lc = H + (t/2);
        Af = 2*Lc*L;
        Ap = H*t;
        Ac = L*t;
        P = 2*L + 2*t;
        Ab = L*S;
        At = N*Af + (N-1)*Ab;

        % Base Convection (Flat Plate)
        RaL = (g*Beta*(Ts-Tinf)*L^3)/(v*a);
        NuL = (0.825 + (0.387*RaL^(1/6))/((1 +
(0.492/Pr)^(9/16))^(8/27)))^2;
        hbase = NuL*kf/L;

        % Heat Dissipation from Plate-Fin Arrays
        m = sqrt(2*hbase/(kfin*t));
        nf = tanh(m*H)/(m*H);
        El = (g*Beta*(Ts-Tinf)*Pr*S^4)/(L*v^2);     % Elenbaas number
        Nu = (576/(nf*El)^2 + 2.87/(nf*El)^(1/2))^(-1/2); % Bar-Cohen
and Rohsenow correlation
        hfin = Nu*kf/S;
        m = sqrt(2*hfin/(kfin*t));
        nf = tanh(m*H)/(m*H);

        % Thermal Resistance Calcuation
        Rfin = 1/(nf*hfin*N*Af);
        Rbase = 1/(hbase*(N-1)*Ab);
        Rconv = (1/Rfin + 1/Rbase)^(-1);

        % Radiation Transport
        Qrad = ((N-1)*e*S + e*(N*t + 2*(H+Bt)))*L*sigma*((Ts+273.15)^4
- (Tinf+273.15)^4);
        Rrad = (Ts-Tinf)/Qrad;

        R = (1/Rconv + 1/Rrad)^(-1);

         % Natural Convection Heat Transfer Coefficient Check
        RAN = g*Beta*(Ts-Tinf)*L^3/(v*a);
        NUN = 0.68+(0.670*RAN^(1/4))/(1+(0.492/Pr)^(9/16))^(4/9);
        NHTC = NUN*kf/L;
    elseif Geom == 1    % Triangular Fins
        % Geometric Properties
        Af = 2*L*(H^2+(t/2)^2)^(1/2);
        Ab = L*S;
        At = N*Af + (N-1)*Ab;
        alpha = atan((0.5*t)/H);
        b = S + 2*((H/2)*tan(alpha));
```

```
        % Base Convection (Flat Plate)
        RaL = (g*Beta*(Ts-Tinf)*L^3)/(v*a);
        NuL = (0.825 + (0.387*RaL^(1/6))/((1 +
(0.492/Pr)^(9/16))^(8/27)))^2;
        hbase = NuL*kf/L;

        % Heat Dissipation from Triangular Fin-Arrays
        m = sqrt(2*hbase/(kfin*t));
        nf = (1/(m*H))*besseli(1,(2*m*H))/besseli(0,(2*m*H));
        Raf = (g*Beta*(Ts-Tinf)*((b^4)/L))/(a*v);
        Nuf = (0.515*(nf*Raf)^(1/4))*(1 + (3.26/(nf*Raf)^0.21)^3)^(-
1/3);
        hfin = Nuf*kf/b;
        m = sqrt(2*hfin/(kfin*t));
        nf = (1/(m*H))*besseli(1,(2*m*H))/besseli(0,(2*m*H));


       % Thermal Resistance Calcuation
        Rfin = 1/(nf*hfin*N*Af);
        Rbase = 1/(hbase*(N-1)*Ab);
        Rconv = (1/Rfin + 1/Rbase)^(-1);

        % Radiation Transport
        Qrad = ((N-1)*e*S + e*(N*t + 2*(H+Bt)))*L*sigma*((Ts+273.15)^4
- (Tinf+273.15)^4);
        Rrad = (Ts-Tinf)/Qrad;

        R = (1/Rfin + 1/Rrad)^(-1);

         % Natural Convection Heat Transfer Coefficient Check
        RAN = g*Beta*(Ts-Tinf)*L^3/(v*a);
        NUN = 0.68+(0.670*RAN^(1/4))/(1+(0.492/Pr)^(9/16))^(4/9);
        NHTC = NUN*kf/L;
    else
        disp('Please select a Geometry')
    end
else
    disp('Please specify Gravitational Orientation')
end

    Tsold = Tsurf;
    Tsurf = Q*R + Tinf;
    Titer(i+1) = Tsurf;
    Error1 = abs(Tsurf-Tsold);
    if flag == 1
        Error1 = -1;    % Divergence Protection
    end

end     % Surface Temperature Convergence Loop
Nfin = nf;
Hbase = hbase;
Hfin = hfin;
Tsurf;
R_finarray = R;
heff = 1/(R*W*L);
```

```
% Natural Convection Heat Transfer Coefficient Verification



% plot((1:i+1),Titer)

%%%%%% Other Resistances %%%%%%
t_cpuB = 0.674*in2m;
kcb = 400;
Acb = (2.588*in2m*2.582*in2m);
R_CPUBlock = t_cpuB/(kcb*Acb);

%%%%%% Through Heat Sink base(in direction of heat flow) %%%%%%%
t_HS = 0.005;
R_HSbase = t_HS/(W*L*kfin);

%%%%%% Spreading Resistance %%%%%%
Rs = Spreading_Resistance(0.39,0.0575,t_HS,hfin,kfin,R_finarray);

%%%%%% Biot Number %%%%%%
Vol_HS = (t_HS*L*W) + N*((1/2)*t*H)*L;     % Total Volume of Heat Sink
m^3
Area_HS = At + 2*(W*t_HS) + 2*(L*t_HS);    % Surface Area of Heat Sink
m^2
Lc = Vol_HS/Area_HS;
Bi = hfin*Lc/kfin;
```

TrendScript.m

```
% Function for heat sink performance trend illustration

% By: Austin Shelnutt
% Last Modified: 28 August 2009

function TrendScript(Q,L,W,Orient,Geom)
% Orient = 0 for horizontal; 1 for vertical
% Geom = 0 for rectangular fins, 1 for triangular

% H = linspace(1,50,1000);  % Fin Heigh/Spacing/Thickness input as
milimeters
% H = [5 10 15 30 40];
H = [5 40];
% H = 5;
S = linspace(0.01,50,1000);
% S = [1 5 10 15 20];
% t = linspace(0.00001,1.5,1000);
t = 2.0;
% 3-D trending Loop
% for i = 1:1000
%      for j = 1:1000
%          R(i,j) = HSAnalysis(Q,L,W,H,S(i),t(j),1,0);
%          count = count + 1;
%      end
% end
% Horizontal Rectangular
for i = 1:2
    for j = 1:1000
        [r,nj,hb,hf,nhtc] = HSAnalysis(Q,L,W,H(i),S(j),t,0,0);
        R1(i,j) = HSAnalysis(Q,L,W,H(i),S(j),t,0,0);
        Nj(i,j) = nj*100;
        Hbase1(i,j) = hb;
        Hfin1(i,j) = hf;
        Hhoriz(i,j) = nhtc;
    end
end
Hhoriz = mean(Hhoriz(2,:));
% Vertical Rectangular
for i = 1:2
    for j = 1:1000
        [r,nj,hb,hf,nhtc] = HSAnalysis(Q,L,W,H(i),S(j),t,1,0);
        R2(i,j) = HSAnalysis(Q,L,W,H(i),S(j),t,1,0);
        Nj(i,j) = nj*100;
        Hbase2(i,j) = hb;
        Hfin2(i,j) = hf;
        Hvertical = nhtc;
    end
end
% Vertical Triangular
for i = 1:2
    for j = 1:1000
        [r,nj,hb,hf,nhtc] = HSAnalysis(Q,L,W,H(i),S(j),t,1,1);
        R3(i,j) = HSAnalysis(Q,L,W,H(i),S(j),t,1,1);
```

```
        Nj(i,j) = nj*100;
        Hbase3(i,j) = hb;
        Hfin3(i,j) = hf;
        Hvertical = nhtc;
    end
end


figure(1)
plot(S,R1(1,:),S,R1(2,:),S,R2(1,:),S,R2(2,:),S,R3(1,:),S,R3(2,:))
% plot(S,R1(4,:),S,R(4,:))
title('Fin Spacing Vs. Thermal Resistance Relationship (Thickness =
2.0mm)')
xlabel('Fin Spacing (mm)')
ylabel('Thermal Resistance (°C/W)')
% legend('Rectangular Fins','Triangular Fins')
% legend('H = 0.5cm','H = 1.0cm','H = 1.5cm','H = 3.0cm','H =
4.0cm','Location','NorthEast')
% legend('S = 1mm','S = 5mm','S = 10mm','S = 15mm','S =
20mm','Location','NorthEast')
legend('H.Rect H = 0.5cm','H.Rect H = 4cm','V.Rect H = 0.5cm','V.Rect H
= 4cm','V.Trig H = 0.5cm','V.Trig H =
4cm','Location','NorthEastOutside')


% figure(2)
% plot(t,Nj(1,:),t,Nj(2,:),t,Nj(3,:),t,Nj(4,:),t,Nj(5,:))
% % plot(H,Nj1(4,:),H,Nj(4,:))
% title('Fin Thickness Vs. Fin Efficiency (Height = 0.5cm)')
% xlabel('Fin Thickness (mm)')
% ylabel('Fin Efficiency (%)')
% % legend('Rectangular Fins','Triangular Fins')
% legend('s = 1mm','s = 5mm','s = 10mm','s = 15mm','s =
20mm','Location','SouthEast')


figure(2)
% plot(S,Hfin(1,:),S,Hfin(2,:),S,Hfin(3,:),S,Hfin(4,:),S,Hfin(5,:))
% plot(H,Hfin(1,:),H,Hfin(2,:),H,Hfin(3,:),H,Hfin(4,:),H,Hfin(5,:))
plot(S,Hfin1(1,:),S,Hfin1(2,:),S,Hfin2(1,:),S,Hfin2(2,:),S,Hfin3(1,:),S
,Hfin3(2,:),S,Hvertical)
title('Fin Spacing Vs. Heat Transfer Coefficient (Thickness = 2.0mm)')
xlabel('Fin Spacing (mm)')
ylabel('Heat Transfer Coefficient (W/m^2K)')
% legend('S = 1mm','S = 5mm','S = 10mm','S = 15mm','S =
20mm','Location','NorthEast')
% legend('Rectangular Fins','Triangular Fins')
% legend('Rectangular H = 3cm','Triangular H = 3cm','Rectangular H =
100cm','Triangular H = 100cm','Location','NorthWest')
% legend('H = 0.5cm','H = 1.0cm','H = 1.5cm','H = 3.0cm','H =
4.0cm','Location','NorthWest')
legend('H.Rect H = 0.5cm','H.Rect H = 4cm','V.Rect H = 0.5cm','V.Rect H
= 4cm','V.Trig H = 0.5cm','V.Trig H = 4cm','Vertical Limit','Location'
```

OptScript.m

```
% Function for Determining the optimum Heat Sink Configuration based
upon
    %   given geometrical constraints

% By: Austin Shelnutt
% Last Modified: 28 August 2009

    % function OptScript(Q,L,W,H,Orient,Geom)
function OptScript(Q,L,W,H)
% Orient = 0 for horizontal; 1 for vertical
% Geom = 0 for rectangular fins, 1 for triangular

tic
S = linspace(0.1,25,200); % Fin Spacing/Thickness input as milimeters
t = linspace(0.1,2,200);
count = 0;
% Horizontal Rectangular
for i = 1:200
     for j = 1:200
         R1(i,j) = HSAnalysis(Q,L,W,H,S(i),t(j),0,0);
         count = count + 1;
     end
end
% Vertical Rectangular
for i = 1:200
     for j = 1:200
         R2(i,j) = HSAnalysis(Q,L,W,H,S(i),t(j),1,0);
         count = count + 1;
     end
end
% Vertical Triangular
for i = 1:200
     for j = 1:200
         R3(i,j) = HSAnalysis(Q,L,W,H,S(i),t(j),1,1);
         count = count + 1;
     end
end
count
% R1
[a,b] = min(R1);          %%
[c,d] = min(a);          %% Algorithm for finding the minimum value and
coordinates within
row = b(d);              %%  Resistance Matrix
column = d;              %%
disp('%%%% Horizontal Rectangular %%%%%')
Sopt = S(row)
topt = t(column)
MinR = min(min(R1))
% R2
[a,b] = min(R2);          %%
[c,d] = min(a);          %% Algorithm for finding the minimum value and
coordinates within
row = b(d);              %%  Resistance Matrix
```

```
column = d;              %%
disp('%%%% Vertical Rectangular %%%%%')
Sopt = S(row)
topt = t(column)
MinR = min(min(R2))
% R3
[a,b] = min(R3);          %%
[c,d] = min(a);          %% Algorithm for finding the minimum value and
coordinates within
row = b(d);              %%  Resistance Matrix
column = d;              %%
disp('%%%% Vertical Triangular %%%%%')
Sopt = S(row)
topt = t(column)
MinR = min(min(R3))

Rinvert1 = 1./R1;
Rinvert2 = 1./R2;
Rinvert3 = 1./R3;

% figure(1)
% surfc(S,t,Rinvert1')
% title('3D Plot of Thermal Resistance Vs. Fin Spacing and Thickness
(Height = 4cm)')
% xlabel('Fin Spacing (mm)')
% ylabel('Fin Thickness (mm)')
% zlabel('1/Rth (W/°C)')
% figure(2)
% surfc(S,t,Rinvert2')
% title('3D Plot of Thermal Resistance Vs. Fin Spacing and Thickness
(Height = 4cm)')
% xlabel('Fin Spacing (mm)')
% ylabel('Fin Thickness (mm)')
% zlabel('1/Rth (W/°C)')
% figure(3)
% surfc(S,t,Rinvert3')
% title('3D Plot of Thermal Resistance Vs. Fin Spacing and Thickness
(Height = 4cm)')
% xlabel('Fin Spacing (mm)')
% ylabel('Fin Thickness (mm)')
% zlabel('1/Rth (W/°C)')
toc
```

Spreading_Resistance.m

```
function [Rs] = Spreading_Resistance(L,W,t,h,k,Rf)

L_HP = 0.36;
W_HP = 0.01;
As = L_HP*W_HP;      % Contact Area of Heat Source
Ap = L*W;            % Area of base plate

lamda = (pi^(3/2)/sqrt(Ap))+(1/sqrt(As));

Rs = ((sqrt(Ap)-
sqrt(As))/(k*sqrt(pi*Ap*As)))*((lamda*k*Ap*Rf+tanh(lamda*t))/(1+lamda*k
*Ap*Rf*tanh(lamda*t)));
```

Conduction3DTransient.m

```
% Function for determining the transient heat diffusion through a
    % 3-Dimensional Rectangular slab with inconsistent heat fluxes
        % Austin Shelnutt 28.October.2008

% function Conduct(Nx,Ny,Nz)
clear
Nx = 16;
Ny = 16;
Nz = 40;
Time = 150;  % Time Length Analyzed (s)
tic

% Problem Specific Constants
L = 0.40;   % Length of Plate (m)       [z-direction]
W = 0.20;   % Width of Plate (m)        [x-direction]
t = 0.02;   % Thickness of Plate (m)    [y-direction]

dz = L/(Nz-1);
dx = W/(Nx-1);
dy = t/(Ny-1);

L = linspace(0,L,Nz);
W = linspace(0,W,Nx);
t = linspace(0,t,Ny);

dt = Time/100;  % Time incriment (s)

% Assumed Constants
ho = 3.0;               % Heat Transfer Coefficient (W/m^2*K)
qo = 6059.2;            % Heat Flux at southern face (W/m^2)
k = 200;                % Aluminum Thermal Conductivity (W/m*K)
p = 2710;               % Aluminum Density (kg/m^3)
Cp = 900;               % Aluminum Specific heat (J/kg*K)
Tinf = 293.15;          % Ambient Air Temperature (K)

% Time Loop
apo = p*Cp*dx*dy*dz/dt; %Transient coefficient

for t = 2:100

iter = 1;               % Spatial Convergence counter
Error1(iter) = 100;     % Error starting value
Error1(iter+1) = 100;
while Error1(iter) >= 0.0000007

    for k = 1:Nz
    for j = 1:Ny
    for i = 1:Nx
     Tnew(i,j,k,1) = Tinf;    % Initial Temperature Field set to
ambient

     % Heat Flux Zone Conditions
```

```
        if j == 1
            if i >= (0.0938/0.233)*Nx
                if i <= (0.186/0.233)*Nx
                    if k >= (0.058/0.39)*Nz
                        if k <= (0.237/0.39)*Nz       % Check for Heat
Flux Zone
                            qzone = 1;
                        end
                    end
                end
            else
                qzone = 0;
            end
        end

            % Iterative Considerations
        if iter == 1    % First Iteration
            if t == 2   % First time step past intial field
                Tstart = 293.15;
                if k == 1       % Top Face
                    if j == 1
                        Testar(i,j,k) = Tstart;
                        Tfstar(i,j,k) = Tstart;
                        Tgstar(i,j,k) = Tstart;
                        Thstar(i,j,k) = Tstart;
                    elseif j == Ny
                        Testar(i,j,k) = Tstart;
                        Tfstar(i,j,k) = Tnew(i,j-1,k,t);
                        Tgstar(i,j,k) = Tstart;
                        Thstar(i,j,k) = Tstart;
                    else
                        Testar(i,j,k) = Tstart;
                        Tfstar(i,j,k) = Tnew(i,j-1,k,t);
                        Tgstar(i,j,k) = Tstart;
                        Thstar(i,j,k) = Tstart;
                    end
                elseif k == Nz      % Bottom Face
                    if j == 1
                        Testar(i,j,k) = Tstart;
                        Tfstar(i,j,k) = Tstart;
                        Tgstar(i,j,k) = Tnew(i,j,k-1,t);
                        Thstar(i,j,k) = Tstart;
                    elseif j == Ny
                        Testar(i,j,k) = Tstart;
                        Tfstar(i,j,k) = Tnew(i,j-1,k,t);
                        Tgstar(i,j,k) = Tnew(i,j,k-1,t);
                        Thstar(i,j,k) = Tstart;
                    else
                        Testar(i,j,k) = Tstart;
                        Tfstar(i,j,k) = Tnew(i,j-1,k,t);
                        Tgstar(i,j,k) = Tnew(i,j,k-1,t);
                        Thstar(i,j,k) = Tstart;
                    end

                elseif j == 1       %South Face
                    if qzone == 1       % West Boundary
```

```
                        Testar(i,j,k) = Tstart;
                        Tfstar(i,j,k) = Tstart;
                        Tgstar(i,j,k) = Tnew(i,j,k-1,t);
                        Thstar(i,j,k) = Tstart;
                    else
                        Testar(i,j,k) = Tstart;
                        Tfstar(i,j,k) = Tstart;
                        Tgstar(i,j,k) = Tnew(i,j,k-1,t);
                        Thstar(i,j,k) = Tstart;
                    end
                elseif j == Ny      % North Face
                    Testar(i,j,k) = Tstart;
                    Tfstar(i,j,k) = Tnew(i,j-1,k,t);
                    Tgstar(i,j,k) = Tnew(i,j,k-1,t);
                    Thstar(i,j,k) = Tstart;
                else
                    Testar(i,j,k) = Tstart;
                    Tfstar(i,j,k) = Tnew(i,j-1,k,t);
                    Tgstar(i,j,k) = Tnew(i,j,k-1,t);
                    Thstar(i,j,k) = Tstart;
                end
            else        % Future Time Steps
                if k == 1       % Top Face
                    if j == 1
                        Testar(i,j,k) = Tnew(i,j+1,k,t-1);
                        Tfstar(i,j,k) = (k*dx*dz/(dy/2)*Tnew(i,j,k,t-1)
+ ho*Tinf*dx*dz)/(ho*dx*dz + k*dx*dz/(dy/2));
                        Tgstar(i,j,k) = (k*dx*dy/(dz/2)*Tnew(i,j,k,t-1)
+ ho*Tinf*dx*dy)/(ho*dx*dy + k*dx*dy/(dz/2));
                        Thstar(i,j,k) = Tnew(i,j,k+1,t-1);
                    elseif j == Ny
                        Testar(i,j,k) = (k*dx*dz/(dy/2)*Tnew(i,j,k,t-1)
+ ho*Tinf*dx*dz)/(ho*dx*dz + k*dx*dz/(dy/2));
                        Tfstar(i,j,k) = Tnew(i,j-1,k,t);
                        Tgstar(i,j,k) = (k*dx*dy/(dz/2)*Tnew(i,j,k,t-1)
+ ho*Tinf*dx*dy)/(ho*dx*dy + k*dx*dy/(dz/2));
                        Thstar(i,j,k) = Tnew(i,j,k+1,t-1);
                    else
                        Testar(i,j,k) = Tnew(i,j+1,k,t-1);
                        Tfstar(i,j,k) = Tnew(i,j-1,k,t);
                        Tgstar(i,j,k) = (k*dx*dy/(dz/2)*Tnew(i,j,k,t-1)
+ ho*Tinf*dx*dy)/(ho*dx*dy + k*dx*dy/(dz/2));
                        Thstar(i,j,k) = Tnew(i,j,k+1,t-1);
                    end
                elseif k == Nz      % Bottom Face
                    if j == 1
                        Testar(i,j,k) = Tnew(i,j+1,k,t-1);
                        Tfstar(i,j,k) = (k*dx*dz/(dy/2)*Tnew(i,j,k,t-1)
+ ho*Tinf*dx*dz)/(ho*dx*dz + k*dx*dz/(dy/2));
                        Tgstar(i,j,k) = Tnew(i,j,k-1,t);
                        Thstar(i,j,k) = (k*dx*dy/(dz/2)*Tnew(i,j,k,t-1)
+ ho*Tinf*dx*dy)/(ho*dx*dy + k*dx*dy/(dz/2));
                    elseif j == Ny
                        Testar(i,j,k) = (k*dx*dz/(dy/2)*Tnew(i,j,k,t-1)
+ ho*Tinf*dx*dz)/(ho*dx*dz + k*dx*dz/(dy/2));
                        Tfstar(i,j,k) = Tnew(i,j-1,k,t);
                        Tgstar(i,j,k) = Tnew(i,j,k-1,t);
```

```
                        Thstar(i,j,k) = (k*dx*dy/(dz/2)*Tnew(i,j,k,t-1)
+ ho*Tinf*dx*dy)/(ho*dx*dy + k*dx*dy/(dz/2));
                    else
                        Testar(i,j,k) = Tnew(i,j+1,k,t-1);
                        Tfstar(i,j,k) = Tnew(i,j-1,k,t);
                        Tgstar(i,j,k) = Tnew(i,j,k-1,t);
                        Thstar(i,j,k) = (k*dx*dy/(dz/2)*Tnew(i,j,k,t-1)
+ ho*Tinf*dx*dy)/(ho*dx*dy + k*dx*dy/(dz/2));
                    end

                elseif j == 1       %South Face
                    if qzone == 1       % West Boundary
                        Testar(i,j,k) = Tnew(i,j+1,k,t-1);
                        Tfstar(i,j,k) = (qo + (k/(dy/2))*Tnew(i,j,k,t-
1))/(k/(dy/2));
                        Tgstar(i,j,k) = Tnew(i,j,k-1,t);
                        Thstar(i,j,k) = Tnew(i,j,k+1,t-1);
                    else
                        Testar(i,j,k) = Tnew(i,j+1,k,t-1);
                        Tfstar(i,j,k) = (k*dx*dz/(dy/2)*Tnew(i,j,k,t-1)
+ ho*Tinf*dx*dz)/(ho*dx*dz + k*dx*dz/(dy/2));
                        Tgstar(i,j,k) = Tnew(i,j,k-1,t);
                        Thstar(i,j,k) = Tnew(i,j,k+1,t-1);
                    end
                elseif j == Ny      % North Face
                    Testar(i,j,k) = (k*dx*dz/(dy/2)*Tnew(i,j,k,t-1) +
ho*Tinf*dx*dz)/(ho*dx*dz + k*dx*dz/(dy/2));
                    Tfstar(i,j,k) = Tnew(i,j-1,k,t);
                    Tgstar(i,j,k) = Tnew(i,j,k-1,t);
                    Thstar(i,j,k) = Tnew(i,j,k+1,t-1);
                else
                    Testar(i,j,k) = Tnew(i,j+1,k,t-1);
                    Tfstar(i,j,k) = Tnew(i,j-1,k,t);
                    Tgstar(i,j,k) = Tnew(i,j,k-1,t);
                    Thstar(i,j,k) = Tnew(i,j,k+1,t-1);
                end
            end
        else        % Second Iteration and on
            if k == 1       % Top Face
                if j == 1
                    Testar(i,j,k) = Told(i,j+1,k,t);
                    Tfstar(i,j,k) = (k*dx*dz/(dy/2)*Told(i,j,k,t) +
ho*Tinf*dx*dz)/(ho*dx*dz + k*dx*dz/(dy/2));
                    Tgstar(i,j,k) = (k*dx*dy/(dz/2)*Told(i,j,k,t) +
ho*Tinf*dx*dy)/(ho*dx*dy + k*dx*dy/(dz/2));
                    Thstar(i,j,k) = Told(i,j,k+1,t);
                elseif j == Ny
                    Testar(i,j,k) = (k*dx*dz/(dy/2)*Told(i,j,k,t) +
ho*Tinf*dx*dz)/(ho*dx*dz + k*dx*dz/(dy/2));
                    Tfstar(i,j,k) = Tnew(i,j-1,k,t);
                    Tgstar(i,j,k) = (k*dx*dy/(dz/2)*Told(i,j,k,t) +
ho*Tinf*dx*dy)/(ho*dx*dy + k*dx*dy/(dz/2));
                    Thstar(i,j,k) = Told(i,j,k+1,t);
                else
                    Testar(i,j,k) = Told(i,j+1,k,t);
                    Tfstar(i,j,k) = Tnew(i,j-1,k,t);
```

```
                    Tgstar(i,j,k) = (k*dx*dy/(dz/2)*Told(i,j,k,t) +
ho*Tinf*dx*dy)/(ho*dx*dy + k*dx*dy/(dz/2));
                    Thstar(i,j,k) = Told(i,j,k+1,t);
                end
            elseif k == Nz      % Bottom Face
                if j == 1
                    Testar(i,j,k) = Told(i,j+1,k,t);
                    Tfstar(i,j,k) = (k*dx*dz/(dy/2)*Told(i,j,k,t) +
ho*Tinf*dx*dz)/(ho*dx*dz + k*dx*dz/(dy/2));
                    Tgstar(i,j,k) = Tnew(i,j,k-1,t);
                    Thstar(i,j,k) = (k*dx*dy/(dz/2)*Told(i,j,k,t) +
ho*Tinf*dx*dy)/(ho*dx*dy + k*dx*dy/(dz/2));
                elseif j == Ny
                    Testar(i,j,k) = (k*dx*dz/(dy/2)*Told(i,j,k,t) +
ho*Tinf*dx*dz)/(ho*dx*dz + k*dx*dz/(dy/2));
                    Tfstar(i,j,k) = Tnew(i,j-1,k,t);
                    Tgstar(i,j,k) = Tnew(i,j,k-1,t);
                    Thstar(i,j,k) = (k*dx*dy/(dz/2)*Told(i,j,k,t) +
ho*Tinf*dx*dy)/(ho*dx*dy + k*dx*dy/(dz/2));
                else
                    Testar(i,j,k) = Told(i,j+1,k,t);
                    Tfstar(i,j,k) = Tnew(i,j-1,k,t);
                    Tgstar(i,j,k) = Tnew(i,j,k-1,t);
                    Thstar(i,j,k) = (k*dx*dy/(dz/2)*Told(i,j,k,t) +
ho*Tinf*dx*dy)/(ho*dx*dy + k*dx*dy/(dz/2));
                end

            elseif j == 1       %South Face
                if qzone == 1       % West Boundary
                    Testar(i,j,k) = Told(i,j+1,k,t);
                    Tfstar(i,j,k) = (qo +
(k/(dy/2))*Told(i,j,k,t))/(k/(dy/2));
                    Tgstar(i,j,k) = Tnew(i,j,k-1,t);
                    Thstar(i,j,k) = Told(i,j,k+1,t);
                else
                    Testar(i,j,k) = Told(i,j+1,k,t);
                    Tfstar(i,j,k) = (k*dx*dz/(dy/2)*Told(i,j,k,t) +
ho*Tinf*dx*dz)/(ho*dx*dz + k*dx*dz/(dy/2));
                    Tgstar(i,j,k) = Tnew(i,j,k-1,t);
                    Thstar(i,j,k) = Told(i,j,k+1,t);
                end
            elseif j == Ny      % North Face
                Testar(i,j,k) = (k*dx*dz/(dy/2)*Told(i,j,k,t) +
ho*Tinf*dx*dz)/(ho*dx*dz + k*dx*dz/(dy/2));
                Tfstar(i,j,k) = Tnew(i,j-1,k,t);
                Tgstar(i,j,k) = Tnew(i,j,k-1,t);
                Thstar(i,j,k) = Told(i,j,k+1,t);
            else
                Testar(i,j,k) = Told(i,j+1,k,t);
                Tfstar(i,j,k) = Tnew(i,j-1,k,t);
                Tgstar(i,j,k) = Tnew(i,j,k-1,t);
                Thstar(i,j,k) = Told(i,j,k+1,t);
            end
        end
```

```
        % Boundary Conditions and Coefficients
        if k == 1       % Top Face
            if j == 1
                if i == 1
                    a(i,j,k) = -(k*dy*dz/(dx/2) + ho*dy*dz + apo);
                    b(i,j,k) = k*dy*dz/(dx/2);
                    c(i,j,k) = 0;
                    e(i,j,k) = 0;
                    f(i,j,k) = 0;
                    g(i,j,k) = 0;
                    h(i,j,k) = 0;
                    dstar(i,j,k) = ho*Tinf*(dy*dz);
                elseif i == Nx
                    a(i,j,k) = -(k*dy*dz/(dx/2) + ho*dy*dz+ apo);
                    b(i,j,k) = 0;
                    c(i,j,k) = k*dy*dz/(dx/2);
                    e(i,j,k) = 0;
                    f(i,j,k) = 0;
                    g(i,j,k) = 0;
                    h(i,j,k) = 0;
                    dstar(i,j,k) = ho*Tinf*(dy*dz);
                else
                    a(i,j,k) = -
((k*dy*dz/dx)+(k*dy*dz/(dx))+(k*dx*dz/dy)+(k*dx*dz/(dy/2))+(k*dx*dy/dz)
+(k*dx*dy/(dz/2))+ apo);
                    b(i,j,k) = k*dy*dz/dx;
                    c(i,j,k) = k*dy*dz/dx;
                    e(i,j,k) = k*dx*dz/dy;
                    f(i,j,k) = (k*dx*dz/(dy/2) + ho*dx*dz);
                    g(i,j,k) = (k*dx*dy/(dz/2) + ho*dx*dy);
                    h(i,j,k) = k*dx*dy/dz;
                    dstar(i,j,k) = -ho*Tinf*(dx*dy+dx*dz);
                end
            elseif j == Ny
                if i == 1
                    a(i,j,k) = -(k*dy*dz/(dx/2) + ho*dy*dz + apo);
                    b(i,j,k) = k*dy*dz/(dx/2);
                    c(i,j,k) = 0;
                    e(i,j,k) = 0;
                    f(i,j,k) = 0;
                    g(i,j,k) = 0;
                    h(i,j,k) = 0;
                    dstar(i,j,k) = ho*Tinf*(dy*dz);
                elseif i == Nx
                    a(i,j,k) = -(k*dy*dz/(dx/2) + ho*dy*dz + apo);
                    b(i,j,k) = 0;
                    c(i,j,k) = k*dy*dz/(dx/2);
                    e(i,j,k) = 0;
                    f(i,j,k) = 0;
                    g(i,j,k) = 0;
                    h(i,j,k) = 0;
                    dstar(i,j,k) = ho*Tinf*(dy*dz);
                else
                    a(i,j,k) = -
((k*dy*dz/dx)+(k*dy*dz/(dx))+(k*dx*dz/dy)+(k*dx*dz/(dy/2))+(k*dx*dy/dz)
+(k*dx*dy/(dz/2)) + apo);
                    b(i,j,k) = k*dy*dz/dx;
```

```
                    c(i,j,k) = k*dy*dz/dx;
                    e(i,j,k) = (k*dx*dz/(dy/2) + ho*dx*dz);
                    f(i,j,k) = k*dx*dz/dy;
                    g(i,j,k) = (k*dx*dy/(dz/2) + ho*dx*dy);
                    h(i,j,k) = k*dx*dy/dz;
                    dstar(i,j,k) = -ho*Tinf*(dx*dy+dx*dz);
                end
            else
                if i == 1
                    a(i,j,k) = -(k*dy*dz/(dx/2) + ho*dy*dz + apo);
                    b(i,j,k) = k*dy*dz/(dx/2);
                    c(i,j,k) = 0;
                    e(i,j,k) = 0;
                    f(i,j,k) = 0;
                    g(i,j,k) = 0;
                    h(i,j,k) = 0;
                    dstar(i,j,k) = ho*Tinf*(dy*dz);
                elseif i == Nx
                    a(i,j,k) = -(k*dy*dz/(dx/2) + ho*dy*dz + apo);
                    b(i,j,k) = 0;
                    c(i,j,k) = k*dy*dz/(dx/2);
                    e(i,j,k) = 0;
                    f(i,j,k) = 0;
                    g(i,j,k) = 0;
                    h(i,j,k) = 0;
                    dstar(i,j,k) = ho*Tinf*(dy*dz);
                else
                    a(i,j,k) = -
((k*dy*dz/dx)+(k*dy*dz/(dx))+(k*dx*dz/dy)+(k*dx*dz/(dy))+(k*dx*dy/dz)+(
k*dx*dy/(dz/2)) + apo);
                    b(i,j,k) = k*dy*dz/dx;
                    c(i,j,k) = k*dy*dz/dx;
                    e(i,j,k) = k*dx*dz/dy;
                    f(i,j,k) = k*dx*dz/dy;
                    g(i,j,k) = (k*dx*dy/(dz/2) + ho*dx*dy);
                    h(i,j,k) = k*dx*dy/dz;
                    dstar(i,j,k) = -ho*Tinf*(dx*dy);
                end
            end
        elseif k == Nz      % Bottom Face
            if j == 1
                if i == 1
                    a(i,j,k) = -(k*dy*dz/(dx/2) + ho*dy*dz + apo);
                    b(i,j,k) = k*dy*dz/(dx/2);
                    c(i,j,k) = 0;
                    e(i,j,k) = 0;
                    f(i,j,k) = 0;
                    g(i,j,k) = 0;
                    h(i,j,k) = 0;
                    dstar(i,j,k) = ho*Tinf*(dy*dz);
                elseif i == Nx
                    a(i,j,k) = -(k*dy*dz/(dx/2) + ho*dy*dz + apo);
                    b(i,j,k) = 0;
                    c(i,j,k) = k*dy*dz/(dx/2);
                    e(i,j,k) = 0;
                    f(i,j,k) = 0;
                    g(i,j,k) = 0;
```

```
                    h(i,j,k) = 0;
                    dstar(i,j,k) = ho*Tinf*(dy*dz);
                else
                    a(i,j,k) = -
((k*dy*dz/dx)+(k*dy*dz/(dx))+(k*dx*dz/dy)+(k*dx*dz/(dy/2))+(k*dx*dy/dz)
+(k*dx*dy/(dz/2)) + apo);
                    b(i,j,k) = k*dy*dz/dx;
                    c(i,j,k) = k*dy*dz/dx;
                    e(i,j,k) = k*dx*dz/dy;
                    f(i,j,k) = (k*dx*dz/(dy/2) + ho*dx*dz);
                    g(i,j,k) = k*dx*dy/dz;
                    h(i,j,k) = (k*dx*dy/(dz/2) + ho*dx*dy);
                    dstar(i,j,k) = -ho*Tinf*(dx*dy+dx*dz);
                end
            elseif j == Ny
                if i == 1
                    a(i,j,k) = -(k*dy*dz/(dx/2) + ho*dy*dz + apo);
                    b(i,j,k) = k*dy*dz/(dx/2);
                    c(i,j,k) = 0;
                    e(i,j,k) = 0;
                    f(i,j,k) = 0;
                    g(i,j,k) = 0;
                    h(i,j,k) = 0;
                    dstar(i,j,k) = ho*Tinf*(dy*dz);
                elseif i == Nx
                    a(i,j,k) = -(k*dy*dz/(dx/2) + ho*dy*dz + apo);
                    b(i,j,k) = 0;
                    c(i,j,k) = k*dy*dz/(dx/2);
                    e(i,j,k) = 0;
                    f(i,j,k) = 0;
                    g(i,j,k) = 0;
                    h(i,j,k) = 0;
                    dstar(i,j,k) = ho*Tinf*(dy*dz);
                else
                    a(i,j,k) = -
((k*dy*dz/dx)+(k*dy*dz/(dx))+(k*dx*dz/dy)+(k*dx*dz/(dy/2))+(k*dx*dy/dz)
+(k*dx*dy/(dz/2)) + apo);
                    b(i,j,k) = k*dy*dz/dx;
                    c(i,j,k) = k*dy*dz/dx;
                    e(i,j,k) = (k*dx*dz/(dy/2) + ho*dx*dz);
                    f(i,j,k) = k*dx*dz/dy;
                    g(i,j,k) = k*dx*dy/dz;
                    h(i,j,k) = (k*dx*dy/(dz/2) + ho*dx*dy);
                    dstar(i,j,k) = -ho*Tinf*(dx*dy+dx*dz);
                end
            else
                if i == 1
                    a(i,j,k) = -(k*dy*dz/(dx/2) + ho*dy*dz + apo);
                    b(i,j,k) = k*dy*dz/(dx/2);
                    c(i,j,k) = 0;
                    e(i,j,k) = 0;
                    f(i,j,k) = 0;
                    g(i,j,k) = 0;
                    h(i,j,k) = 0;
                    dstar(i,j,k) = ho*Tinf*(dy*dz);
                elseif i == Nx
                    a(i,j,k) = -(k*dy*dz/(dx/2) + ho*dy*dz + apo);
```

```
                    b(i,j,k) = 0;
                    c(i,j,k) = k*dy*dz/(dx/2);
                    e(i,j,k) = 0;
                    f(i,j,k) = 0;
                    g(i,j,k) = 0;
                    h(i,j,k) = 0;
                    dstar(i,j,k) = ho*Tinf*(dy*dz);
                else
                    a(i,j,k) = -
((k*dy*dz/dx)+(k*dy*dz/(dx))+(k*dx*dz/dy)+(k*dx*dz/(dy))+(k*dx*dy/dz)+(
k*dx*dy/(dz/2)) + apo);
                    b(i,j,k) = k*dy*dz/dx;
                    c(i,j,k) = k*dy*dz/dx;
                    e(i,j,k) = k*dx*dz/dy;
                    f(i,j,k) = k*dx*dz/dy;
                    g(i,j,k) = k*dx*dy/dz;
                    h(i,j,k) = (k*dx*dy/(dz/2) + ho*dx*dy);
                    dstar(i,j,k) = -ho*Tinf*(dx*dy);
                end
            end

        elseif j == 1       %South Face
            if i == 1       % West Boundary
                a(i,j,k) = -(k*dy*dz/(dx/2) + ho*dy*dz + apo);
                b(i,j,k) = k*dy*dz/(dx/2);
                c(i,j,k) = 0;
                e(i,j,k) = 0;
                f(i,j,k) = 0;
                g(i,j,k) = 0;
                h(i,j,k) = 0;
                dstar(i,j,k) = ho*Tinf*(dy*dz);
            elseif i == Nx    % East Boundary
                a(i,j,k) = -(k*dy*dz/(dx/2) + ho*dy*dz + apo);
                b(i,j,k) = 0;
                c(i,j,k) = (k*dy*dz/(dx/2));
                e(i,j,k) = 0;
                f(i,j,k) = 0;
                g(i,j,k) = 0;
                h(i,j,k) = 0;
                dstar(i,j,k) = ho*Tinf*(dy*dz);
            elseif qzone == 1
                a(i,j,k) = -
((k*dy*dz/dx)+(k*dy*dz/(dx))+(k*dx*dz/dy)+(k*dx*dz/(dy/2))+(k*dx*dy/dz)
+(k*dx*dy/(dz)) + apo);
                b(i,j,k) = k*dy*dz/dx;
                c(i,j,k) = k*dy*dz/dx;
                e(i,j,k) = k*dx*dz/dy;
                f(i,j,k) = k*dx*dz/(dy/2);  % South face with heat flux
May need qo in here
                g(i,j,k) = k*dx*dy/dz;
                h(i,j,k) = k*dx*dy/dz;
                dstar(i,j,k) = qo*(dx*dz);
            else
                a(i,j,k) = -
((k*dy*dz/dx)+(k*dy*dz/(dx))+(k*dx*dz/dy)+(k*dx*dz/(dy/2))+(k*dx*dy/dz)
+(k*dx*dy/(dz)) + apo);
                b(i,j,k) = k*dy*dz/dx;
```

```
                c(i,j,k) = k*dy*dz/dx;
                e(i,j,k) = k*dx*dz/dy;
                f(i,j,k) = (k*dx*dz/(dy/2) + ho*dx*dz);
                g(i,j,k) = k*dx*dy/dz;
                h(i,j,k) = k*dx*dy/dz;
                dstar(i,j,k) = -ho*Tinf*(dx*dz);
            end
        elseif j == Ny      % North Face
            if i == 1       % West Boundary
                a(i,j,k) = -(k*dy*dz/(dx/2) + ho*dy*dz + apo);
                b(i,j,k) = k*dy*dz/(dx/2);
                c(i,j,k) = 0;
                e(i,j,k) = 0;
                f(i,j,k) = 0;
                g(i,j,k) = 0;
                h(i,j,k) = 0;
                dstar(i,j,k) = ho*Tinf*(dy*dz);
            elseif i == Nx    % East Boundary
                a(i,j,k) = -(k*dy*dz/(dx/2) + ho*dy*dz + apo);
                b(i,j,k) = 0;
                c(i,j,k) = k*dy*dz/(dx/2);
                e(i,j,k) = 0;
                f(i,j,k) = 0;
                g(i,j,k) = 0;
                h(i,j,k) = 0;
                dstar(i,j,k) = ho*Tinf*(dy*dz);
            else
                a(i,j,k) = -
((k*dy*dz/dx)+(k*dy*dz/(dx))+(k*dx*dz/dy)+(k*dx*dz/(dy/2))+(k*dx*dy/dz)
+(k*dx*dy/(dz)) + apo);
                b(i,j,k) = k*dy*dz/dx;
                c(i,j,k) = k*dy*dz/dx;
                e(i,j,k) = k*dx*dz/dy;
                f(i,j,k) = (k*dx*dz/(dy/2) + ho*dx*dz);
                g(i,j,k) = k*dx*dy/dz;
                h(i,j,k) = k*dx*dy/dz;
                dstar(i,j,k) = -ho*Tinf*(dx*dz);
            end
        elseif i == 1   % West Face
            a(i,j,k) = -(k*dy*dz/(dx/2) + ho*dy*dz + apo);
            b(i,j,k) = k*dy*dz/(dx/2);
            c(i,j,k) = 0;
            e(i,j,k) = 0;
            f(i,j,k) = 0;
            g(i,j,k) = 0;
            h(i,j,k) = 0;
            dstar(i,j,k) = ho*Tinf*(dy*dz);
        elseif i == Nx  % East Face
            a(i,j,k) = -(k*dy*dz/(dx/2) + ho*dy*dz + apo);
            b(i,j,k) = 0;
            c(i,j,k) = k*dy*dz/(dx/2);
            e(i,j,k) = 0;
            f(i,j,k) = 0;
            g(i,j,k) = 0;
            h(i,j,k) = 0;
            dstar(i,j,k) = ho*Tinf*(dy*dz);
        else        % Any intermediate point (Non Face/Non Flux)
```

```
            a(i,j,k) = -((2*k*dy*dz/dx)+(2*k*dx*dz/dy)+(2*k*dx*dy/dz) +
apo);
            b(i,j,k) = k*dy*dz/dx;
            c(i,j,k) = k*dy*dz/dx;
            e(i,j,k) = k*dx*dz/dy;
            f(i,j,k) = k*dx*dz/dy;
            g(i,j,k) = k*dx*dy/dz;
            h(i,j,k) = k*dx*dy/dz;
            dstar(i,j,k) = 0;
        end

        d(i,j,k) = -(apo*Tnew(i,j,k,t-1) + e(i,j,k)*Testar(i,j,k) +
f(i,j,k)*Tfstar(i,j,k) + g(i,j,k)*Tgstar(i,j,k) +
h(i,j,k)*Thstar(i,j,k) + dstar(i,j,k));
      if i == Nx
          % TDMA
            abc = zeros(Nx,Nx);
            for l = 1:Nx
                for m = 1:Nx
                    if l == m
                        abc(m,l) = a(l,j,k);
                    elseif l == (m+1)
                        abc(m,l) = b(l-1,j,k);
                    elseif l == (m-1)
                        abc(m,l) = c(l+1,j,k);
                    else
                        abc(m,l) = 0;
                    end
                end
                D(l) = d(l,j,k);
            end
            Tnew(:,j,k,t) = abc\D';
            abc = 0; D = 0;
      end

        qzone = 0;

    end
    end
    end


if iter > 1
error1(iter) = abs(mean(mean(mean(Tnew(:,:,:,t)))))-
mean(mean(mean(Told(:,:,:,t))));
Error1(iter+1) = sum(error1(iter).^2)/iter;
end
Told = Tnew;
iter = iter + 1;

end
iter = 1;
end
```

```
for i = 1:Nx
    for k = 1:Nz
        Txz1(i,k) = Tnew(i,1,k,1);
    end
end
for i = 1:Nx
    for k = 1:Nz
        Txz2(i,k) = Tnew(i,1,k,2);
    end
end
for i = 1:Nx
    for k = 1:Nz
        Txz3(i,k) = Tnew(i,1,k,100);
    end
end
figure(1)
% subplot(1,3,1)
surfc(W,L,Txz1')
title('3D plot of Temperature across the South (Heat Flux input) face
(xz plane)')
xlabel('Width (m)')
ylabel('Length (m)')
zlabel('Temperature (K)')
% subplot(1,3,2)
figure(2)
surfc(W,L,Txz2')
title('3D plot of Temperature across the Mid-Plane (xz plane)')
xlabel('Width (m)')
ylabel('Length (m)')
zlabel('Temperature (K)')
% subplot(1,3,3)
figure(3)
surfc(W,L,Txz3')
title('3D plot of Temperature across the North face (xz plane)')
xlabel('Width (m)')
ylabel('Length (m)')
zlabel('Temperature (K)')


toc
```